TECHNISCHE UNIVERSITÄT MÜNCHEN
LEHRSTUHL FÜR CHEMIE DER BIOPOLYMERE
VERHELST LAB

# Substrate-free Rhomboid Protease Assays for the Discovery of Novel Inhibitors

*Eliane* Viola Wolf

Vollständiger Abdruck der von der Fakultät Wissenschaftszentrum Weihenstephan für Ernährung, Landnutzung und Umwelt der Technischen Universität München zur Erlangung des akademischen Grades eines

Doktors der Naturwissenschaften

genehmigten Dissertation.

Vorsitzender:             Univ.-Prof. Dr. D. Langosch

Prüfer der Dissertation:    1.  TUM Junior Fellow Dr. St. Verhelst

2.  Univ.-Prof. Dr. St. Lichtenthaler

3.  Univ.-Prof. Dr. I. Antes

Die Dissertation wurde am 28.01.2015 bei der Technischen Universität München eingereicht und durch die Fakultät Wissenschaftzentrum Weihenstephan für Ernährung, Landnutzung und Umwelt am 19.06.2015 angenommen.

# Table of Contents

## Abstract

Rhomboid proteases are intramembrane serine proteases that reside within various cellular membranes and cleave their substrates in the plane of the membrane. They can be found in almost all organisms and are implicated in various biological processes and some important diseases such as malaria and cancer. Currently, rhomboid research is being hampered by the lack of selective inhibitors, which could be useful as research tools and lead compounds in drug research. All available inhibitor screening assays have the limitation of being substrate based, which prevents them from being applied to many members of the rhomboid family.

In order to address this issue, in this work a new, substrate-free, rhomboid inhibitor screening assay was developed that allows for rapid screening of a rhomboid protease by using activity-based probes (ABPs) - the "Rhomboid FluoPol ABPP" assay. A screen performed with this new assay uncovered novel rhomboid inhibitors, among these an entirely new structural class. Some of these inhibitors were shown to function as ABPs and are therefore new research tools available to the rhomboid community.

In follow-up experiments it was shown that the screening environment - detergent micelles or liposomes - has no influence on the identification of the rhomboid inhibitors, so that rhomboid inhibitor screens can easily be performed in detergent micelles in the future. During these experiments, the reconstitution protocol and the first rhomboid-containing giant unilamellar vesicles (GUVs) were developed, that allow future systematic study of the membrane environment.

In a comprehensive inhibitor fingerprinting of 13 rhomboid proteases from prokaryotic, archaean, and eukaryotic origins with 51 small molecules performed in this thesis, many new inhibitors and ABPs were discovered, which is especially important for the not well studied rhomboid proteases. As an additional result from these experiments, a new phenomenon has been uncovered: the rhomboid auto-cleavage. In first experiments it was shown that rhomboid proteases are able to truncate N-terminal extra membranous rhomboid domains, and that many of these truncated rhomboid species retain their catalytic activity.

Taken together the results from this thesis, for example the "Rhomboid FluoPol ABPP" assay, the Rhomboid-GUVs and the new inhibitors and ABPs will allow future study of rhomboids from various organisms, activity profiling as well as auto-processing.

# Zusammenfassung

Rhomboidproteasen sind intramembranäre Serinproteasen, die in vielzähligen zellulären Membranen lokalisiert sind und ihre Substrate in der Membranebene spalten. Sie kommen in fast allen Organismen vor und werden mit verschiedensten biologischen Prozessen und einigen wichtigen Krankheiten wie Malaria und Krebs in Verbindung gebracht. Im Moment wird die Rhomboidforschung durch das Fehlen selektiver Inhibitoren behindert; letztere könnten nützliche Forschungswerkzeuge und Ausgangsstrukturen für die Medikamentenforschung darstellen. Alle bislang verfügbaren Testmethoden zum Screening von Inhibitoren haben die Einschränkung, dass sie substratbasiert sind, und somit für viele Vertreter der Rhomboid-Familie nicht angewendet werden können.

Um dieses Problem zu überwinden, wurde in dieser Arbeit eine neue, substratfreie Testmethode zum Inhibitorscreening für Rhomboide entwickelt, welche das schnelle Suchen nach Rhomboidinhibitoren mit Hilfe von aktivitätsbasierten Sonden (englisch: activity-based probes, ABPs) erlaubt – das „Rhomboid FluoPol ABPP" Testverfahren. In einem mit dieser Testmethode durchgeführten Screening konnten neue Rhomboidinhibitoren gefunden werden, darunter auch Vertreter einer komplett anderen strukturellen Klasse. Einige dieser Inhibitoren konnten erfolgreich als ABPs angewendet werden und stellen daher neue Forschungswerkezuge für Rhomboidforscher dar.

In Folgeexperimenten konnte gezeigt werden, dass die Art der Umgebung in der ein Inhibitorscreening durchgeführt wird – Detergensmizellen oder Liposomen – keinen Einfluss auf die korrekte Identifizierung von Inhibitoren hat, und somit künftig immer einfache Detergensmizellen verwendet werden können. Das während dieser Untersuchungen entwickelte Rekonstitutionsprotokoll und die ersten rhomboidhaltigen rießigen unilamellaren Vesikel erlauben eine zukünftige systematische Untersuchung der Membranumgebung von Rhomboiden.

In einem umfangreichen Inhibitorfingerabdruck-Experiment mit 13 Rhomboiden aus prokaryotischer, achaeeller und eukaryotischer Herkunft, sowie 51 kleinen Molekülen, wurden in dieser Arbeit viele neue Inhibitoren und ABPs entdeckt, was für die wenig untersuchten Rhomboidproteasen besonders wichtig ist.

Ein weiteres Ergebnis dieser Experimente ist die Entdeckung eines neuen Phänomens, der Rhomboid-Selbstspaltung. In ersten Experimenten konnte gezeigt werden, dass Rhomboidproteasen ihre N-terminale extramembranäre Domäne abspalten können, und dass viele dieser gekürzten Rhomboide ihre Aktivität beibehalten.

Zusammengefasst werden die Ergebnisse dieser Arbeit, beispielsweise die "Rhomboid FluoPol ABPP" Testmethode, die Rhomboid-Liposomen-Rekonstitutionsmethode, sowie die neuen Inhibitoren und ABPs, zukünftige Untersuchungen von Rhomboiden aus verschiedenen Organismen, des Aktivitätsprofiles, und der Selbstspaltung ermöglichen.

# 1. Introduction

## 1.1. The intramembrane protease rhomboid

Classical proteases are soluble enzymes that cleave proteins and polypeptides by hydrolysis. According to their catalytic mechanism proteases can be classified into the following groups: serine, cysteine, and threonine proteases, which are named after the catalytic residue that nucleophilically attacks the peptide bond, as well as aspartic, glutamic and metalloproteases, which in contrast are named after the catalytic residues or chemical entity that activates the hydrolyzing water molecule [1].

A common nomenclature for proteases is used for describing substrate binding sites and side chains: The substrate side chains upstream and downstream of the scissile bond are termed Pn-P1 and P1'-Pn' respectively, while the corresponding binding pockets in the protease are termed Sn-S1 and S1'-Sn' (Figure 1).
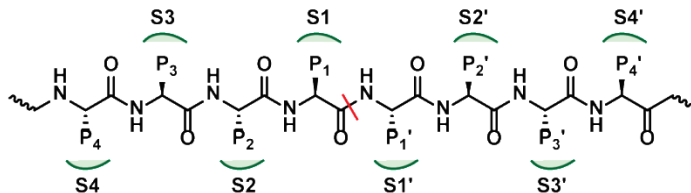


**Figure 1 Nomenclature of the substrate binding pockets in a protease and the substrate side chains.** Nomenclature according to Schechter and Berger [2]: The location of cleavage site is indicated in red. Residues N-terminal of the scissile bond are termed P1-P4, residues C-terminal of the scissile bond P1'-P4'. The binding pockets of the protease are termed accordingly with an S instead of a P. The scheme has been modified after Strisovsky 2013 [3].

In contrast to these classical proteases, novel types of proteases have been discovered some years ago - the intramembrane proteases.

### 1.1.1. Intramembrane proteases

Intramembrane proteases are enzymes that are located within the membrane and cleave in the plane of the membrane within or very close to the substrate's transmembrane domain (TMD), which is also located within the membrane. This was seen as a paradox for a while, because the proteolytic cleavage requires water molecules, which are not very abundant in hydrophobic membranes. Today, with crystal structures available for some members of the intramembrane proteases [4-8], the process of cleavage within the membrane is better understood and intramembrane proteases have turned from unconventional exceptions to accepted protease-members. Cleavage of membrane proteins by intramembrane proteases, also termed regulated intramembrane proteolysis (RIP), is an important cellular process which leads to the release of protein fragments to either the exterior or the interior of the cell or organelle, with the fragments having a function different from their full-length precursors [9, 10]. Similar to soluble proteases, intramembrane proteases can be classified according to their active site, and commonly are divided into three classes: (1) the site-2 protease (S2P) family, which are metalloproteases [11-13]; (2) the 'GxGD'-type aspartyl protease family, including both the γ-secretase family and the signal peptide peptidase (SPP) family [9, 14-18]; (3) and the rhomboid-like family, which are serine proteases [19, 20].

The first known intramembrane proteases were those of the S2P family, which are involved in activating transcription factors: they cleave both the sterol regulatory element-binding protein (SREBP), which is involved in feedback regulation of the sterol and lipid biosynthesis; and also the activating transcription factor 6 (ATF6), which triggers the ER unfolded protein response [11, 21]. The SREBP-cleavage is a good example for regulation of intramembrane cleavage, as regulated trafficking of the SREBP substrate controls the availability of it for the S2P [22]. Furthermore S2Ps require a prior trimming event of the substrate before they cleave their substrate. This is another important way to regulate the intramembrane cleavage. S2Ps contain two motives, HExxH and EG, that coordinate a prosthetic zinc ion which activates the water molecule required for proteolysis [23]. They can be found in in many organisms ranging from metazoans and fungi, to plants and animals, but not in the yeast *Saccharomyces cerevisiae* [23, 24].

The two aspartyl protease families, γ-secretase and SPP, both contain two conserved active site motives, a YD motif on one transmembrane (TM) helix, and a GxGD motif on a neighboring TM helix. Due to these common motives, the two families are combined under the name "GxGD type aspartyl proteases" [9, 17]. Of these, the γ-secretase is the best characterized protease, probably because it is implicated in early onset familial Alzheimer's disease (AD) [25, 26]. After prior cleavage by either α-secretase or the β-secretase (BACE), γ-secretase intramembranously cleaves off the N-terminus of the amyloidogenic precursor protein (APP). Some of the secreted short N-terminal fragments are prone to aggregate and are a major risk factor for AD [27]. In addition to APP, over 60 γ-secretase substrates have been identified, emphasizing the importance of this protease in RIP [28]. In contrast to all other membrane proteases, γ-secretase requires other non-catalytic subunits in addition to its catalytic subunit, presenilin [29, 30]. While this makes obtaining a crystal structure of the complex difficult, it provides the cell with an additional regulation mechanism: through interference with the assembly process and retrieval of unassembled complexes γ-secretase activity can be further influenced [31].

The other GxGD family, the SPPs, remove signal peptides from the membrane. These signal peptides are initially cleaved from their precursor proteins by a signal peptidase and remain in the membrane, where they are degraded by the SPP [17]. In addition to the removal of signal peptides, SPP have also been shown to be involved in antigen presentation and cleavage of the hepatitis C virus core protein [32-34]. Eukaryotic SPP-like (SPPL) proteases have additionally been implicated in processing of the tumor necrosis factor TNFα as well as being involved in parasite invasion in *Plasmodium falciparum* [14, 35].

The third intramembrane group, the rhomboids, is the focus of this thesis and will be discussed in greater detail in the next paragraph.

### 1.1.2.   Rhomboids

Rhomboids are a family of intramembrane serine proteases, which can be found in the membranes of almost all organisms of prokaryotic, archaean and eukaryotic origin [20, 36]. They were first discovered in the fruit fly *Drosophila melanogaster*, where Rhomboid-1 cleaves the transmembrane protein Spitz, a homolog of the mammalian TGFα and primary epidermal growth factor receptor (EGFR) activating ligand [10, 19, 37-43]. Rhomboids are named after their mutant phenotype, an abnormally shaped *Drosophila melanogaster* head [44].

**Biological relevance of rhomboids**

Rhomboids are involved in numerous cellular processes and have various biological functions, a few of which are listed here.

In *Drosophila melanogaster* as well as in *Caenorhabditis elegans*, they have been shown to control EGFR signaling [19, 45].

In the gram-negative bacterium *Providencia stuartii,* the rhomboid AarA is indirectly involved in intercellular communication – quorum sensing – by cleavage of the twin-arginine protein translocator subunit TatA [46]. Upon cleavage the TatA can multimerize and form a channel, which translocates fully folded, modified, and cofactor-containing proteins with a twin-arginine motif into the periplasm [46-48].

In apicomplexan parasites such as *Plasmodium falciparum* and *Toxoplasma gondii*, which cause malaria and toxoplasmosis respectively, rhomboids are important for cleavage of adhesins, which then leads to the invasion of the host cell by the parasite [49-53].

In the yeast *Saccharomyces cerevisiae* the mitochondrial rhomboid PcP1, also named Rbd1, is involved in mitochondrial membrane dynamics through cleavage of the dynamine-like GTPase Mgm1 [54-57]. The mammalian mitochondrial rhomboid PARL (presenilin associated rhomboid-like) in contrast, is thought to be involved in the regulation of apoptosis in lymphocytes by cleavage and release of the protease HtrA2 from the mitochondrial inner membrane [58, 59]. Additionally, human PARL has been shown to cleave PINK1, thereby inhibiting recruitment of the Parkin ubiquitin ligase onto the mitochondria [60, 61].

The Parkin/PINK1 pathway has been shown to malfunction in Parkinson's disease. PARL mutations have been found in patients suffering from Parkinson's disease and diabetes, but the involved mechanisms is not yet completely understood [60, 62].

As proteases, they are in principle targetable by inhibitors, and on the basis of their biological roles in EGFR-signaling, quorum sensing, apicomplexan infections and mitochondrial dynamics, rhomboids might prove to be valuable therapeutical targets in the future for treatment of cancer, infections, parasites or type 2 diabetes respectively.

**Structure of rhomboids**

Various crystal structures of the rhomboid GlpG from *Haemophilus influenza* (HiROM) and the rhomboid GlpG from *Escherichia coli* (EcGlpG) (Figure 2) have provided insight into the structure and architecture of rhomboids [6-8, 63].
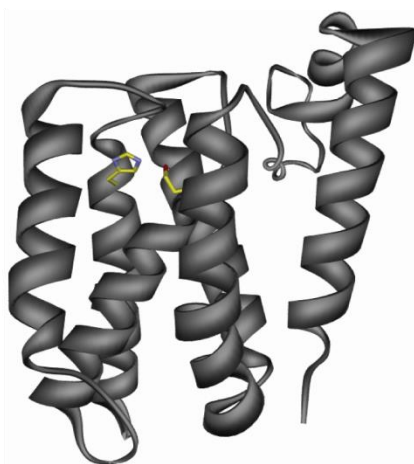


**Figure 2 Crystal structure of the rhomboid EcGlpG.** The 6 TM helices are of different lengths and angles and form a water-filled cavity directed towards the periplasm. The catalytic site is located in this cavity, ~ 10 Å below the surface. The catalytic Ser201 at the start of TM4 is hydrogen bonded to the catalytic His254 in the middle of TM6 with a distance of ~ 3.1 Å (both residues are indicated in yellow). The crystal structure of PDB entry 4NJP was visualized by ViewerLite and rendered with POVRay [64].

In contrast to soluble serine proteases, whose catalytic triad consists of a serine, histidine and aspartate, rhomboids possess a serine-histidine dyad [65] (Figure 3).

While this is uncommon, there are examples for soluble serine proteases that forego the classical serine-histidine-aspartic acid triad [66].
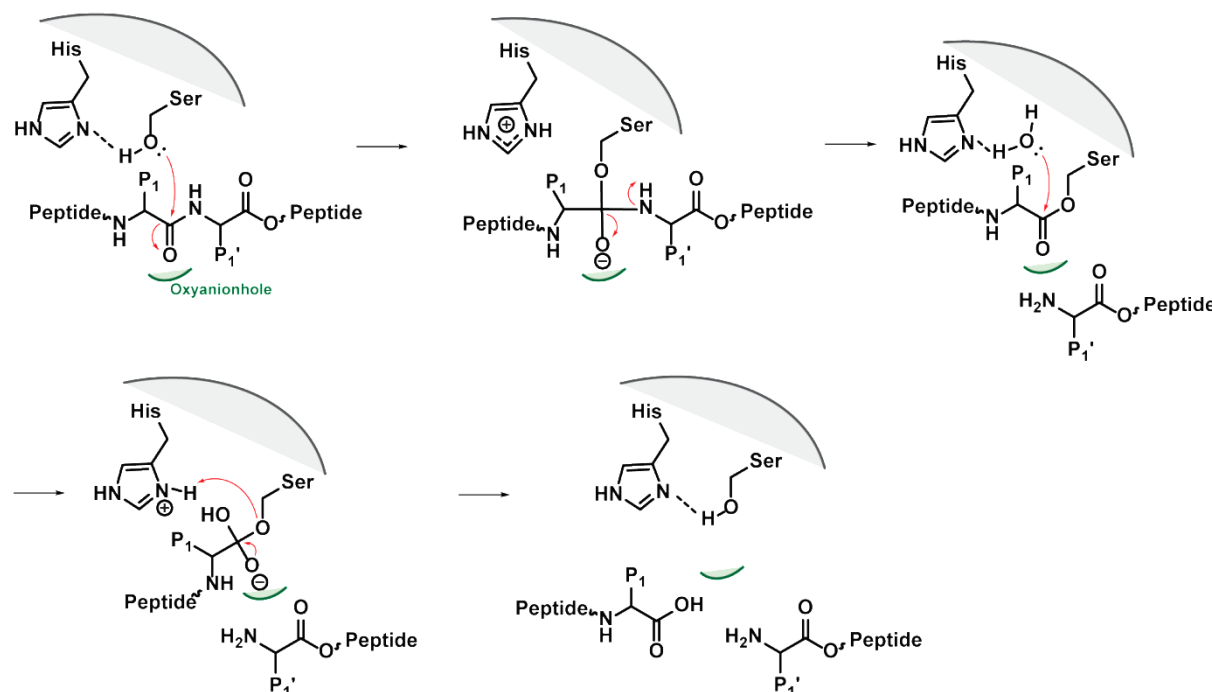


**Figure 3 Catalytic mechanism of the serine-histidine dyad in rhomboids.** The histidine acts as a base and deprotonates the hydroxyl group of the serine. The now nucleophilic serine can attack onto the carbonyl in the scissile bond of the substrate. A tetrahedral intermediate is formed, which is stabilized by several hydrogen bonds with the rhomboid's oxyanion hole. The tetrahedral intermediate is formed into the acyl-enzyme intermediate and an amine product. Water attacks on the acyl-enzyme complex and forms a second tetrahedral complex, which is then deacylated and the carboxylic acid product leaves. Rhomboids lack the stabilizing proton-withdrawing aspartate soluble serine proteases possess.

The serine-histidine dyad is located several Å below the surface of the bilayer, at the bottom of a water-filled cavity which is open towards the aqueous environment outside the membrane [67]. The catalytic serine is located on top of the short TM4 and is surrounded and shielded by the longer, membrane-spanning TM2, 3 ,5, and 6.

The catalytic histidine is located on TM6 and oriented towards the serine [4, 5] stabilized by a stacking interaction with Tyr205 [68]. The oxyanion hole, according to inhibitor-bound crystal structures, is formed by the main chain NH group of Ser201 and the side chains of His150 and Asn154 (EcGlpG nomenclature) [69].

There are four major motives present in rhomboids, which are important for stability and activity [70]: (1) a conserved E/QxWRxxS/T motif in the L1 loop, between TM1 and 2, wherein arginine and threonine form hydrogen bonds with other residues in the L1 loop thereby greatly stabilizing it; (2) a conserved GxxxExxxG motif on the bottom of TM2 and beginning of the L2 loop, wherein the first glycine leads to a bend in TM2, the glutamate forms hydrogen bonds with the bottom of TM1 and 3, and finally the second glycine forming a cytosolic bend before TM3, overall bringing together the TM1, 2, and 3 into a V-shape on the cytosolic side of the enzyme; (3) a conserved GxSG motif in TM4 and hallmark for rhomboid enzymes [19, 36], with the glycines extending the L3 loop far into the membrane so that the active serine sits on top of TM4, and hydrogen bonding to the L1 loop, overall leading to a stabilization of the cavity; (4) and lastly a conserved alanine followed by the active site histidine in an AHxxGxxxG motif on TM6, forming a tight interaction with TM4 and thus bringing the two catalytic residues, serine (TM4) and histidine (TM6) within close proximity [5, 68, 70].

Crystal structures of the rhomboid-inhibitor complex have defined the polar S1 cavity and the hydrophobic S2' cavity, which bind the substrates P1 and P2' residues respectively [71]. The S2' cavity is not observed in the apoenzyme structure, but only when inhibitor is bound, will loop 5, TM5, and the side chain W236 (EcGlpG nomenclature) move to form this plastic cavity. A recent rhomboid-peptidic inhibitor crystal structure has delineated the S1 to S4 subsides, with most importantly the S1 cavity merging into the so-called 'water-retention site' and the S4 pocket being plastically formed by the L1 loop [72, 73].

The basic rhomboid structure, also called the rhomboid catalytic core, is found in most prokaryotic rhomboids and consist of 6 TM helices [74, 75], with most eukaryotic rhomboids possessing an additional TM helix on the C-terminus (6+1 topology) [19], and mitochondrial PARL-type rhomboids having an extra TM helix at the N-terminus (1+6 topology) [20, 36] (Figure 4). This has implications on the substrate cleavage: Prokaryotic rhomboids and eukaryotic 6+1 rhomboids have a $N_{in}$ orientation, leaving the catalytic residue-containing TM helices 4 and 6 pointing towards the inside, and cleave type 1 membrane proteins that have a $N_{out}$ orientation [10].

PARL-like rhomboids on the other side, due to their 1+6 topology, have their catalytic residue containing TM helices pointing outwards, and they cleave type 2 membrane proteins with a $N_{in}$ orientation [54, 55]. To what degree this orientation influences the preferred orientation of the substrate remains unclear at this point.
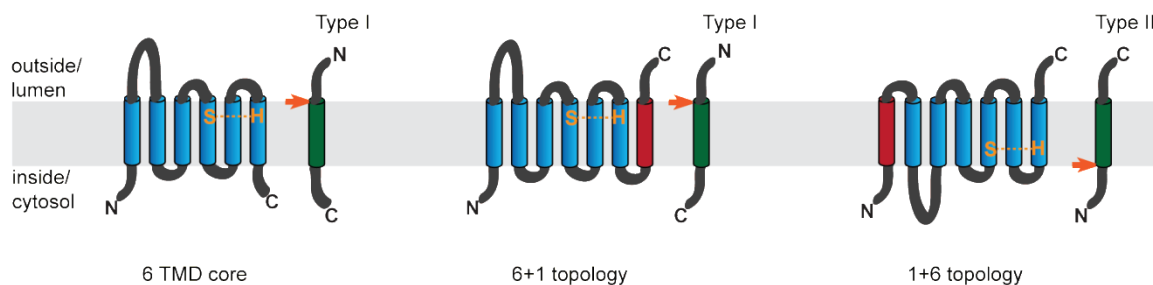


**Figure 4 Topology of prokaryotic, eukaryotic and mitochondrial rhomboids.** Most prokaryotic rhomboids like EcGlpG consist of only the 6 TMD core, with an inside N- and C-terminus. They cleave type 1 membrane proteins. Eukaryotic rhomboids like Rhomboid-1 have an additional TM helix on the C-terminus of the 6 TMD core, giving them a 6+1 topology with an outside C-terminus. They also cleave type 1 membrane proteins. The mitochondrial rhomboid PARL has an additional TM helix on the N-terminus of the 6 TMD core, with a 1+6 topology and an outside C-terminus. PARL cleaves type 2 membrane proteins. The scheme has been modified after Strisovsky 2013 [3].

**Classification of rhomboids**

Despite their ubiquitous presence in all kingdoms of life, rhomboids as a whole share a low sequence identity of only about 6% [20, 36, 76]. The rhomboid 'superfamily' includes active proteases and inactive members.

The active eukaryotic rhomboids can be further subdivided into two subgroups: the mitochondrial PARL-like rhomboids, and the secretase rhomboids, which are part of the secretory pathway. In mammals, the secretase rhomboids are called RHBDL1-4 (for rhomboid-like protein 1-4), and are localized in the Golgi (RHBDL1), plasma membrane (RHBDL2), endosomes (RHBDL3), or endoplasmatic reticulum (ER) (RHBDL4) [77, 78].

In addition to the catalytically active rhomboid serine proteases, there are also rhomboid pseudoproteases, which share rhomboid sequences and topologies as well as the GxxxG motive in TM6, but lack the catalytic residues. The two major groups are the iRhoms (inactive rhomboids) and Derlins [20, 65, 79].

iRhoms are present in animals and have a 6+1 topology, furthermore they share an universal proline before the catalytic serine (in a GPxG motive), an extended N-terminus, as well as a highly conserved loop 1, the iRhom homology domain (IRHD) [20]. Derlins are present in eukaryotes and consist of the rhomboid 6 TMD core and have the WR motive in their L1 loop, that is also present in active rhomboids [79].

Unless otherwise specified, this thesis uses the term rhomboids for the active rhomboid protease members.

**Rhomboid substrates**

The questions what makes a protein a rhomboid substrate as well as how this substrate then gains access to the active site, are the most controversially discussed topics in the rhomboid field. The fundamental problem when arguing about substrate recognition is the lack of natural substrates: there are only a handful of substrates known for a few rhomboids, with most of them being eukaryotic substrates and only one prokaryotic substrate [80, 81]. Notably for EcGlpG, the best studied rhomboid, the natural substrate has still not been identified [74].

To overcome the lack of substrates, some effort has been undertaken to investigate possible selectivity motives in known substrates and to design a possibly "universal" substrate [82, 83]. This approach seems reasonable, as rhomboid substrates have been shown to be often interchangeable: It has been shown that Rhomboid-1 from *Drosophila* and AarA from *Providencia stuartii* can functionally replace each other in vivo [84, 85]. Although recognition motives have been found on rhomboid substrates that confer selectivity (small residue in P1, hydrophobic and large residues in P4 and P2' positions) [83], other experiments have shown that a non-substrate can be turned into a substrate by the introduction of a helix-destabilizing residue [86]. As such it seems that a rhomboid substrate needs to at least partially unfold to allow access to the scissile bound, this has been evidenced by various studies which have found that helix-destabilizing residues are common near the cleavage site in many rhomboid substrates [74, 87, 88].

The relationship between such helix-breaking residues and specific recognition motives identified remains unclear at this point, with two competing theories being discussed: The 'recognition motif' theory favors an interaction of the substrate's recognition motive with the top of the membrane through specific subsites, and the need for helix-destabilizing residues depends mainly on whether the substrate is cleaved within the TMD or at the interface [5, 83, 89]. The 'TMD dynamics' theory relies on a lateral interaction of the substrate with the TM helices in the membrane, where the substrate automatically unwinds, when moving from the hydrophobic membrane into the hydrophilic interior of the rhomboid [63, 70, 86]. Both theories are consistent with existing crystal structures, so that only a structure of the rhomboid-substrate complex might give further insight into this.

The mechanism of substrate-entry into the active site is up to date still a much discussed issue, with two competing models favored by the rhomboid community: In the first, the L5 loop forms a cap on top of the active site and thus plugs the cavity, and is then displaced by the substrate [4], whereas in the second model, a lateral gate between TM2 and 5 is proposed, with TM5 being the mobile entity [63]. For both theories applicable, an observed thinning of the lipid bilayer around the rhomboid would lead to a hydrophobic mismatch and thus would enhance recruitment of the substrate [6], although it is not clear at this point whether this observation is at all valid [6, 90].

While there are multiple experimental observations favoring either the 'lateral gate' [7, 63, 68, 86, 91-93] or the 'L5 cap' [4, 69, 71, 90, 94, 95] theory, the precise mechanism remains unclear: mutation studies have shown that the substrate gate is most likely the semi-mobile TM5. It is the only helix not hydrogen-bonded but still relatively stable, effectively being able to limit the access to the active side, so that opening of the gate is the rate-limiting step. A recent crystal structure of a covalent peptidic inhibitor with the rhomboid, points toward the 'L5 cap' and the 'recognition motive' theories [72]. Indeed the peptidic inhibitor showed various hydrogen bonds and van der Waals interactions with residues in the L3, L5, and L1 loop, which could point towards a function of these loops in not only substrate stabilization but also recognition. Although this inhibitor mimics the substrate, only the P4 to P1 positions were analyzed and the carbonyl group of the P1 residue did not overlay with previous inhibitors in the putative oxyanion hole [96, 97]. As such this crystal structure does not provide an ultimate conclusion on these controversial matters.

Indeed the cleavage sites and topologies of different rhomboid substrates are so diverse, that a more refined and complex mechanisms in gating and recognition might be needed to explain the wide range of rhomboid functions within different organelles and organisms [98-101].

On a final note, a recent catalytic analysis conducted in proteoliposomes determined the $K_M$ of EcGlpG with 135 μM, the $k_d$ with 191 μM, and the $k_{cat}$ with 0.0063 s$^{-1}$, which mounts up to a catalytic efficiency of only 47 M$^{-1}$s$^{-1}$ [64]. While the $k_M$ stayed basically the same in all 10 rhomboid proteases investigated, the $k_{cat}$ ranged ~10,000-fold. These findings are thought to indicate that rhomboid catalysis does not rely on substrate affinity, but is rather a kinetically controlled reaction. Another steady-state kinetic analysis performed in detergent found similar kinetic parameters, but additionally uncovered a cooperative and homotropic allosteric effect for the rhomboid AarA from *Providencia stuartii* with its natural substrate TatA [102]. These findings point towards the existence of an exosite, formed by rhomboid dimerization that recognizes a TMD-substrate, which would necessarily require the existence of a recognition motive.

With these somewhat contradictory findings, it seems that the conundrum about substrate recognition and access is far from resolved.

**Regulation and of rhomboid activity**

The regulation of rhomboid activity is still poorly understood; since rhomboids are not produced as inactive zymogens, but already as active enzymes, the question has been raised how the cleavage of substrates is regulated by the cell. This regulation is especially necessary since rhomboids cleave the full length form of their substrates, and do not require a prior cleavage event, like all other transmembrane protease families, and can serve as a regulation mechanism [10, 74, 103, 104].

A few observed regulation mechanisms are transcriptional control [105], compartmentalization, where the substrate and rhomboid are not in the same compartment prior to cleavage [10, 49, 106], and the translocation of the cleavage site into the membrane prior to cleavage, a process called alternative topogenesis [98].

Both mechanisms restrict the access of the rhomboid to its substrate. It was shown in liposomes that rhomboid activity is influenced by the lipid composition, but further studies are required to assess the extent of the influence of the lipid environment, so that for now it remains unclear if certain lipid environments are used in vivo to control rhomboid activity [107]. An open question is whether direct regulation mechanisms exist at all, for example through specific binding of other proteins, such as for example iRhoms. A further point for speculations are the highly diverse extra-membranous domains: In the *Toxoplasma gondii* rhomboids 1 and 2 they have been shown to be important for protein trafficking [108], the C-terminal domain of RHBDL4 contains a ubiquitin interacting motive that is important for substrate degradation [77], and RHBDL2 has a cytoplasmic domain that is important for thrombomodulin cleavage [78]. Taken together, these examples indicate that extramembranous rhomboid domains could be a widespread regulation feature. While full length rhomboid crystal structures are not available, NMR and X-ray structures of the cytosolic domains have been solved for *Pseudomonas aeruginosa* and *E.coli* GlpG [109-111]. Excitingly, the EcGlpG cytoplasmic domains appear in dimers with extensive domain swapping between the two domains. While it has been shown that the cytosolic domains do not interact with the lipid bilayer and thus are not involved in regulation by the lipid environment, this domain swapping could explain the dimeric occurrence of some rhomboids in vivo, which has been observed in *E.coli*, *Haemophilus influenza, Providencia stuartii* and B*acillus subtilis* [102, 112].

**Environments for rhomboid study**

Rhomboids can be found in many cellular bilayers including the Golgi, the plasma membrane, endosomes, the endoplasmatic reticulum (ER), mitochondria and chloroplasts [77, 78, 113-115]. Due to the fact that rhomboids are present in various organelles and organisms, they are adapted to completely different lipid environments. Despite this, rhomboid proteases have been classically studied either in *E.coli* cells [19] or solubilized in detergent [65, 107].

The latter method is especially useful for bacterial rhomboids such as EcGlpG or BsYqgP (rhomboid YqgP from *Bacillus subtilis*), where solubilization and purification results in relatively highly concentrated rhomboid samples readily usable for assays [65, 97, 107, 116]. Although detergent solubilization is easy and well established for some rhomboid proteases [65], they do not account for the natural lipid environment which is required for the activity of many eukaryotic rhomboids. This is why for these rhomboids cell culture assays are used [77, 117]. The disadvantage of using cell cultures for inhibitor testing is that compounds might be generally toxic to the cells, and may cause differences in cell growth, and rhomboid and substrate expression levels. Both in vitro assays and cell culture assays are relatively laborious which is why in the past, some work has been done on the reconstitution of rhomboids into liposomes [64, 107].

While still artificial, liposomes offer a more natural lipid-based environment compared to detergent micelles, and at the same time a more controlled environment compared to cells. The reported works on the reconstitution of EcGlpG into liposomes used either very simplified liposome compositions of only one to two lipids, or whole *E.coli* membrane extracts [64, 107]. The fact that whole *E.coli* membrane extracts can be used is surprising considering that work presented by Urban and co-workers in 2005 suggested that EcGlpG is inactive in its own membrane [107]. To date the experiments performed in membranes are still few and future research on the influence of the lipid environment on various rhomboids will further illuminate rhomboid mechanism, regulation and function.

**Rhomboid inhibitors and inhibitor screening assays**

A major caveat in the research of rhomboid activity and regulation is the lack of selective inhibitors. Rhomboids are in general not susceptible to broad-spectrum serine protease inhibitors, with the exception of tosyl phenylalanyl chloromethyl ketone (TPCK) and dichloroisocoumarin (DCI) [19]. The resistance of the rhomboids towards classical serine proteases inhibitors has been shown to not be due to an accessibility problem, but may rather be due to the active site architecture.

The catalytic serine approaches the peptide bond from the 'si'-face, unlike other serine proteases, but much like α/β-hydrolyses - β-lactamases, lipases, and bacterial leader peptidases, which are also immune to the common serine protease inhibitors [118, 119]. Both TPCK and DCI are not selective and are therefore neither good lead compounds for drug research nor very effective research tools.

Due to the fact that selective rhomboid inhibitors can provide powerful research tools allowing for a better characterization of biological functions, efforts have been made in the past to identify more inhibitors.

Hitherto, all rhomboid inhibitors belong to four different structural classes: chloromethylketones [19, 72], 4-chloroisocoumarins [19, 71, 97], fluorophosphonates [69, 94, 110], and N-sulfonylated beta-lactams [82]. While the inhibitors identified from these structural classes are not yet selective towards rhomboids, they provide a lead structure that, through modification of different substituents, might be turned into a selective rhomboid inhibitor in the future. Despite this, efforts have continued to detect novel rhomboid inhibitors, especially ones belonging to different structural classes, which will make it more likely to obtain selective inhibitors.

In order to identify such inhibitors, various screening assays have been developed that allow for a more or less rapid search of libraries of small compounds. While the first rhomboid experiments were performed in cells [10, 19], the key to a more direct rhomboid study was the successful solubilization of the active enzyme [65, 74, 107]. All rhomboid inhibitor screening assays developed so far are substrate-based and use either a gel-based detection [65, 74, 107] of the substrate cleavage, or a read-out by Förster resonance energy transfer (FRET) [82] or matrix-assisted laser desorption/ionization (MALDI) mass spectrometry [97]. Since these screening assays are all substrate based, they all share the same limitation: The natural substrate is not known for most rhomboids, and additionally not all rhomboids are able to cleave substrates from other species or artificial substrates.

This severely limits the number of rhomboids that can be studied with the available screening assay. One way to circumvent this caveat is to monitor rhomboid activity without using a substrate at all, but a small mechanism-based molecular reporter.

## 1.2. Activity-based protein profiling

Proteomic techniques allow the identification and quantification of countless proteins from even the smallest amounts of tissues and cells [120]. Yet while the techniques have become ever more powerful, they cannot report on the activity of an enzyme. Standard methods such as western blot or mass spectrometry only report on the overall abundance, yet most often only a fraction of present enzyme is also active. In order to uphold the fine balance between proper enzymatic function and disease, enzymatic function is tightly controlled: Enzymes are often expressed as inactive zymogens and inactivated by inhibitors or degradation processes shortly after activation. Activity-based protein profiling (ABPP) has emerged as a powerful technique that reports on the activity of the enzymes and thus allows for a more accurate estimation of the actually active sub fraction in a protein sample or even within a living cell. The first ABPP experiments were performed in gel, and while many more detection methods can be used with this method today, for example florescence polarization, the gel-based approach remains very popular [121, 122]. The small molecular tools utilized in this method are called activity-based probes (ABPs).

### 1.2.1. Activity-based probes

ABPs are small molecules that covalently bind to active enzyme in a mechanism-based manner, and therefore do not react with inhibitor-inactivated or zymogen forms. ABPs usually consist of three parts: a reactive group, a spacer, and a tag (Figure 5).
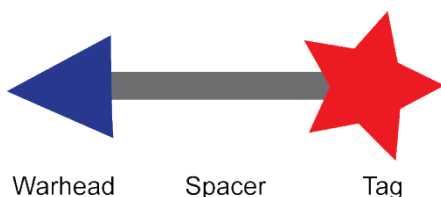


Warhead    Spacer    Tag

**Figure 5 Schematic representation of a general ABP.** An ABP consist of three elements: (1) The warhead or reactive group that covalently binds to the active side in a mechanism-based manner; (2) a spacer which separates warhead and tag and can include selectivity motives, ligation handles or cleavable linkers; (3) and a chemical tag for purification or detection.

The reactive group, sometimes also called 'warhead', can covalently react with the active enzyme. Classical ABPs for hydrolases use an electrophile that acts as a nucleophilic trap for the catalytic residue, which can be a serine or cysteine. Common reactive groups that have been used so far are fluorophosphonates [123], epoxides [124-126], β-lactones and β-lactams [127, 128], as well as many other electrophile containing groups. ABPs directed towards enzymes that cannot form a covalent enzyme-inhibitor complex, such as metallo and aspartic proteases, employ photocrosslinkers for the covalent attachment of the probes [129, 130]. More correctly though, such probes are called 'affinity-based probes'. There are also sulfonate probes that can react with reactive glutamate, aspartate, tyrosine and histidines that do not have to be the catalytic residues, and as such the probes are called "reactivity probes" [131]. In summary it is useful to classify probes, based on the warhead, into activity, affinity, and reactivity based probes.

The spacer is the part of the ABP between the reactive group and the tag. While it can simply act to allow spatial separation between the two entities, it can also confer selectivity: by introduction of a peptide motive into the spacer, the ABP can be directed towards a certain protease or also group of proteases. Through modifications in the spacer region, the degree of selectivity of the ABP can be finely tuned to suit the requirements of the analysis technique used, with selective ABPs being preferred for techniques such as imaging, and less selective ABPs being required for profiling experiments [132]. Furthermore, the spacer region can include a cleavable linker, which allows for specific release of a part of the ABP, a ligation handle which allows functionalization with different tags, or even trifunctional linkers that enable the combination of multiple tags onto the same ABP molecule [125, 126].

The third part of an ABP, the tag, is a functional moiety that can be used for detection or purification. Detection tags can be radiotracers, biotin, fluorophores, mass tags or antibody recognition motives, which can be used for microscopy, fluorescence polarization, microarrays, mass spectrometry, or gel electrophoresis. The tags are chosen according to the employed detection method [122]. The second use for the tag is for purification, which for example allows pulling out active enzyme from a whole-cell lysate. Tags like biotin are advantageous because they can simultaneously be used for both detection and purification. Alternatively in order to combine detection and a purification moiety, clickable ABPs or trifunctional linkers can be used [126, 133].

### 1.2.2. Tandem labeling with ABPs

While simple ABPs are very straightforward to synthesize, the detection and purification tags they contain are often bulky and impair the labeling reaction or cell permeability. Furthermore many enzymes are only active in situ or in vitro, and can only therefore only be probed in the cell [134]. To circumvent this caveat, strategies have been employed which separate the reactive group from the tag: in the so-called tandem ABPP, a smaller ABP version in which the bulky tag is replaced by a ligation handle, is first reacted with the target enzyme in vitro, in situ, or in vivo, and is only latter functionalized with a tag, which can easily be done in vitro. Several bioorthogonal labeling techniques can be used for tandem ABPP, and are selected according to the specific needs individually or in combination [135, 136].

While the Staudinger-Bertozzi ligation[137] and the Diels-Alder ligation have both been successfully used for tandem ABPP with the proteasome and cysteine cathepsins [136, 138, 139], the most often used click chemistry technique is the azide-alkyne cycloaddition. This method, also referred to as Huisgen 1,3-dipolar cycloaddition, uses Cu(I) as a catalyst and thereby greatly increases the reaction rate of the alkyne with the azide. The reactants themselves are very stable and easy to store, furthermore they do not cross-react with biopolymers making them a perfect choice for bioorthogonal reactions. In most experiments, the reactive group is functionalized with an alkyne, while the reporter tag carries the azide moiety, as this decreases the background [134, 140]. The azide-alkyne cycloaddition is widely used, and consequently both alkyne and azide-derivatized biotins and fluorophores are commercially available, making this technique also available for non-chemists. One a side note, there is an alternative, copper-free version of the azide-alkyne cycloaddition available, the strain-promoted reaction that utilized strained alkynes in eight membered rings [141]. While this variety of the azide-alkyne cycloaddition is not as reactive as the copper-catalyzed variant or the Bertozzi-Staudinger ligation, and suffers from a high background labeling, it is an alternative for click reactions performed in cells, as copper is cytotoxic [142]. All these tandem ABPP methods have been used in combination for probing of various enzyme targets by different probes at the same time in a two-step approach.

### 1.2.3. Gel-based activity-based protein profiling

Both one-step and two-step (tandem) ABPP have classically been and are still very often performed in gel [134, 140], despite novel platforms such as live cell imaging, microarrays or fluorescence plate-reader assays. The advantage of gel-based methods is that complex proteomes can easily be resolved on the gel and the target protein, bound to the ABP, can easily be identified over the background proteome. This makes it possible to work in lysates or even whole cells or tissues and circumvent a purification step. This is especially advantageous for profiling purposes or the search for inhibitors which can be performed as a high-throughput screen (HTS) and allows the simultaneous probing of multiple enzymes or inhibitors. For inhibitor screening, the target enzyme, purified or in vivo or in situ, is reacted with a potential inhibitor for a defined amount of time. Afterwards, the active site of the enzyme is probed by the ABP: if the active site is blocked by the inhibitor, the ABP cannot bind and migrates away during electrophoresis; otherwise the ABP can bind to the uninhibited active site and through the ABP's tag the enzyme can be seen as a gel band in a fluorescent gel. This experiment can easily be performed with rhomboids (Figure 6).
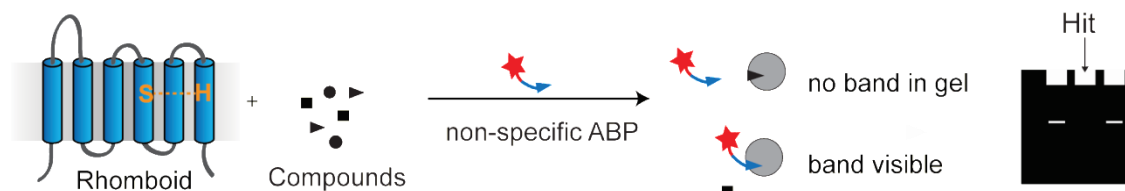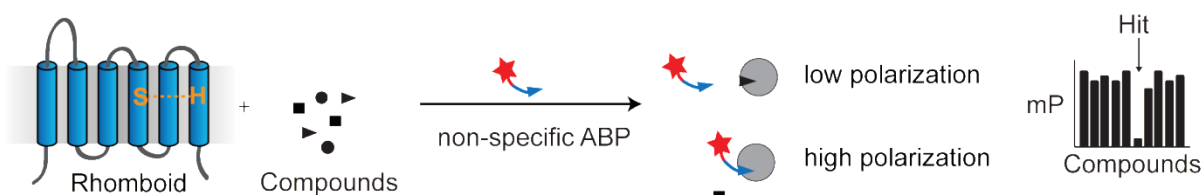


**Figure 6 Gel-based rhomboid inhibitor screening by ABPP.** Purified rhomboid in detergent is first incubated with the compound and then with a nonspecific ABP. If the active site is blocked by an inhibitor, the ABP cannot bind and no gel band is visible in gel. Otherwise if the ABP can bind a gel band is visible. In an inhibitor screening, many samples are analyzed and lanes without the gel band signify a hit compound.

The advantage of the gel-based ABPP is that although it is low-throughput, the experiments is easy to set up for new enzymes and can be performed not only on purified enzymes, but also in lysates, whole cells or tissues. This is why this method is still used very often in ABPP today.

### 1.2.4. Fluorescence polarization activity-based protein profiling

Fluorescence polarization activity-based protein profiling (FluoPol ABPP) was first introduced by Cravatt and co-workers as an HTS for protease inhibitors [143], and has since been used successfully for various purified hydrolases [144-149]. Similarly to the gel-based ABPP, the enzyme is first incubated with a potential inhibitor and then reacted with the ABP. The labeling reaction is then directly monitored in a fluorescence polarization plate reader. The basic principle is that stationary fluorescence molecules, upon excitation with plane-polarized light, emit this light in the same plane. Molecules in solution tumble and rotate though, and thus emit the polarized light in a different plane. Smaller molecules rotate faster than larger ones, depolarizing the light more strongly. Consequently it is possible to distinguish between smaller and larger molecules by the amount of depolarized light, and ultimately between unbound (smaller) and enzyme-bound (larger) ABPs. This way an inhibitor bound enzyme, which cannot be labeled with an ABP will result in a high depolarization and low polarization, while uninhibited enzymes can bind the ABPs, leading to a high polarization (Figure 7).



**Figure 7 Rhomboid inhibitor screening by FluoPol ABPP.** Purified rhomboid in detergent is first incubated with a compound and then a nonspecific ABP is added. The binding of the ABP to the active site of the rhomboid is monitored in a fluorescence polarization plate reader. If the active site is blocked by an inhibitor, the ABP cannot bind and the polarization is low. Otherwise the ABP can bind to the active site, giving rise to a high polarization. In an inhibitor screen, compounds that cause a low polarization are considered potential hits and can be further verified by a secondary gel-based ABPP.

The advantage of the FluoPol ABPP is that it can be easily performed in a HTS format enabling the screening of libraries with thousands of compounds [143]. It requires purified enzymes though, as the read-out cannot differentiate between the enzyme and off-targets. Furthermore the reaction conditions need to be optimized for each studied enzyme accordingly. Once set-up, this assay allows fast assaying of many compounds and requires little experimental work.

## 2. Aim of This Work

Rhomboids are intramembrane proteases that are involved in many important processes in the cell. One major obstacle in their research is the lack of selective inhibitors, universally applicable inhibitor screening assays and ABPs as study tools.

The general aim of this thesis was to develop substrate-free and ABP-based rhomboid inhibitor screening assays. The first objective was to use such an assay for the screening of a small focused compound library. Inhibitors discovered in this screen were to be further analyzed for their binding site, reversibility, apparent $IC_{50}$ and potential use as ABP.

A second objective of the presented work was to investigate the influence of the rhomboid environment on inhibitor screening results, in order to evaluate if inhibitor screens can be performed in detergent micelles or if they should rather be performed in a membrane environment. Furthermore, in order to do this and also enable future research on rhomboids in membranes, a suitable proteoliposome preparation protocol for rhomboids was to be established first.

The final aim was to create ABP-based inhibitor fingerprints for rhomboids from different species, which would enable rapid discovery of inhibitors and ABPs. These inhibitor profiles were to be compared and analyzed for selective and non-selective inhibitors. Inhibitors discovered from these fingerprints were to be further analyzed and tested for their applicability as ABPs.

# 3. Materials and Methods

Unless otherwise specified, solvents and salts were purchased from Applichem, biochemical reagents from Carl Roth.

Thin layer chromatography (TLC) was performed using ALUGRAM sil G/UV254 silica plates (Carl Roth) to verify full conversion of the starting isocoumarin. Spots were detected by both UV light and cerium ammonium molybdate (CAM) staining (solution contains 1 g $Ce(SO_4)_2$, 5 g $(NH_4)_6Mo_7O_{24} \cdot 4H_2O$, 10 mL $H_2SO_4$ and 90 mL $H_2O$). After confirmation by TLC, samples were purified by HPLC. All solvents used were purchased at Applichem at HPLC grade and filtered and degassed before use. The HPLC was performed on a Waters system with a FlexInject injector, two 515 HPLC pumps, aWaters Xbridge C18, 5 µm (4.6 x 150 mm) column (for analytical scale runs), a Waters Xbridge BEH130 Prep C18 5 µm (19 x 150 mm) column (for preparative scale runs), a 2487 Dual Wavelength Absorbance Detector and a Fraction Collector III. For separation, gradients of solvent A (100% ACN + 0.1% TFA) and B (100% $H_2O$ + 0.1% TFA) were used. The samples were detected at 215 nm and 254 nm. For analysis of identity and purity, the purified compound was analyzed by mass spectrometry using an Agilent 1100 Series LC system with an Agilent 6210 electrospray ionization-time of flight (ESI-ToF) mass spectrometer. Separation was done at RT on a Zorbax SB C18 5 µm (0.5 x 150 mm) capillary column. A gradient of solvents A (5% ACN/$H_2O$ + 0.1% FA) and B (95% ACN/$H_2O$ + 0.1% FA) was used for 35 min, starting with solvent A and progressing with an increase of 2.57% ACN/min at a flow rate of 20 µl/min. The measurements were performed in positive ion mode. The data was analyzed using the Masshunter Software B.03.01 (Agilent).

## 3.1. Synthesis of 116 and EK2

**Click reactions to synthesize 116**

Benzylazide (2 eq., 19 µmol) was dissolved in 0.7 ml THF. The isocoumarin SV-105 (1 eq.), 5 µl 100mM TBTA and Cu(I)Br (0.1 eq.) were added and the reactions stirred o/n at 50 °C under a $N_2$ atmosphere. TLC, HPLC and LC-MS were performed as described above.

ESI-MS: m/z 397.1041 (detected) m/z 397.0989 (calculated for $C_{20}H_{17}ClN_4O_3^+$).

**Click reactions to synthesize EK2**

TAMRA-azide (tetramethylrhodamine 5-carboxamido-(6-azidohexanyl)-azide) (1 eq., 2.06 µmol) was dissolved in 0.5 ml THF. The isocoumarin SV-105 (1.5 eq.) and 5 µl TBTA and Cu(I)Br (0.1 eq.) were added and the reactions stirred o/n at 50 °C under a $N_2$ atmosphere. TLC, HPLC and LC-MS were performed as described above.

ESI-MS: m/z 776.2430 (detected) m/z 776.25 (calculated for $C_{41}H_{37}ClN_7O_7^+$).

## 3.2. Plasmid propagation

For plasmid propagation, the plasmid was transformed into competent DH5α cells and grown in a 50 ml o/n culture with the appropriate antibiotic. The cells were pelleted and the plasmid purified using the E.Z.N.A. Plasmid Mini Kit I (VWR) according to the manufacturer's instructions but using 30 µl of ddH$_2$O for elution. Plasmid concentration was determined in an Ultrospec 3100 pro photometer (Amersham Biosciences).

## 3.3. Preparation of competent cells and transformation

**Bacterial strains**

In this study two different bacterial strains were used for plasmid propagation and protein expression (Table 1).

**Table 1 Overview of bacterial strains used for plasmid propagation and rhomboid protease expression.**

| Strain | Resistance | Comment |
| --- | --- | --- |
| DH5α | none | plasmid propagation |
| BL21(DE3)gold pRARE2 | chloramphenicol | protein expression, contains vector encoding rare amino acids |

**Antibiotics**

For selection in LB media and on LB agar plates, antibiotics were used as listed in Table 2.

**Table 2 Concentrations of antibiotic stocks.**

| Antibiotic | Concentration of stock | Final concentration |
| --- | --- | --- |
| ampicillin | 50 mg/ml in $H_2O$ | 50 µg/ml |
| chloramphenicol | 34 mg/ml in EtOH | 34 µg/ml |
| kanamycin | 30 mg/ml in $H_2O$ | 30 µg/ml |

**Preparation of electro competent cells**

400 ml LB medium (Carl Roth; containing appropriate antibiotics, see Table 1 and Table 2) were inoculated with 4 ml of an o/n culture of bacteria, and grown at 37 °C to an $OD_{600} = 0.4$. The cells were cooled on ice for 30 min and then pelleted for 15 min at 4000 g and 4 °C. The cell pellet was resuspended in 100 ml ice cold sterile 10% (w/v) glycerol. The centrifugation and resuspension procedure was repeated twice, using first 50 ml of ice cold sterile 10% (w/v) glycerol for resuspension and finally 20 ml. From this final volume 100 µl aliquots were created in 1.5 ml reaction tubes and snap frozen in liquid nitrogen and stored at -80 °C.

**Transformation of electro competent cells**

Cells were thawed on ice for approximately 10 min. Then 100 ng of plasmid DNA were added and gently mixed with the cells. The DNA-cell suspension was pipetted into an ice cooled electroporation cuvette (1 mm, PEQLAB), which was then put into a MicroPulser electroporator (Bio-Rad) and a voltage pulse of 18 kV/cm applied. After electroporation 500 µl of LB medium were added and the whole suspension transferred to a 1.5 ml reaction tube. The sample was incubated for 1 h at 37 °C shaking and then plated onto LB agar plates (LB medium containing 1.5% (w/v) agar-agar and appropriate antibiotics), and the plates then incubated o/n at 37 °C.

**Preparation of chemically competent cells**

This method is modified after Chung et al. [150]. 50 ml LB medium (containing appropriate antibiotics, see Table 1 and Table 2) were inoculated with 500 µl of an o/n culture of bacteria, and grown at 37 °C to an $OD_{600} = 0.3$. The cells were pelleted for 10 min at 1000 g and 4 °C and resuspended in 5 ml ice cold TSS medium (LB medium containing 10% (w/v) PEG 3350, 5% (v/v) DMSO, 50 mM $MgCl_2$, sterile filtered). The sample was divided into aliquots of 100 µl and transferred to 1.5 ml reaction tubes. The aliquots were snap frozen in liquid nitrogen and stored at -80 °C.

**Transformation of chemically competent cells**

As the preparation of competent cells method above, this transformation protocol is modified after Chung et al. [150]. Cells were thawed on ice. Then 100 ng of plasmid DNA were added and the cells incubated for 30 min on ice. The heat shock was performed for 1 min in a 42 °C warm water bath. The sample was immediately cooled on ice for 2 min. After the addition of 900 µl LB medium without antibiotics the sample was incubated for 1 h at 37 °C shaking. The sample was streaked out onto LB agar plates (LB medium containing 1.5% (w/v) agar-agar and appropriate antibiotics), and the plates then incubated o/n at 37 °C.

## 3.4.   Subcloning of AaROM

The gene coding for the rhomboid from Aquifex aeolicus (AaROM) was initially localized on a pcDNA3.1 vector (donor plasmid), but subcloned into a pET21d+ vector (acceptor plasmid) for expression in *E.coli*. To this end 1 µg each of donor and acceptor plasmids were digested separately for 1 h at 37 °C in 1x Tango buffer with 10 U of the restriction enzyme NheI (Thermo Scientific) according to the manufacturer's instructions. Next, the concentration of Tango buffer was increased to 2x and 10 U of EcoRI (Thermo Scientific) were added. The samples were incubated at 37 °C for 2 h. Next the digested acceptor plasmid was dephosphorylated for 10 min at 37 °C with 0.5 U Fast AP Thermosensitive Alkaline Phosphatase (Thermo Scientific). The enzyme was inactivated for 20 min at 80 °C. The digested donor plasmid was mixed with 1x DNA loading dye (Carl Roth) and then separated in a 1% (w/v) agarose (Carl Roth) gel in 1x TBE buffer (AppliChem) with 0.5 µg/ml ethidium bromide (AppliChem) at 120 V. The separated vector fragments were visualized in the gel under UV light and the DNA band corresponding to the DNA-insert of AaROM was excised from the gel. The DNA insert was extracted from the gel using the NucleoSpin Plasmid Kit (Macherey-Nagel) according to the manufacturer's instructions and the concentration of the purified insert DNA photometrically determined.

For the ligation 100 ng of dephosphorylated pET21d+ vector backbone (acceptor plasmid) and 60 ng of insert AaROM (from donor plasmid) were incubated for 10 min at RT with T4 DNA ligase (Thermo Scientific) according to the manufacturer's instructions. The ligase was inactivated by incubation of the sample at 65 °C for 10 min. 1.5 µl of the ligation reaction were used for transformation into competent DH5α cells.

## 3.5.  Protein expression and purification

**Rhomboids used in this study**

Fourteen rhomboids from 13 different bacterial, archaean and eukaryotic organisms were used in this work. An overview of abbreviations, origins, vector construct and sources is provided below (Table 3).

**Table 3 Overview of rhomboids used in this study.** The topology (6 or 7 TM helices) is indicated in the description, as predicted by Phobius [151].

| Rhomboid | Organism | Description | Kindly provided by |
|---|---|---|---|
| EcGlpG WT | *Escherichia coli* | pET25b+ vector, C-terminal TEV-cleavage site and His$_6$ tag, (6 TM helices) | Matthew Freeman [65] |
| EcGlpG S201A | *Escherichia coli* | pET25b+ vector, C-terminal TEV-cleavage site and His$_6$ tag, (6 TM helices) | Matthew Freeman [65] |
| BsYqgP WT | *Bacillus subtilis* | pET25b+ vector, C-terminal TEV-cleavage site and His$_6$ tag, (7 TM helices) | Matthew Freeman [65] |
| PsAarA WT | *Providencia stuartii* | pET25b+ vector, C-terminal TEV-cleavage site and His$_6$ tag, (7 TM helices) | Matthew Freeman [65] |

| | | | |
|---|---|---|---|
| AaROM | *Aquifex aeolicus* | pET21d+ vector, C-terminal His$_6$ tag, (6 TM helices) | This work |
| MmRHBDL3 | *Mus musculus* | pRSET Vector, C-terminal His$_6$ tag, (7 TM helices) | Marius Lemberg [117] |
| DmRho1 | *Drosophila melanogaster* | pGEX-6P-1 vector, N-terminal GST tag followed by PreScission protease site, (7 TM helices) | Sin Urban [93, 107] |
| VcROM | *Vibrio cholera* | pGEX-6P-1 vector, N-terminal GST tag followed by PreScission protease site, (6 TM helices) | Sin Urban [93, 107] |
| MmRHBDL1 | *Mus musculus* | pGEX-6P-1 vector, N-terminal GST tag followed by PreScission protease site, (7 TM helices) | Sin Urban [93, 107] |
| PhROM | *Pyrococcus horikoshii* | pGEX-6P-1 vector, N-terminal GST tag followed by PreScission protease site, (6 TM helices) | Sin Urban [93, 107] |
| AfROM | *Archaeoglobus fulgidus* | pGEX-6P-1 vector, N-terminal GST tag followed by PreScission protease site, (6 TM helices) | Sin Urban [93, 107] |
| MjROM | *Methanocalcococcus jannaschii* | pGEX-6P-1 vector, N-terminal GST tag followed by PreScission protease site, (6 TM helices) | Sin Urban [93, 107] |

| TmROM | *Thermotoga maritima* | pGEX-6P-1 vector, N-terminal GST tag followed by PreScission protease site, (7 TM helices) | Sin Urban [93, 107] |
|---|---|---|---|
| HiGlpG | *Haemophilus influenzae* | pBAD/Myc-His vector, C-terminal TEV cleavage site and His$_6$ tag, (6 TM helices) | Joanne Lemieux [7] |

**Protein expression**

*EcGlpG.* The EcGlpG pET25b+ plasmid was transformed into BL21 (DE3) gold pRARE2 cells. 1 l LB medium containing chloramphenicol and ampicillin was inoculated with 10 ml o/n culture and grown at 37 °C shaking to an OD$_{600}$ = 0.6. Expression was induced by addition of 1 mM IPTG (Carl Roth) for 3 h. The cells were pelleted for 1 h at 5000 g and 4 °C and the pellet stored at -80 °C.

*HiGlpG.* The HiGlpG pBAD/Myc-His plasmid was transformed into BL21 (DE3) gold pRARE2 cells. 1 l LB medium containing chloramphenicol and ampicillin was inoculated with 10 ml o/n culture and grown at 37 °C shaking to an OD$_{600}$ = 0.7. The expression culture was shifted to 18 °C shaking and expression induced by addition of 0.002% (w/v) arabinose (Carl Roth) o/n. The cells were pelleted for 1 h at 5000 g and 4 °C and the pellet stored at -80 °C.

*Other rhomboids.* For all other rhomboids the corresponding plasmids were transformed into BL21 cells. 1 l LB medium containing chloramphenicol and ampicillin was inoculated with 10 ml o/n culture and grown at 37 °C shaking to an OD$_{600}$ = 0.6. The expression culture was shifted to 16 °C shaking and expression induced by addition of 1 mM IPTG (Carl Roth) o/n. The cells were pelleted for 1 h at 5000 g and 4 °C and the pellet stored at -80 °C.

**Protein purification for FluoPol**

Cells were resuspended in 50 ml of 20 mM HEPES (pH 7.4) containing 100 mM NaCl, 10% (v/v) glycerol and one complete EDTA-free protease inhibitor tablet (Roche). The sample was sonicated using a Branson digital W-250 D sonifier (G.HEINEMANN) using 50% amplitude with 2 s pulse and 5 s pause for a total time of 5 min. The sonicated cells were pelleted in a CE-80K ultracentrifuge (Beckman Coulter) for 1 h at 50,000 g and 4 °C. The pellet was resuspended in 10 ml of 20 mM HEPES (pH 7.4) containing 300 mM NaCl, 10% (v/v) glycerol and 10 mM imidazole and solubilized o/n at 4 °C by addition of 1.5% (w/v) *n*-dodecyl β-D-maltoside (DDM). Unsolubilized cell-debris was removed by ultracentrifugation for 30 min at 50,000 g and 4 °C. The supernatant was incubated with 0.5 ml of equilibrated Ni-NTA agarose beads (Qiagen) for 4 h shaking at 4 °C. The supernatant with the beads was then filled into a 3 ml polypropylene cartridge with a frit (ERC GmbH). The next steps were all performed on ice with gravity-flow. The beads were washed three times with 10 ml of a buffer consisting of 20 mM HEPES (pH 7.4), 300 mM NaCl, 10% (v/v) glycerol, 0.0125% (w/v) DDM and an increasing concentration of imidazole for each washing step (25 mM, 50 mM, 100 mM). Elution was done with 3 ml of 20 mM HEPES (pH 7.4) containing 300 mM NaCl, 10% (v/v) glycerol, 0.0125% (w/v) DDM and 750 mM imidazole. The eluted sample was dialyzed o/n at 4 °C in a Spectra/Por 7 MWCO 1000 membrane (Carl Roth) against 20 mM HEPES (pH 7.4) containing 300 mM NaCl, 10% (v/v) glycerol, 0.0125% (w/v) DDM.

**Protein purification for liposomes**

For the liposome experiments EcGlpG was purified in three different buffers containing either *n*-dodecyl β-D-maltoside (DDM), 3-[(3-cholamidopropyl) dimethylammonio]-1-propanesulfonate (CHAPS), or octyl β-D-glucopyranoside (OG; from Sigma) as detergents. An overview is given below (Table 4). For all steps of purification, the buffers contained the required detergent for each sample according to this overview.

**Table 4 Overview of detergent concentrations used in the liposome experiments.**

| Rhomboid | Detergent | Concentration | Equals |
|---|---|---|---|
| EcGlpG WT | DDM[1] | 0.0125% (0.2 mM) | 1x CMC[4] |
| EcGlpG WT | CHAPS[2] | 40 mM | 4x CMC[4] |
| EcGlpG WT | OG[3] | 100 mM | 4x CMC[4] |
| EcGlpG S201A | OG[3] | 100 mM | 4x CMC[4] |

[1] = $n$-dodecyl β-D-maltoside
[2] = 3-[(3-cholamidopropyl) dimethylammonio]-1-propanesulfonate
[3] = octyl β-D-glucopyranoside
[4] = critical micellular concentration

Cells were resuspended in 50 ml of 20 mM HEPES (pH 7.4) containing 100 mM NaCl, 50 mM MgCl$_2$, 10% (v/v) glycerol and half a complete EDTA-free protease inhibitor tablet (Roche). The sample was sonicated using a Branson digital W-250 D sonifier (G.HEINEMANN) using 50% amplitude with 2 s pulse and 5 s pause for a total time of 5 min. The sonicated cells were pelleted in a CE-80K ultracentrifuge (Beckman Coulter) for 1 h at 50,000 g and 4 °C. The pellet was resuspended in 10 ml of 20 mM HEPES (pH 7.3) containing 200 mM NaCl, 10% (v/v) glycerol and 5 mM imidazole and solubilized o/n at 4 °C by addition of 1.5 % (w/v) DDM. Unsolubilized cell-debris was removed by ultracentrifugation at 50,000 g and 4 °C for 30 min. The supernatant was incubated with 0.5 ml of equilibrated Ni-NTA agarose beads (Qiagen) for 1.5 h shaking at 4 °C. The supernatant with the beads was then filled into a 3 ml polypropylene cartridge with a frit (ERC GmbH). The next steps were all performed on ice with gravity-flow. The beads were washed with 20 ml of 50 mM HEPES (pH 7.3), 500 mM NaCl, 10% (v/v) glycerol, 20 mM imidazole and the required detergent. Next the beads were washed with 20 ml of 50 mM HEPES (pH 7.3), 200 mM NaCl, 10% (v/v) glycerol, 50 mM imidazole and the required detergent. The proteins were eluted from the beads with three times 250 µl of the same buffer as before but containing 250 mM imidazole, and then three times with 250 µl buffer containing 500 mM imidazole. The eluted sample was dialyzed o/n at 4 °C in a Spectra/Por 7 MWCO 1000 membrane (Carl Roth) against 20 mM HEPES (pH 7.4) containing 300 mM NaCl, 10% (v/v) glycerol, and required detergent.

**Protein purification for ABPP**

*Purification of EcGlpG, PsAarA, BsYqgP, HiGlpG, MmRHBDL3, and AaROM.* Cells were resuspended in 20 ml of 20 mM HEPES (pH 7.4) containing 100 mM NaCl, 5 mM MgCl$_2$, 10% (v/v) glycerol with one complete EDTA-free protease inhibitor tablet (Roche). The cells were lysed in an Amino French press (G.HEINEMANN) at 17 MPa. The lysate was centrifuged for 20 min at 4500 g and 4 °C to remove cell debris. The supernatant was ultra-centrifuged for 1 h at 50,000 g and 4 °C. The pellet was resuspended in 4 ml of 50 mM HEPES (pH 7.4), 200 mM NaCl, 1 mM MgCl$_2$, 1 mM CaCl$_2$, 10% (v/v) glycerol and 5 mM imidazole and the membrane proteins solubilized by addition of 1% (w/v) DDM o/n at 4 °C. Next the sample was centrifuged for 30 min at 50,000 g and 4 °C. The supernatant was incubated with 0.5 ml of equilibrated Ni-NTA agarose beads (Qiagen) for 1.5 h shaking at 4 °C. The supernatant with the beads was then filled into a 3 ml polypropylene cartridge with a frit (ERC GmbH). The next steps were all performed on ice with gravity-flow. The beads were washed with 10 ml of 50 mM HEPES (pH 7.4), 500 mM NaCl, 1 mM MgCl$_2$, 1 mM CaCl$_2$, 10% (v/v) glycerol, 30 mM imidazole and 0.1% (w/v) DDM and then with 10 ml of 50 mM HEPES (pH 7.4), 200 mM NaCl, 1 mM MgCl$_2$, 1 mM CaCl$_2$, 10% (v/v) glycerol, 30 mM imidazole and 0.1% (w/v) DDM. Elution was done three times with 500 µl of 50 mM HEPES (pH 7.4), 200 mM NaCl, 1 mM MgCl$_2$, 1 mM CaCl$_2$, 10% (v/v) glycerol, 400 mM imidazole and 0.1% (w/v) DDM. The eluted samples were dialyzed o/n at 4 °C against 20 mM HEPES (pH 7.4) containing 100 mM NaCl, 5 mM MgCl$_2$, 10% (v/v) glycerol and 0.1% (w/v) DDM.

*Purification of TmROM, PhROM, MjROM, VcROM, AfROM, DmRho1, and MmRHBDL1.* Cells were resuspended in 20 ml of 20 mM HEPES (pH 7.4) containing 100 mM NaCl, 10% (v/v) glycerol with one complete EDTA-free protease inhibitor tablet (Roche). The cells were lysed in an Amino French press (G.HEINEMANN) at 17 MPa. The lysate was centrifuged for 20 min at 4500 g and 4 °C to remove cell debris. The supernatant was ultracentrifuged for 1 h at 50,000 g and 4 °C. The pellet was resuspended in 4 ml of 50 mM HEPES (pH 7.4), 200 mM NaCl, 1 mM MgCl$_2$, 1 mM CaCl$_2$, 10% (v/v) glycerol and 5 mM imidazole and the membrane proteins solubilized by addition of 1% (w/v) DDM o/n at 4 °C. The sample was centrifuged for 30 min at 50,000 g and 4 °C.

1 ml equilibrated sepharose GST beads (Thermo Fisher Scientific) were added to the supernatant. The sample was incubated for 2 h shaking at 4 °C. Next the GST beads were washed twice with 10 ml of 50 mM HEPES (pH 7.4), 200 mM NaCl, 1 mM MgCl$_2$, 1 mM CaCl$_2$, 10% (v/v) glycerol, 5 mM imidazole and 0.1% (w/v) DDM. The last washing step was performed with 10 ml cleavage buffer (50 mM HEPES (pH 7.0), 150 mM NaCl, 1 mM DTT, 1 mM EDTA and 0.1% (w/v) DDM). 960 µl of cleavage buffer and 40 µl PreScission protease (GE Healthcare) were added to the beads and the whole sample incubated o/n at 4 °C shaking. The sample was centrifuged for 5 min at 1000 g and 4 °C and the supernatant then applied to 0.5 ml of equilibrated sepharose GST beads. After an incubation of 2 h at 4 °C, the sample was centrifuged for 10 min at 1000 g and 4 °C. The supernatant was dialyzed o/n at 4 °C against 20 mM HEPES (pH 7.4), 100 mM NaCl, 10% (v/v) glycerol and 0.1% (w/v) DDM.

**Determination of protein concentration**

Protein concentration was determined by DC protein assay II (Bio-Rad) according to the manufacturer's instructions.

## 3.6. Gel-based visualization of rhomboids

**SDS-PAGE**

SDS-polyacrylamide gel electrophoresis (PAGE) was performed either with a PerfectBlue dual gel system Twin S (Peqlab) or a triple-wide gel system (VWR) according to the number of samples to be analyzed. For preparation of two triple-wide or 5 small 15% Tris-Glycine gels, the same protocol was used: First, for creating the 15% separating gel, 12.5 ml ddH$_2$O, 12.5 ml 1.5 M Tris-HCl (pH 8.8), 25 ml 30% acrylamide (acrylamide:bisacrylamide 37.5:1), 250 µl 10% (w/v) APS, and 25 µl TEMED were mixed together, poured into the bottom of the pouring equipment and covered with 2-propanol. Once polymerization was completed, the 2-propanol was removed.

Next for the stacking gel, 8.75 ml ddH$_2$O, 3.75 ml 0.5 M Tris-HCl (pH 6.8), 2.5 ml 30% acrylamide (acrylamide:bisacrylamide 37.5:1), 100 μl 10% (w/v) APS, and 10 μl TEMED were mixed, poured on top of the separating gel, and a comb inserted. After polymerization, poured gels were wrapped in wet tissues and aluminum foil and stored at 4 °C for up to two weeks.

Samples were mixed with 4x sample buffer (500 mM Tris-HCL (pH 6.8), 40% (v/v) glycerol, 12% (w/v) SDS, 20% (v/v) 2-mercaptoethanol, 0.04% (v/v) bromphenol blue). Gels were run at 120 V in SDS-PAGE running buffer (620 mM TRIS-HCl (pH 8.3), 4.8 M glycine, 0.5% (w/v) SDS) until the bromphenol blue running front reached the bottom of the gel. As a reference, the BenchMark$^{TM}$ Fluorescent Protein Standard (Invitrogen) and the SeeBlue® Plus2 Pre-Stained Standard (Invitrogen) were used.

**Fluorescence scanning**

For all experiments, in which fluorescence samples were analyzed in an SDS-polyacrylamide gel, the gel bands were visualized by a Typhoon Trio+ scanner (GE Healthcare) using 532 nm excitation wavelength and 580 nm emission wavelength to detect both samples and marker.

**Coomassie staining of SDS-PAGE gels**

Gels were stained o/n shaking at RT using Biosafe Coomassie (Bio-Rad) according to the manufacturer's instructions. For destaining, gels were repeatedly washed for 15 min in 25% (v/v) methanol.

**Ammoniacal silver staining of SDS-PAGE gels**

For visualization of low protein amounts in the gels, the much more sensitive but also elaborate silver staining method was used [152]. All steps were performed at RT. After SDS-PAGE, gels were taken out of the glass plates and incubated for 45 min in a fixative solution containing 50% ethanol and 10% acetic acid, followed by an overnight incubation in a freshly prepared 10% glutaraldehyde solution.

The gels were then washed extensively for up to 6 h with several changes of $H_2O$ to completely remove residual glutaraldehyde. The gels were stained for 5 min in 150 ml freshly prepared silver stain solution (1.17% $NH_4OH$, 19 mM $NaOH$ and 15.2 mM $AgNO_3$) and afterwards washed twice for 3 min in $H_2O$. For band development, gels were incubated shaking in 0.0185% formaldehyde and 0.238 mM citric acid until bands appeared. The reaction was stopped by incubating the gels for 1 h in $H_2O$.

**Western-Blot**

Proteins separated by SDS-PAGE were transferred onto a nitrocellulose membrane (Carl Roth) with a semi-dry blotter (Scie-Plas) and Roti-Blot 2 transfer buffer (Carl Roth) at 1.5 mA/cm$^2$ of gel for 1.5 h. Next the membrane was blocked in 3% (w/v) milk powder in PBST (101 mM $Na_2HPO_4$, 17.6 mM $KH_2PO_4$, 1.37 M $NaCl$, 27 mM $KCl$, 0.1% (v/v) Tween) for 1 h and then incubated in 20 ml of 3% (w/v) milk powder in PBST with 2 µl of anti-His$_6$ peroxidase (Roche). The membrane was washed three times for 15 min at RT in PBST and then luminescence was detected using the ECL plus western blot detection system (GE Healthcare) either on Kodak X-Omat LS films (VWR) with varying exposure times from 5 s to 5 min, or on the Typhoon Trio+ scanner (GE Healthcare).

## 3.7. Activity-based labeling of rhomboids

**Competitive activity-based protein profiling for FluoPol assay confirmation**

For the activity-based labeling of rhomboids performed for the FluoPol assay confirmation, 45 nM of rhomboid in 20 µl of 50 mM HEPES (pH 7.4) containing 10% (v/v) glycerol and 0.0125% (w/v) DDM were incubated for 30 min at 37 °C shaking with either 100 µM compound or an equal volume of DMSO as vehicle control. Then either EK2 or FP-R (ActivX TAMRA-FP Serine Hydrolase Probe, Thermo Fisher Scientific) were added to a final concentration of 1 µM and incubated for either 30 min or 2 h at 37 °C shaking in the dark. The reaction was stopped by addition of 4x SDS sample buffer. 10 µl of the reaction were applied to a 15% SDS-polyacrylamide gel.

**Competitive activity-based protein profiling in micelles**

For the competitive activity-based protein profiling experiment in micelles, 200 ng of rhomboid in 20 µl of 50 mM HEPES (pH 7.4) containing 10% (v/v) glycerol and 0.0125% (w/v) DDM were incubated for 30 min at 37 °C shaking with either 100 µM compound or an equal volume of DMSO as vehicle control. Then FP-R was added to a final concentration of 1 µM and incubated for 2 h at 37 °C shaking in the dark. The reaction was stopped by addition of 4x SDS sample buffer. 10 µl of the reaction were applied to a 15% SDS-polyacrylamide gel.

**Competitive activity-based protein profiling in micelles for auto-cleavage experiments**

200 ng of rhomboid in 20 µl of 50 mM HEPES (pH 7.4) containing 10% (v/v) glycerol and 0.0125% (w/v) DDM were incubated for 30 min up to 24 h at 37 °C shaking with either 100 µM compound, an equal volume of DMSO as vehicle control, or 1/25 of a 25x stock solution containing one complete EDTA-free protease inhibitor tablet (Roche) in 2 ml H$_2$O. For silver staining experiments, the reaction was immediately stopped by addition of 4x SDS sample buffer, and the samples frozen at -20 °C. For fluorescence scanning, samples were first treated with 1 µM FP-R for 2 h at 37 °C shaking in the dark. The reaction was stopped by addition of 4x SDS sample buffer, and the samples frozen at -20 °C. 10 µl of each sample was applied to a 15% SDS-polyacrylamide gel.

**Competitive activity-based protein profiling in liposomes**

For the competitive activity-based protein profiling experiment in liposomes, 20 µl of large unilamellar vesicles (LUVs) were incubated for 30 min at 37 °C shaking with either 100 µM compound or an equal volume of DMSO as vehicle control. Then FP-R was added to a final concentration of 1 µM and incubated for 2 h at 37 °C shaking in the dark. The reaction was stopped by addition of 4x SDS sample buffer. 10 µl of the reaction were applied to a 15% SDS-polyacrylamide gel.

**Competitive activity-based protein profiling in membranes**

For the competitive activity-based protein profiling experiment in membranes, unsolubilized membranes containing overexpressed EcGlpG from 500 ml expression culture were harvested by French press and ultracentrifuged as described above. The membrane pellet after ultracentrifugation was not solubilized with detergent, but resuspended in 2 ml 1x PBS (101 mM $Na_2HPO_4$, 17.6 mM $KH_2PO_4$, 1.37 M NaCl, 27 mM KCl; pH 7.4), and diluted 1:10 with 1x PBS. 20 µl of this sample was incubated for 30 min at 37 °C shaking with either 100 µM compound or an equal volume of DMSO as vehicle control. Then FP-R was added to a final concentration of 1 µM and incubated for 2 h at 37 °C shaking in the dark. The reaction was stopped by addition of 4x SDS sample buffer. 10 µl of the reaction were applied to a 15% SDS-polyacrylamide gel.

## 3.8.  Fluorescence polarization assay (FluoPol ABPP)

500 nM rhomboid in 99 µl of 50 mM HEPES (pH 7.3) containing 0.01% (w/v) Pluronic F-127 (Invitrogen) and 0.0125% (v/v) Triton X-100 were incubated with 100 µM of either compound or an equal amount of DMSO for 30 min at 37 °C shaking in the dark in a black 96-well plate (NeoLab). Then 1 µl of FP-R was added to a final concentration of 75 nM and the measurement immediately started. The plates were measured at 37 °C in a POLARstar Omega fluorescence polarimeter (BMG Labtech) in continuous intervals for up to 7 h.

**Data evaluation and Z-determination for FluoPol ABPP**

For each sample the starting value was subtracted from the polarization value at 4 h to achieve a baseline correction. To obtain an assay window, the value for the EcGlpG S201A mutant was subtracted from all samples and the value of the EcGlpG WT was defined as 100% value. All other data thus represents percentages relative to 100% of WT activity.

To evaluate and validate the suitability of the rhomboid FluoPol ABPP for high-throughput applications, the Z'-factor was calculated based on the data of 10 positive controls (EcGlpG WT) and 10 negative controls (EcGlpG S201A), using the formula below [153].

$$Z' = 1 - \frac{3 \times SD_{pos} + 3 \times SD_{neg}}{|mean_{pos} - mean_{neg}|}$$

**Formula to calculate the Z'-factor, an indication for the robustness and reproducibility of an assay** [153]**.** $SD_{pos}$ = standard deviation of the positive controls, $SD_{neg}$ = standard deviation of the negative controls, $mean_{pos}$ = mean of the positive controls, $mean_{neg}$ = mean of the negative controls.

## 3.9.   Gel-based substrate cleavage assay

For assaying the inhibition of substrate cleavage by the EcGlpG rhomboid, a fluorescence substrate based on the TatA protein from *Providencia stuartii* was used. The substrate was constructed to contain a LPRTG-motif for sortase mediated protein labeling [154] on the C-terminus followed by a His$_6$ tag for purification. Expression and purification was done as described above. For the sortase-mediated labeling reaction, 33 µM of the unlabeled substrate, 50 µM sortase A from *S.aureus* [154] and 500 µM of the label NH$_2$-Ala-Ala-Ahx-Lys(TAMRA) [154] were added together in 50 mM Tris (pH 7.5) containing 150 mM NaCl, 10 mM CaCl$_2$ and 0.05% (w/v) DDM. The reaction was allowed to take place o/n at 37 °C in the dark. During the reaction the glycine and the His$_6$ tag are exchanged for the TAMRA-label, so that labeled substrate did no longer carry a His$_6$ tag. Thus the sortase and unlabeled substrate were removed by incubation of the labeling reaction with Ni-NTA agarose beads. In order to remove excess label, the supernatant was applied to a ZEBA-spin column (VWR; MW-cut-off 7 kDa). 40 µl of a 500 nM rhomboid solution in 50 mM HEPES (pH 7.4) containing 10% (v/v) glycerol and 0.0125% (w/v) DDM were incubated for 30 min at 37 °C shaking with 100 µM of compound or an equal amount of DMSO. Then the fluorescently labeled substrate described above was added to a final concentration of 83 nM, and the cleavage reaction was allowed to take place o/n at 37 °C shaking in the dark. The reaction was stopped by the addition of 4x SDS-sample buffer and 10 µl of the reaction were applied to a 15% SDS-polyacrylamide gel.

## 3.10. Direct labeling of rhomboids by Cu(I)-mediated click reaction

Compounds carrying an alkyne group were subjected to the two-step azide-alkyne cycloaddition in order to attach a 5-(and-6)-carboxytetramethylrhodamine succinimidyl ester fluorophore to them. To this end, 36 nM of rhomboid in 50 µl phosphate buffer (pH 7.4) containing 0.0125% (w/v) DDM were incubated with 100 µM of compound carrying an alkyne group or an equal amount of DMSO as vehicle control for 30 min at 37 °C. Next 0.5 µl each of 100 mM TCEP (in $H_2O$), 100 mM $CuSO_4$ (in $H_2O$), 1.7 mM TBTA (in DMSO) and 5 mM TAMRA-azide (in DMSO) were added and the reaction incubated for 1 h at RT in the dark. The reaction was stopped by the addition of 4x SDS-sample buffer and 10 µl analyzed on a 15% SDS-polyacrylamide gel.

## 3.11. Reversibility check

For determining the reversibility of selected compounds, 500 nM rhomboid in 100 µl of 50 mM HEPES (pH 7.3) containing 10% (v/v) glycerol and 0.0125% (w/v) DDM were incubated for 30 min at 37 °C shaking with 100 µM compound or an equal volume of DMSO. The sample was then applied to an equilibrated ZEBA-spin column (VWR; MWCO 7 kDa) to remove unbound compound. Next the flow-through was incubated for 30 min at 37 °C shaking in the dark with 1 µM EK2 or FP-R.

## 3.12. Apparent IC$_{50}$ determination

**Apparent IC$_{50}$ determination by Rhomboid FluoPol**

To characterize the potency of the inhibitors, the apparent half maximal inhibitory concentration (IC$_{50}$) was determined. To this end 500 nM rhomboid in 99 µl of 50 mM HEPES (pH 7.4) containing 0.01% (w/v) Pluronic (Invitrogen) and 0.0125% (v/v) Triton X-100 were incubated for 30 min at 37 °C shaking in a black 96-well plate with a range of concentrations of the compounds or an equal amount of DMSO.

Then 75 nM FP-R was added and the measurement immediately started. The plates were measured at 37 °C in a Polarstar Omega fluorescence polarimeter (BMG Labtech) for up to 7 h in continuous intervals. The logarithm of the compounds in nM was plotted against the % remaining active enzyme (normalized to 100% WT activity) in the software Prism (GraphPad) and the apparent $IC_{50}$ value calculated by the same software.

**Apparent $IC_{50}$ determination by competitive ABPP in polyacrylamide gel**
200 ng of rhomboid in 20 µl of 50 mM HEPES (pH 7.4) containing 10% (v/v) glycerol and 0.0125% (w/v) DDM, 20 µl LUVs or 20 µl membrane in PBS were incubated for 30 min at 37 °C shaking with either a range of concentrations of the compounds or an equal volume of DMSO as vehicle control. Then FP-R was added to a final concentration of 1 µM and incubated for 2 h at 37 °C shaking in the dark. The reaction was stopped by addition of 4x SDS sample buffer. 10 µl of the reaction were separated in a 15% SDS-polyacrylamide gel and detected on a Trio+ fluorescence scanner (GE Healthcare). Band intensities were densitometrically determined using ImageJ (http://imagej.nih.gov/ij/). The logarithm of the compounds in nM was plotted against the % remaining active enzyme (normalized to 100% WT activity) in the software Prism (GraphPad) and the apparent $IC_{50}$ value calculated by the same software.

## 3.13. Generation of liposomes

**Generation of LUVs**
Large unilamellar vesicles (LUVs) containing reconstituted rhomboid were created using the mixed-micelle approach [155-157]. All lipids were obtained dissolved in chloroform from Avanti Polar Lipids. A total of 2 mg of lipids consisting of 50% (w/v) 1-palmitoyl-2-oleoyl-sn-glycero-3-phosphocholine (POPC), 25% (w/v) L-α-phosphatidylinositol from soy (Soy-PI), 24% (w/v) 1,2-dioleoyl-sn-glycero-3-phosphoethanolamine (DOPE) and 1% (w/v) 1,2-dioleoyl-sn-glycero-3-phosphoethanolamine-N-(5-dimethylamino-1-aphthalenesulfonyl)-(ammonium salt) (Dansyl-PE) were pipetted into a 2 ml reaction tube and mixed thoroughly.

The mixture was dried to a lipid film under a faint $N_2$-stream and then further dried for 1 h at RT in a SC110 vacuum centrifuge (Savant). 1 ml liposome buffer (10 mM HEPES (pH 7.4) containing 250 mM NaCl) containing either 0.6 mM DDM, 30 mM CHAPS or 75 mM OG (this equals ~ 3x critical micelle concentration (CMC)) and a total of 0.02 mg rhomboid were added to the lipid film and vortexed for 1 min. This resulted in a peptide to lipid (P/L) ratio of 1:100. The mixture was incubated in a thermomixer (VWR) for 1 h at 37 °C and 900 rpm in the dark and then dialyzed with three buffer changes o/n at 4 °C in a Spectra/Por 7 MWCO 1000 membrane (Carl Roth) against lipsome buffer without detergent. Next the sample was mixed with 1.5 ml of 80% (w/v) nycodenz (Axis-Shield PoC) and put into a clear 4 ml ultracentrifugation tube (Beckman Coulter). 750 µl of 30% (w/v) nycodenz were added on top of the liposomes/nycodenz sample and finally 250 ml of liposome buffer on top of the gradient. Ultracentrifugation took place for 16 h at 4 °C and 50,000 g in a CE-80K ultracentrifuge (Beckman Coulter). The liposomes were harvested from the top layer of the gradient under UV light which excited the dabcyl and made harvest easier. The liposomes were stored at 4 °C for up to 3 days.

**Generation of GUVs**

To generate giant unilamellar vesicles (GUVs) from LUVs the dehydration-rehydration method was used [157, 158]. 100 µl LUVs were applied onto a clean microscopy glass slide and the glass slide then dried in a dessicator with a running vacuum pump at approximately 160 mbar at RT in the dark for 24 h. Rehydration took place by addition of 250 µl liposome buffer to the dried lipid film on the glass slide. The sample was carefully removed from the glass slide and transferred to a 1.5 ml reaction tube.

**Labeling of LUVs and GUVs**

After addition of 100 µM compound or an equal amount of DMSO the liposome sample was incubated for 30 min at 37 °C gently shaking in the dark. 1 µM EK2 was added to the liposomes and the sample then incubated for 2 h at 37 °C gently shaking in the dark. Finally the liposome sample was dialyzed o/n at 4 °C in a Spectra/Por 7 MWCO 1000 membrane (Carl Roth) against liposome buffer without detergent.

## 3.14. Fluorescence microscopy

LUVs and GUVs were analyzed by fluorescence microscopy using a BX51 fluorescence microscope (Olympus) with a UMNG2 filter set (excitation wavelength 530-550 nm; emission wavelength 590 nm; dichromatic filter 570 nm) and a UMNU2 filter set (excitation wavelength 360-370 nm; emission wavelength 420 nm; dichromatic filter 400 nm) at 100x magnification. Pictures were taken using a CCD camera (Olympus) and analyzed using the software cell$^F$ (Olympus) and saved as jpg files. The background noise and jpeg artifacts were removed using Photoshop (Adobe) and the background set to black using the "levels" function to improve overall visibility in the pictures. For the overlay figures, the two corresponding pictures of the dansyl and TAMRA channels were colored separately in green and red respectively using Photoshop's layer channel function. An overlay was then created in which the top picture, the green dansyl channel, was set to 50% opacity.

## 3.15. Dynamic light scattering

The size of the LUVs was determined by dynamic light scattering using a NanoSight NS300 (NanoSight Ltd). Samples were diluted 1:1000 with $ddH_2O$ and injected into the NANOSIGHT and measured three times over 45 s at RT. After measurement, the samples were evaluated by NTA Analytical Software (NanoSight Ltd) for calculation of the average size of the liposomes.

## 3.16.  Edman degradation

Protein samples to be analyzed by Edman degradation were first separated by SDS-PAGE and transferred onto a nitrocellulose membrane (see 3.6). The sample was reacted with phenylisothiocyanate and the stepwise fragmented N-terminal amino acids analyzed using the Procise Protein Sequencing System (Applied Biosystems, 494 cLC Protein Sequencer). All experiments were kindly performed by Kvido Strisovsky and co-workers at the Institute of Organic Chemistry and Biochemistry AS CR in Prague, Czech Republic.

## 3.17.  TEM

For analysis of the LUVs and GUVs by transmission electron microscopy (TEM), a JEOL JEM-1011 device at 80 kV beam acceleration voltage was used. Liposome samples were negatively stained with 2% phosphotungstic acid on carbon-coated EM grids. All experiments were kindly performed by Kvido Strisovsky and co-workers at the Institute of Organic Chemistry and Biochemistry AS CR in Prague, Czech Republic.

## 3.18.  Docking

The ring-opened compound **48** was geometry optimized by 500 steps of steepest descent, using the MMFF94 force field in the program Avogadro 1.0.1 in order to optimize bond length [159]. It was then built onto the S201 side chain of GlpG (PDB structure 3ZMI) and defined as a side chain of S201. Docking of the inhibitor was performed as a flexible side chain using AutoDock Vina [160]. Structures were visualized and overlaid with the L29 inhibitor (from PDB structure 3ZMI) using VMD 1.9 [161]. The validity of the molecular docking approach was confirmed by docking the original L29 inhibitor using the same method, resulting in a good overlay and an RMSD of 1.005 with the crystal data.

## 3.19. Heat map and clustering

The SDS-polyacrylamide gels were run and detected by fluorescence scanning as described above. The gel band intensities were quantified densitometrically using ImageJ, and the data for every rhomboid was normalized to its DMSO control, which was set as 100% activity. Inhibition percentage was defined as 100 minus the percentage of residual activity, and negative values were set to zero. Hierarchical clustering (complete linkage) of the activity data was performed using Cluster 3.0 [162] with distance measures based on Pearson correlation (uncentered) for inhibitors and rhomboids, and visualized using TreeView 1.60.

For phylogenetic clustering, a multiple sequence alignment of the amino acid sequences of the rhomboids was performed by Clustal Omega [163], and the alignment manually reviewed and further analyzed in MEGA6 [164] as described by the caption function: The minimum evolution method [165] was used for evolutionary analysis, and tested using the bootstrap test (1000 replicates) [166]. The analysis involved 13 amino acid sequences. All positions containing gaps and missing data were deleted. There were a total of 148 positions in the final dataset. The evolutionary distances were computed using the JTT matrix-based method [167] and are in the units of the number of amino acid substitutions per site. The ME tree was searched using the Close-Neighbor-Interchange (CNI) algorithm [168] at a search level of 1. The Neighbor-joining algorithm [169] was used to generate the initial tree. The optimal tree with the sum of branch length = 9.61613319 is shown in Figure 29. The percentage of replicate trees in which the associated taxa clustered together in the bootstrap test is shown next to the branches [166]. The tree was drawn to scale, with branch lengths in the same units as those of the evolutionary distances used to infer the phylogenetic tree.

Sequence identity was determined by aligning the sequences of MmRHBDL1 and 3 with the program "needle" using the matrix EBLOSUM62, a gap penalty of 10 and an extend penalty of 0.5. The identity reported was 208/404 including 31 gaps and the score 1137.0.

## 3.20. FRET peptide cleavage assay

The original Förster resonance energy transfer (FRET) peptide, containing a QSY21 dark quencher and a Chromis-645 fluorophore, was derived from the rhomboid substrate Gurken and designed by Freeman and co-workers [82]. For this work, the peptide was synthesized by PSL Peptide Specialty Laboratories GmbH with different fluorophores (dabcyl and edans) and a PEG-9 instead of a PEG-4 linker (Figure 8).



Dabcyl    Edans

Ac-4x(PEG-9)-QRKVRMAHIVFSFPE-amide
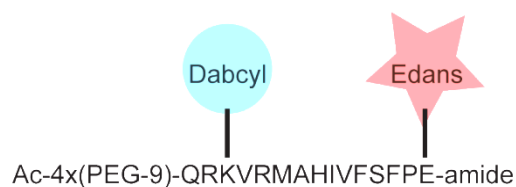
**Figure 8 Design of the Gurken-based FRET peptide.** The peptide sequence is based on the rhomboid substrate Gurken and carries the fluorophore edans and the quencher dabcyl. The acetylated N-terminus contains four PEG linkers for better solubility of the peptide. The C-terminus is amidated.

1 µM FRET-peptide was added to 1.5 µM purified rhomboid protease in 50 mM HEPES (pH 7.3) containing 0.01% (w/v) Pluronic F-127 and 0.0125% (v/v) Triton X-100, and the fluorescence measured at 340 nm excitation and 485 nm emission wavelength in a fluorescence plate reader (POLARstar, BMG) at 37 °C over the course of 8 h.

# 4. Results

Up to the start of the work presented here, known rhomboid inhibitors were based on four distinct scaffolds: chloromethylketones [19, 72], 4-chloroisocoumarins [19, 71, 97], fluoro-phosphonates [69, 94, 110] and N-sulfonylated β-lactams [82]. Since inhibitors are useful as research tools or lead compounds for drug development, various rhomboid screening assays have been developed in the past to discover further structural classes of rhomboid inhibitors. All rhomboid assays share the limitation of being substrate based. Although rhomboid proteases can cleave substrates across species, a universal substrate that can be efficiently cleaved by all of them is not available. To circumvent this caveat, part one of this work presents the development of a substrate-free rhomboid inhibitor screening assay. For this work the previously reported FluoPol ABPP [143] was for the first time adopted for use with membrane proteins, which led to the discovery of a novel class of rhomboid inhibitors. The second part of this work discusses the reconstitution and visualization of rhomboids into large and giant unilamellar vesicles and the effect of the rhomboid environment on inhibitor screening results. Lastly, in the third part another application of the substrate-free inhibitor screening approach is presented that allows for gel-based fingerprinting and easy comparison of inhibitory profiles of various rhomboids. As a result of this work, the phenomenon of rhomboid auto-cleavage is presented.

Results presented in this thesis have been or will be published in peer-reviewed international journals [116].

## 4.1. Rhomboid protease fluorescence polarization activity-based protein profiling

### 4.1.1. Development of a fluorescence polarization assay for rhomboids

The high-throughput FluoPol ABPP was reported first in 2009 by Cravatt and co-workers and has been successfully applied to various soluble enzymes [143, 144, 146-149, 170]. In order to adopt the FluoPol ABPP to rhomboid proteases, a suitable ABP was needed. Previous work from the Verhelst lab and another group reported the first ABPs for rhomboid proteases [97, 110]. The ABP from the Verhelst lab is based on the isocoumarin rhomboid inhibitor **5** (appendix, Table 10) discovered in a MALDI-based rhomboid protease screen [97]. It contains an alkyne handle enabling copper-catalyzed click chemistry for attaching a fluorophore. While the click chemistry can be performed easily for each individual sample after the inhibitor has bound to the enzyme, it can be advantageous to have an already pre-clicked version of this ABP ready at hand. A benzyl-azide was first clicked to the inhibitor **5** to test the reaction conditions and create the rhomboid inhibitor **116** later used in the screens (Figure 9A).
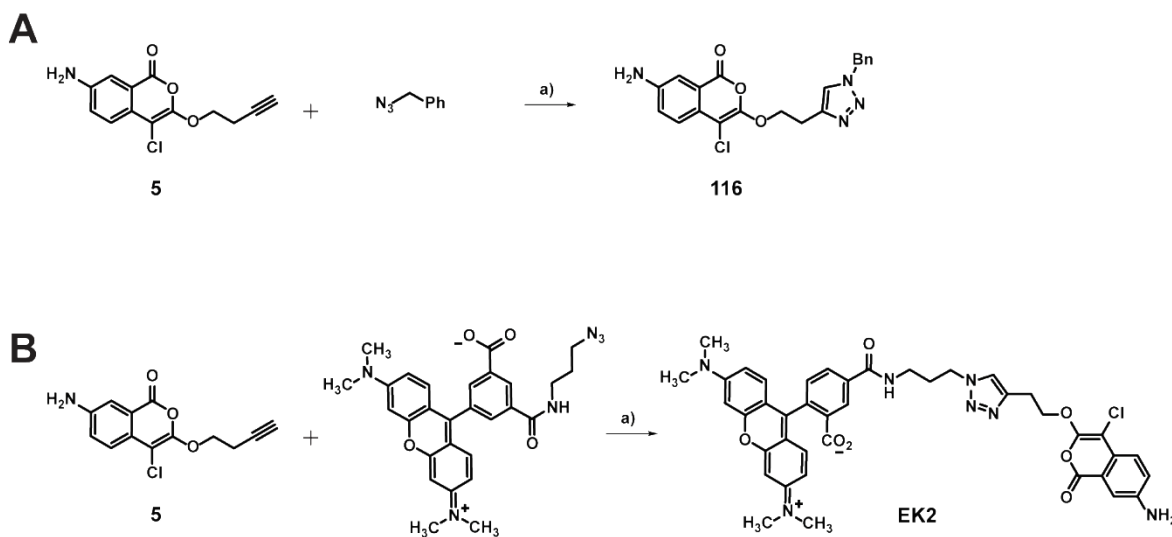


**Figure 9 Synthesis of the inhibitor 116 and the ABP EK2.** (A, B) Synthesis of the inhibitor **116** and the ABP EK2 a) 0.5 µM TBTA, 1 eq. Cu(I)Br, THF.

Next, using the same reaction conditions, TAMRA-azide was clicked to inhibitor **5** creating the ABP EK2 (Figure 9B). Both compounds were purified by HPLC and their identity confirmed by high resolution mass spectrometry.

In addition to the ABP EK2 there is another fluorescent ABP available for rhomboids, the ActivX TAMRA-FP Serine Hydrolase Probe (FP-R) from Thermo Fisher (Figure 10A), originally developed by Cravatt and co-workers [171]. While EK2 is isocoumarin-based, the FP-R has a fluorophosphonate group as warhead. Both probes carry a TAMRA fluorophore for detection. FP-R is a general serine hydrolase probe and had not been used for rhomboids at the time this work was started. To test whether both ABPs are suitable for rhomboids, labeling was tested against the *Escherichia coli* rhomboid EcGlpG (Figure 10B): EcGlpG WT and S201A mutant were incubated with either known inhibitor **97** or DMSO as vehicle control for 30 min and then labeled with 1µM of either ABP for 30 min.
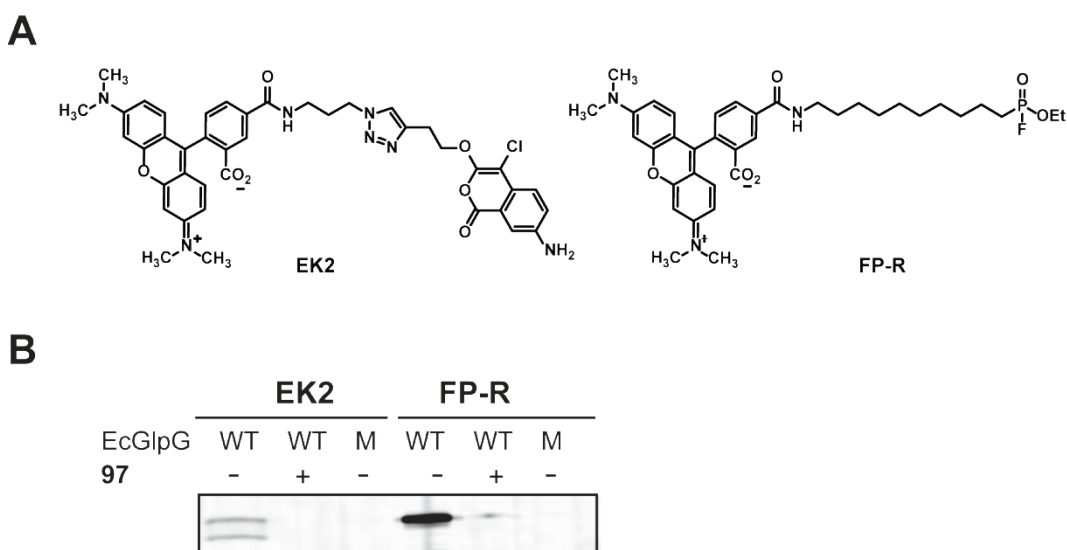


**Figure 10 Labeling of EcGlpG with the two ABPs EK2 and FP-R.** (A) Structures of EK2 and the commercially available FP-R used as ABPs in this study. Based on either an isocoumarin (EK2) or an fluorophosphonate (FP-R), both ABPs carry a TAMRA fluorophore for visualization. (B) 45 nM EcGlpG wild-type (WT) or the inactive S201A mutant (M) were incubated for 30 min at 37 °C with either 100 µM **97** or an equal amount of DMSO as vehicle control, followed by labeling with 1 µM of either EK2 or FP-R for 30 min at 37 °C.

While both EK2 and FP-R labeled the EcGlpG WT, there is no labeling of the catalytically inactive S201A mutant. Additionally, labeling could be completely abolished by pre-incubation with an inhibitor.

The suitability of FP-R as an ABP for the rhomboid protease was reported by another group during the course of this work [110]. While both probes labeled active rhomboids, the labeling intensity with FP-R was much stronger, which is probably due to the higher reactivity of the fluorophosphonate's electrophile.

With two ABPs available for labeling of the rhomboid protease, the first requirement for the FluoPol-ABPP – the availability of suitable ABPs – was fulfilled. The next step involved finding the right assaying conditions for a good FluoPol signal. All enzymes used before in the FluoPol ABPP assay were soluble enzymes [143, 144, 146-149, 170]. In these studies, Tris-HCL or HEPES buffers with 0.01% Pluronic F-127 were used [143, 146]. The latter is a surfactant that helps solubilization of the hydrophobic FP-R in the polar buffer. Rhomboids are membrane proteases and require detergents in order to stay in solution. A commonly used detergent for rhomboids is the mild non-ionic DDM, which has been successfully used for both rhomboid purification and during rhomboid activity assays [82, 97].

In order to confirm that execution of the FluoPol assay was possible in our laboratory and with our equipment, and to additionally test the effect of Pluronic F-127 in combination with the required detergent on the polarization signal, the first polarization experiment was not conducted with the membrane enzyme rhomboid, but with the soluble serine protease porcine pancreas elastase (PPE) in the presence or absence of both DDM and Pluronic F-127 (Figure 11A) in a standard rhomboid buffer (50 mM HEPES, pH 7.5). Due to gradual binding of the free probe to the enzyme, a successful polarization experiment should result in an increase of polarization over time, signified by a smooth, inclining signal curve.

The sample without detergent and surfactant showed a smooth curve, but a relatively flat slope (Figure 11A, orange curve). In the presence of the surfactant Pluronic F-127 however, the polarization signal improved, with a steeper slope and a smooth curve with little noise (Figure 11A, red curve). The sample with no surfactant but 1x CMC DDM resulted in a very noisy curve with almost no increase in signal when comparing the starting time point to the 60 min time point (Figure 11A, blue curve). In presence of both DDM and Pluronic F-127 the polarization signal showed an increase in polarization over 60 min with a slope comparable to the no-detergent samples, but the curve itself remained very noisy (Figure 11A, grey curve).

Having replicated the FluoPol ABPP from the literature [143] with a soluble enzyme in a buffer suitable for rhomboids, the next experiments were performed with rhomboid in order to see if similar results could be achieved (Figure 11B). Since the presence of a detergent is essential for rhomboid activity, three different DDM concentrations were tested and compared to the 1x CMC DDM with 0.01% Pluronic F-127 composition that gave rise to a decent polarization signal with elastase (Figure 11A, grey curve).

The samples containing 4x, 2x or 1x CMC of DDM all showed no significant increase in polarization signal over time, and only the 1x CMC DDM plus 0.01% Pluronic F-127 sample resulted in an inclining, albeit still noisy curve (Figure 11B). It seems thus that regardless of the tested enzyme, the presence of 0.01% Pluronic F-127 enhances the overall quality of the polarization signal. This is why the surfactant was added to every sample for all subsequent polarization experiments. Although 1x CMC DDM with 0.01% Pluronic F-127 already gave rise to an increasing polarization curve, the values for consecutive time points still varied a lot resulting in a very noisy curve. Other labs have successfully used Triton X-100 as detergent for rhomboids [65, 77], so it was decided to the use different Triton concentrations in the next experiment (Figure 11C). To confirm that also in the FluoPol ABPP settings FP-R labels only active rhomboid and not the inactive mutant, for all Triton concentrations two samples were measured: one containing EcGlpG WT and the other inactive EcGlpG S201 mutant. As expected, the polarization signal increased only for samples containing EcGlpG WT (Figure 11C, bright colored curves), while EcGlpG S201A samples result in a flat line (Figure 11C, pastel colored curves). Each corresponding pair of WT and S201A mutant samples already gave a first indication of what the assay window would be in the later screening: While the difference in the 5x CMC Triton X-100 samples between WT and S201A mutant (Figure 11C, red curves) was large and the slope of the WT curve steep, the curves themselves were quite noisy. The 0x CMC Triton X-100 samples (Figure 11C, grey curves) showed merely a slight increase of signal intensity for the WT, leaving only a small assay window between WT and mutant curves. Additionally the slope of the WT curve (Figure 11C, dark grey curve) was very flat.

The best polarization data was produced by the 1x CMC Triton X-100 samples: while the mutant sample produced an almost straight, flat line (Figure 11C, light blue curve), the WT sample showed a nice curve with a steep increase and little noise.

49
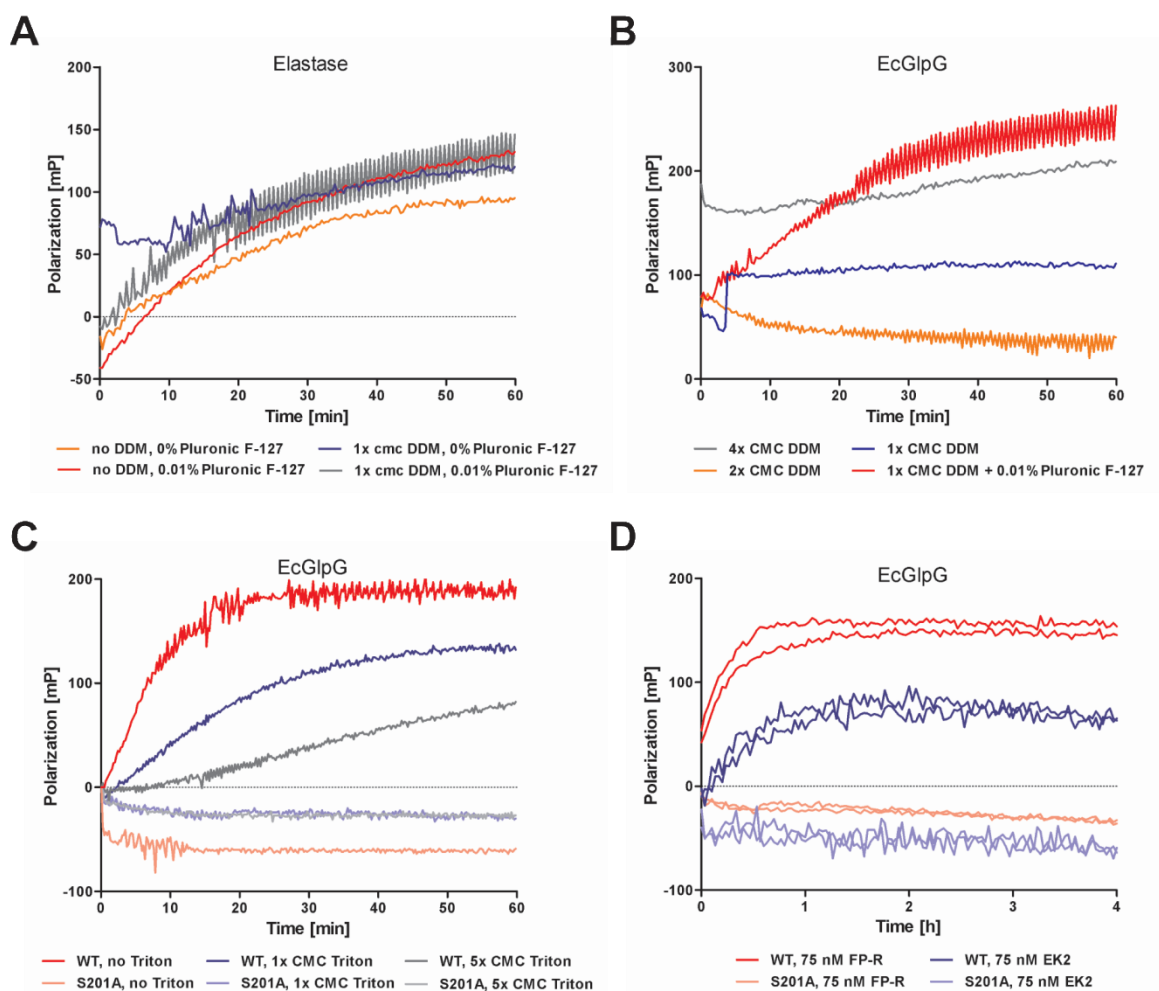
**Figure 11 Optimization of the Rhomboid FluoPol ABPP.** (A) Influence of detergent DDM and Pluronic F-127 on the polarization curve of elastase with FP-R: 500 nM elastase in 50 mM HEPES (pH 7.5) with or without 1x CMC DDM and 0.01% Pluronic F-127 were assayed with 75 nM FP-R in a fluorescence polarimeter at 37 °C for 60 min. (B) Influence of DDM concentration and Pluronic F-127 on EcGlpG: 500 nM EcGlpG in 50 mM HEPES (pH 7.5) with either 4x, 2x, or 1x CMC DDM and 0.01% Pluronic F-127 were reacted with 75 nM FP-R for 60 min in a fluorescence polarimeter at 37 °C. (C) Influence of Triton X-100 concentration on GlpG polarization curve. 500 nM EcGlpG WT and S201A mutant in HEPES (pH 7.5) were subjected to different Triton-X100 concentrations (0x, 1x, and 5 x CMC detergent) and assayed with 75 nM FP-R for 60 min at 37 °C in a fluorescence polarimeter. (D) 75 nM of EK2 or FP-R as ABPs were reacted with 500 nM of either EcGlpG WT or S201A mutant over 4 h at 37 °C in a fluorescence polarimeter.

From these experimental data it was decided that 1x CMC Triton and 0.1% Pluronic F-127 in a 50 mM HEPES buffer was a well suited choice to obtain reliable polarization signals with a good separation of the WT and the mutant polarization values. It was therefore used in all subsequent polarization experiments.

Up to this point all polarization experiments had been performed using FP-R as probe, since it was well established in the FluoPol ABPP literature [143, 148]. Having also an additional probe, the isocoumarin EK2 at hand, the last assay development experiment was conducted to determine whether the more selective [97] EK2 or the more reactive [116] FP-R is better suitable for the Rhomboid FluoPol assay (Figure 11D). EcGlpG WT and S201A samples were both assayed with either 75 nM FP-R (reds) or 75 nM EK2 (blues). While both probes work well in the FluoPol assay, FP-R gave smother curves and a more stable assay window between WT and mutant samples.

In addition to a purely visual evaluation of the graphs, the assay window can also be evaluated by calculation of the Z'-factor. The factor combines the average and standard deviations of positive controls (EcGlpG WT) and negative controls (EcGlpG S201A) and is an indication for the robustness and reproducibility of an assay. Calculation of the Z'-factor of duplicate measurements for each individual time point showed very good Z'-values of $> 0.8$ after 1 h for both probes, with slightly better Z'-values for the probe FP-R. Because of the better Z'-value and the smoother curves in the plot, FP-R was chosen as ABP for all subsequent FluoPol assays. In turn, EK2 was used for the confirmation of results obtained using FP-R to ensure that no probe-specific effects were observed. The optimized assaying conditions were thus determined as follows: 500 nM EcGlpG with 75 nM FP-R in 50 mM HEPES with 1x CMC Triton-X100 and 0.01% Pluronic F-127.

After determining the best assaying conditions for the rhomboid EcGlpG in FluoPol ABPP, the suitability for an inhibitor screen was tested by replicating some results of another rhomboid screening assay [97]. To this end, a selection of known inhibitors and enhancers were tested against EcGlpG in the FluoPol ABPP assay under the optimized conditions for 60 min (Figure 12A). In this short time span it was already possible to clearly distinguish between inhibitors (**2**, **17**, **97**), which resulted in a flat line in the plot, and inactive molecules or enhancers (**96**, **98**), which gave increasing polarization values (Figure 12A). All inhibitors were correctly identified in this experiment. It should be noted that after 20 min the sample with compound **2** showed an increase in polarization caused by the EcGlpG WT regaining its activity.
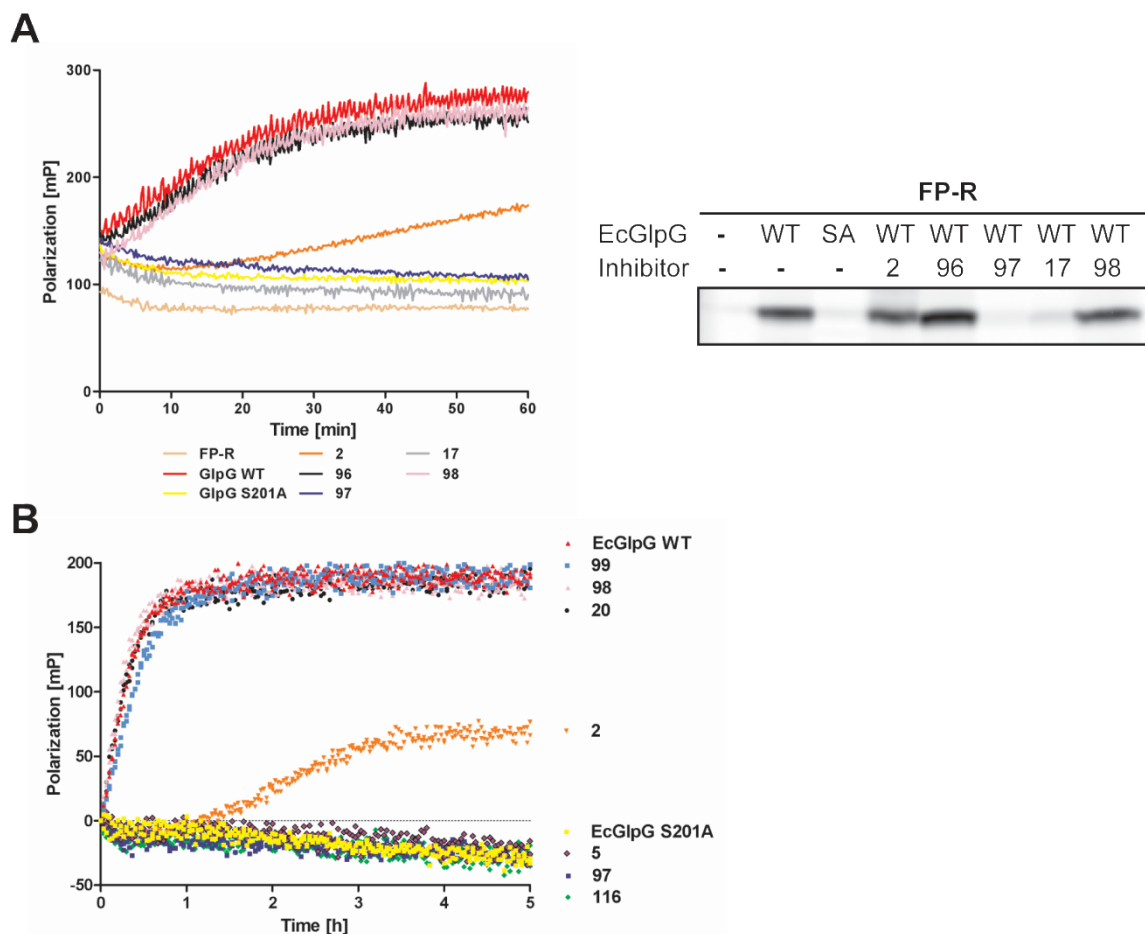
**Figure 12 Verification of the optimized FluoPol assay using known rhomboid inhibitors and enhancers.** (A) 500 nM EcGlpG WT was incubated with 100 µM each of five known inhibitors and enhancers for 30 min at 37 °C. The samples together with the EcGlpG s201A and no enzyme controls were then reacted with 75 nM FP-R over 60 min at 37 °C in order to observe the initial slope development. After the FluoPol assay, the samples were separated on a fluorescent 15% SDS-polyacrylamide gel to assess whether the FP-R bound irreversibly to the active site during the assay. (B) 100 µM of different rhomboid inhibitors and enhancers were incubated for 30 min at 37 °C with 500 nM EcGlpG WT. Then samples and the inactive S210A mutant control were reacted with 75 nM FP-R for 5 h at 37 °C and measured in a fluorescence polarimeter in order to assess slope development over time and visualize irreversible inhibitors as well as the hydrolysis of **2**.

This illustrates that the Rhomboid FluoPol ABPP is a suitable tool not only for identifying irreversible inhibitors, but also testing if they result in a stable covalent modification during the assayed time-frame by monitoring the kinetic. In the literature compound **2** had previously been reported to form an unstable covalent complex with EcGlpG, with the protease regaining activity due to deacylation [69].

To confirm whether the negative samples in the FluoPol assay were truly negative, all samples were separated on an SDS-polyacrylamide gel after the 60 min FluoPol assay. Only uninhibited EcGlpG WT samples have the FP-R bound irreversibly to the active site and can be seen in the fluorescence scan, while inhibited samples and the EcGlpG S201A mutant remain unlabeled. The enhancer **96** showed an increased labeling of EcGlpG WT compared to the uninhibited WT control. The inhibitor **2** sample meanwhile showed about the same labeling intensity as the uninhibited samples, which confirms that EcGlpG WT is regaining its activity probably caused by hydrolysis of **2**. The experiment showed that 60 min assaying time already gave good enough results to correctly identify the small molecules for their inhibitory capacity. While 60 min assaying time seemed sufficient, the next question to be addressed was whether an increase of measurement time would result in even more robust data. To this end EcGlpG WT was incubated with four inhibitors and three enhancers and assayed over 5 h in the Rhomboid FluoPol ABPP (Figure 12B). All inhibitors (**2**, **5**, **97**, **116**) and enhancers (**20**, **89**, **99**) were again correctly identified. While a good separation of polarization values for uninhibited and inhibited samples was achieved after 1 h, an even larger assaying window could be observed after 4 h of measurement time. Additionally the hydrolysis of **2** was even more pronounced during a longer assaying time. Since time was not an issue as measurements can be easily run over night, it was decided that all subsequent Rhomboid FluoPol screening assays where to be performed for at least 4 h.

Having determined the best assaying conditions and the optimal length for the measurement, the final step of the Rhomboid FluoPol assay development was to find out whether the assay is compatible with high-throughput screening. Ten replicates of each EcGlpG WT and EcGlpG S201A mutant were assayed under the optimized conditions for 5 h (Figure 13A). The assay window was then quantified by calculating the Z'-factor (see page 37) for each time point and plotting the resulting curve (Figure 13B).
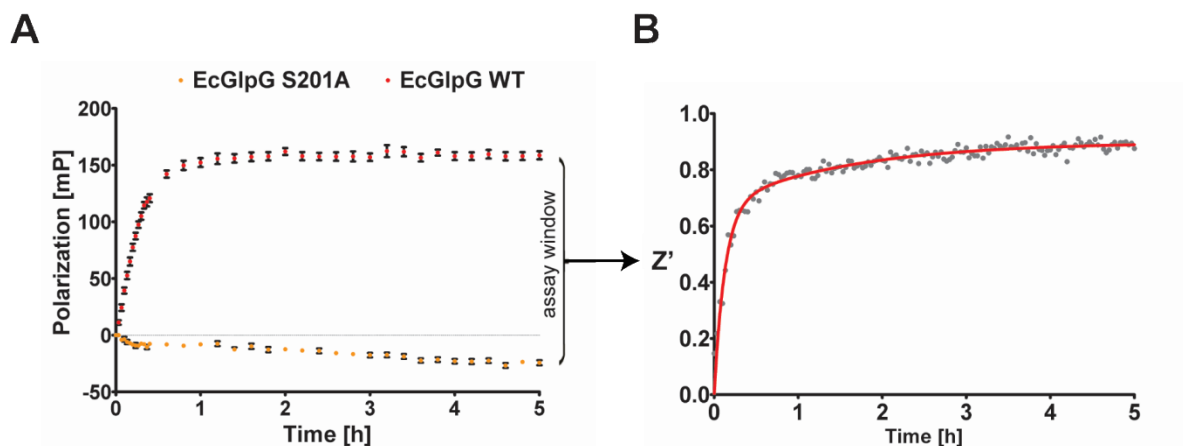
**Figure 13 Robustness and Reproducibility of the FluoPol ABPP.** (A) Ten replicates of EcGlpG WT and EcGlpG S201A were assayed in the FluoPol under optimized conditions: 500 nM enzyme with 75 nM FP-R in 50 mM HEPES (pH 7.5) with 1x CMC Triton X-100 and 0.1% Pluronic F-127. The area between the graphs is the assay window. (B) The assay window can be further evaluated by calculating the Z'-factor, which is an indication for the robustness and reproducibility of the assay.

The Z'-values increased rapidly in the first hour, and reached an Z'-factor > 0.8, close to 0.9 after 4 h, which makes it by definition an excellent assay [153]. Since the Z'-factor was so good after 4 h, it was decided to use the 4 h time point for data evaluation in the following FluoPol screens.

### 4.1.2. Screening a small molecule library by Rhomboid FluoPol ABPP

After determining the best assaying conditions and verifying that the results of other rhomboid screening assays can be replicated in the Rhomboid FluoPol ABPP, a set of 85 compounds was screened for rhomboid inhibitors. The small focused library screened in this work consisted of reactive electrophiles that all contain electrophiles that potentially react with the active site of rhomboid proteases: isocoumarins [172], phosphonates, phosphoamidates, β-lactones [127, 173], β-sultams, epoxides and thiiranes [174] (Table 10, page 118). In duplicate measurements, the 85 compounds were screened under optimized conditions and the polarization values at the 4 h time point were plotted in a bar graph (Figure 14).
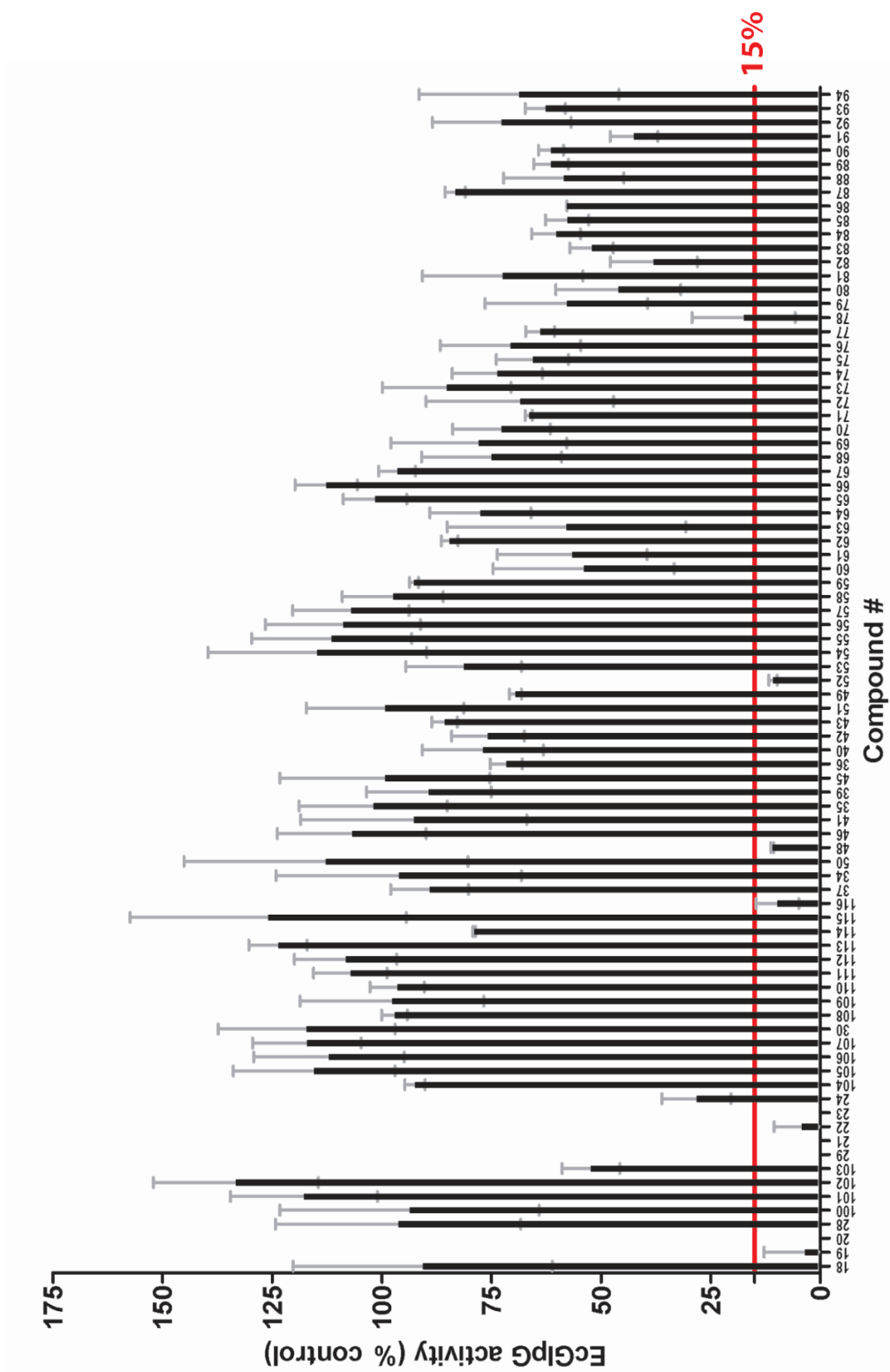
**Figure 14 A small molecule screen by Rhomboid FluoPol ABPP.** Screening data of 85 small molecules analyzed by the FluoPol assay normalized to 100% EcGlpG WT activity. A 15% cut-off was set to select potential hits. For compounds **20, 21, 23, 101** the slightly negative values are depicted as zero.

Nine compounds (**19**, **20**, **21**, **22**, **23**, **29**, **48**, **52**, **116**) gave 15% or less of the WT activity and were considered as potential hits together with a compound (**78**) that was slightly above the arbitrary 15% cut-off.

Next, the potential hits were confirmed by two different secondary gel-based assays (Figure 15). First, competitive ABPP was conducted with the ABP EK2 (Figure 15, upper panel) to ensure that the hits were not dependent on the nature of the ABP used in the screen. EcGlpG was first pre-incubated with the potential hits and then reacted with EK2. For this assay, labeled band should only be visible for samples containing uninhibited EcGlpG, which is the case for the untreated control or false positive hits.

The second assay was a substrate cleavage experiment, where EcGlpG was again pre-treated with the potential hits and then added to a fluorescent substrate and the cleavage visualized in gel (Figure 15, lower panel).
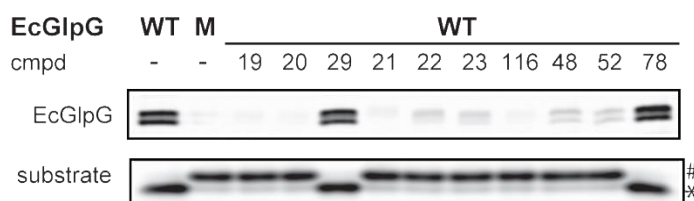


**Figure 15 Confirmation of potential hits.** Upper panel: Competitive ABPP with EcGlpG WT and S201A (M) against the ABP EK2. Lower panel: Substrate cleavage assay with EcGlpG WT and S201A and a fluorescence substrate. Uncleaved (#) and cleaved (*) substrate is indicated.

For both confirmation assays, the positive (WT) and the negative control (S201A mutant, M) reacted as expected: Labeling or substrate cleavage was seen for the active EcGlpG, and no labeling and no substrate cleavage could be observed for the inactive EcGlpG. The compounds **21** and **78**, both diphenyl phosphonates, turned out to be false positive hits, as they could prevent neither labeling nor substrate cleavage. Therefore compounds **19**, **20**, **22**, **23**, **29**, **48**, **52** and **116** were confirmed as inhibitors for the rhomboid protease EcGlpG.

In order to verify that the confirmed inhibitors were indeed irreversibly binding (see Figure 12), the inhibitors were subjected to a reversibility test (Figure 16): A positive control, the two false positives, a negative control and the confirmed inhibitors were incubated with EcGlpG for 30 min and the samples then subjected to a gel filtration to remove unbound molecules. After filtration, the samples were incubated with the ABP EK2 and visualized on a SDS-polyacrylamide gel.
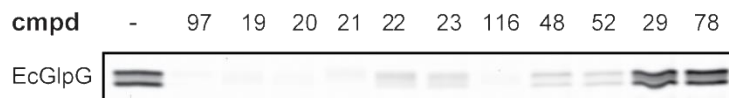


**Figure 16 Reversibility test with potential hit compounds.** To assess irreversibility of the potential hits, EcGlpG was incubated with the compounds and the samples purified in desalting columns to remove non-irreversibly bound compounds.

The positive control and all confirmed inhibitors still prevented EK2-labeling after the gel filtration, while the negative control and the false positive-treated samples showed labeling. This confirmed that the confirmed hits of the Rhomboid FluoPol ABPP are all irreversibly binding and stable in the time frame of the experiments, as can be expected from the reported mechanism of action with soluble serine hydrolases.

The structures of the confirmed compounds identified in the Rhomboid FluoPol ABPP screen are shown in Figure 17 together with the structure of the positive control and known inhibitor **97** (Figure 17A and B). The compounds **19**, **20**, **21**, **22**, **23** and **116** are all based on the isocoumarin scaffold, a structural class which had been reported before to yield rhomboid inhibitors [19, 71, 97].

Excitingly, compound **38** is a monocyclic and **52** a bicyclic β-lactone. The β-lactones have never been described to inhibit rhomboids and therefore represent a novel class of rhomboid inhibitors.
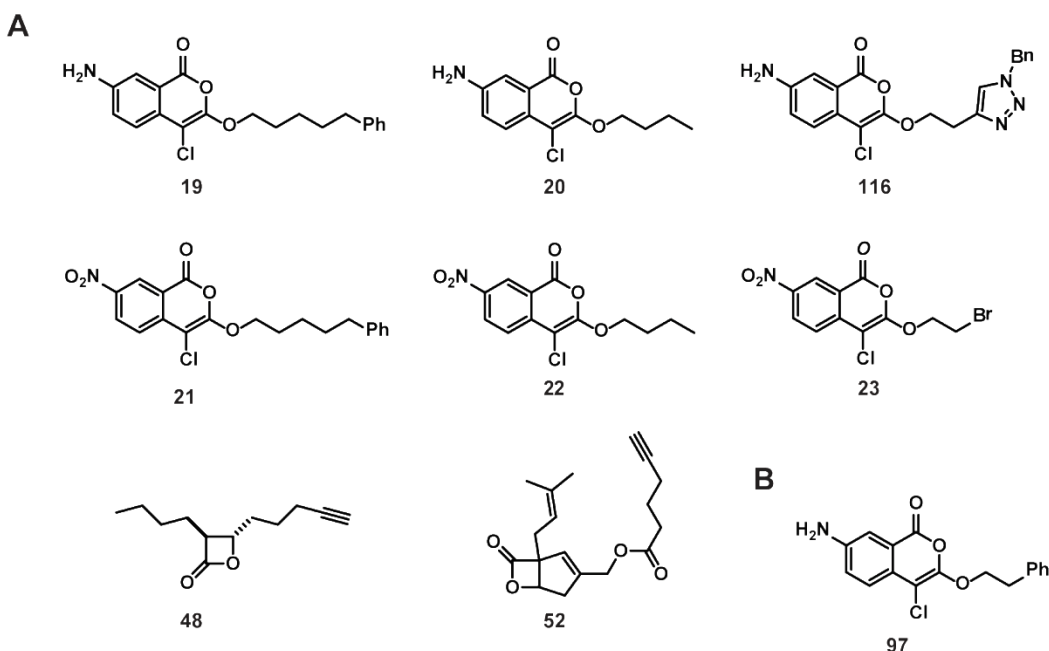
**Figure 17 Inhibitors found in the FluoPol screen.** (A) Chemical structures of the confirmed hits found in the FluoPol screen (B), and of the positive control, the known inhibitor **97**.

### 4.1.3. Further studies on hit compounds

For further investigation on the hit compounds, the apparent $IC_{50}$s were determined by FluoPol ABPP (Table 5). They are called "apparent" $IC_{50}$s, because regular $IC_{50}$-values determined in kinetic assays are only applicable to reversible inhibitors using a (reversibly bound) substrate. The apparent $IC_{50}$ determinations give a first indication of the inhibitory potency of the hit compounds, especially when compared to the apparent $IC_{50}$ of a known inhibitor.

The compounds based on the isocoumarin scaffold (**19**, **20**, **21**, **22**, **23**, **116**) showed a similar potency to **97** and inhibited in the single digit to sub µM-range. Compounds **19**, **20 and 116** have a close structural resemblance to **97** and inhibited up to one order of magnitude better than the compounds **21**, **22** and **23**, which all have a nitro group instead of an amine.

This confirms previous findings of the Verhelst group that indicated that an amino group at the 7-position of the isocoumarin scaffold is important for a stable and potent inhibition [97].

The β-lactones **48** and **52** with an apparent $IC_{50}$ of 26 and 44 μM respectively are less potent than the isocoumarins, but are comparable in potency to the structurally related rhomboid inhibitors, the β-lactams [82].

**Table 5 Apparent $IC_{50}$ (μM) of the hit compounds and 97, determined in duplicate measurements by FluoPol ABPP.** The β-lactones are indicated in bold letters.

| Compound | Apparent $IC_{50}$ [μM] |
|---|---|
| 97 | $1.1 \pm 0.6$ |
| 19 | $0.8 \pm 0.2$ |
| 20 | $0.4 \pm 0.1$ |
| 116 | $3.1 \pm 0.9$ |
| 21 | $5.2 \pm 0.8$ |
| 22 | $5.5 \pm 0.5$ |
| 23 | $8.4 \pm 1.7$ |
| **48** | **$26 \pm 6$** |
| **52** | **$44 \pm 10$** |

To get a first impression of the specificity of the two β-lactone hits **48** and **52**, the apparent $IC_{50}$ of them was determined for two canonical serine proteases: bovine chymotrypsin and bovine trypsin. Against these targets, both compounds showed an apparent $IC_{50} > 50$ μM for chymotrypsin and an apparent $IC_{50} > 150$ μM for trypsin.

Both β-lactone inhibitors **48** and **52** have an alkyne group attached to their scaffold, making them suitable for bio-orthogonal, tandem activity-based labeling. To test whether they can be used as novel ABPs, both compounds and DMSO as vehicle control were first allowed to irreversibly react with either EcGlpG WT or S201A mutant. In the second step the covalently bound inhibitors were functionalized with a TAMRA azide by copper-catalyzed azide-alkyne cycloaddition, thereby making the enzyme-inhibitor complex visible in fluorescence (Figure 18).
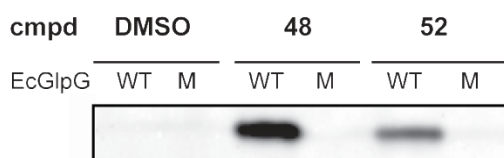


**Figure 18 Confirmation of the two β-lactones as novel ABPs for rhomboids.** Tandem labeling of EcGlpG with the two hit compounds **48** and **52**: 36 nM of EcGlpG WT or S201A (M) was incubated with 100 μM of the hit compounds or 1% (v/v) DMSO as vehicle control, followed by copper-mediated click reaction to attach a TAMRA-azide.

The EcGlpG WT, but not the inactive S201A mutant (M) was visualized as a band in a fluorescent gel by both **48** and **52** confirming covalent and activity-based labeling.

## 4.2.    Inhibitor screening in rhomboid-containing proteoliposomes

### 4.2.1.   Optimization of a reconstitution protocol and characterization of liposomes

An often encountered question when using a detergent-based approach like the Rhomboid FluoPol ABPP (and other rhomboid assays) is, whether inhibitors identified and characterized in such an artificial environment are transferable to natural conditions. While assaying in a detergent environment is easy, it might thus make sense to switch to a liposome-based assay or even using cells altogether. To address this question at least for rhomboid inhibitor screening assays, EcGlpG was reconstituted into liposomes and assayed against a selection of inhibitors. For designing the composition of the LUVs with reconstituted EcGlpG for this work, two aspects were considered: (1) The lipids that had been reported [107] in the past to positively influence EcGlpG activity and (2) the lipid composition of the *E.coli* membrane [175, 176], the natural environment of EcGlpG. The aim was to choose a composition where the EcGlpG would be active, and at the same time would still resemble a natural *E.coli* membrane. For the liposome experiments performed in this work, a ternary liposome composition of mostly phosphocholine (PC) with phosphoethanolamine (PE) and phosphatidylinositol (PI) was chosen. Fluorescently-labeled PE was added for visualization of the liposomes during preparation and under the fluorescence microscope (Table 6).

**Table 6 Lipid composition of the liposomes used for reconstitution of rhomboid proteases.**

| Lipid | Amount [%] |
| --- | --- |
| POPC[1] | 50 |
| Soy-PI[2] | 25 |
| DOPE[3] | 24 |
| Dansyl-PE[4] | 1 |

[1] = 1-palmitoyl-2-oleoyl-sn-glycero-3-phosphocholine
[2] = L-α-phosphatidylinositol from soy
[3] = 1,2-dioleoyl-sn-glycero-3-phosphoethanolamine
[4] = 1,2-dioleoyl-sn-glycero-3-phosphoethanolamine-N-(5-dimethylamino-1-naphthalenesulfonyl) (ammonium salt)

The next important variable was the reconstitution method. There are different methods available that allow for reconstitution of membrane proteins into liposomes: mechanical methods, freeze-thaw-cycles, using organic solvents, and detergents [177]. Since membrane proteases are susceptible to heating (during sonication), repeated freeze-thawing and organic solvents which denature the protein [177], the first three preparation methods are not very well suitable for rhomboid proteases. The much gentler detergent-reconstitution methods seemed much better suited, especially since rhomboids are solubilized and purified in detergents anyway.

For reconstitution with detergents, the purified membrane proteins in detergent are in the first step mixed with the lipids to form mixed micelles, and the detergent is then removed in the second step by various means leaving liposomes with inserted membrane proteins [178]. The detergent can be removed by gel chromatography, dilution, polystyrene beads or dialysis [177]. Rhomboids have been reported to loose activity during gel filtration [111], so that detergent removal by chromatography as well as polystyrene beads seemed less suited for rhomboids. While rapid dilution of the detergent is very easy and has been used before for rhomboids [64, 107], it vastly dilutes the sample and additionally does not remove the detergent completely. This implies that residual detergent molecules could still remain in the liposome and may even preferably position themselves around the rhomboid, so that all effects observed in such a system might be caused by the detergent, and not the lipid environment. Due to these deliberations, it seemed reasonable to use dialysis as method of choice for the removal of detergent.

Whether a detergent is removable by dialysis depends on the size of the micelles formed, which again depends on the aggregation number (the number of detergent molecules forming one micelle) and on the CMC (the concentration of detergent needed to form micelles). DDM is the preferred detergent for rhomboids, that has been used in many rhomboid studies including the Rhomboid FluoPol ABPP [19, 64, 93, 97, 107, 116]. Because of its large micelle size, DDM cannot be dialyzed within 24 h using a rhomboid-suitable dialysis membrane, making is not suitable for this method. Two other common detergents, CHAPS and OG, can easily be dialyzed due to their much smaller micelle size. The rhomboid BsYqgP has been reported to be inactive in both OG and the CHAPS-variant CHAPSO [107], so it seemed likely that EcGlpG would be also inactive in these detergents.

This was reasoned to not be problematic since correct reconstitution should restate the rhomboid activity, and might even be advantageous since regain of activity would confirm correct reconstitution and removal of all detergent molecules.

For testing the most suitable detergent for reconstituting EcGlpG into liposomes, EcGlpG was purified into DDM (as control), CHAPS or OG. Using the selected lipid composition (Table 6), liposomes were created through dialysis. Samples of EcGlpG in the three different detergents and of EcGlpG in liposomes prepared from these detergents were reacted with FP-R and visualized on a fluorescent gel (Figure 19).
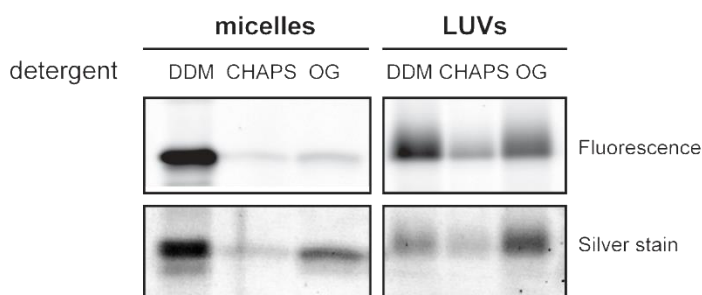


**Figure 19 Reconstitution of EcGlpG from three different detergents into liposomes.** Left side of the panel: EcGlpG in DDM, CHAPS and OG micelles labeled with FP-R in fluorescence scan and silver stain. Right side of the panel: The EcGlpG micelle samples were used for reconstitution into liposomes without detergent and the EcGlpG labeled with FP-R for fluorescence scan and silver stain. In fluorescence scan, only active rhomboids can be visualized with FP-R.

Only active rhomboid can react with FP-R and thus be visualized in fluorescence. As can be seen in Figure 19, although similar amounts of EcGlpG were used for the buffer exchanges, the rhomboid was most abundant in the DDM sample. Comparing the silver stain intensities to the fluorescence signal, it can be concluded that the present EcGlpG is active in DDM, and less so in CHAPS and OG. Once reconstituted, EcGlpG was active in all liposomes made from all three different detergents. EcGlpG was most active in liposomes made from DDM. However, these liposomes are likely not pure lipid-liposomes, but rather mixed micelles consisting of both lipids and DDM, since the detergent cannot be fully removed through dialysis.

Having confirmed that both CHAPS and OG can be used to reconstitute active EcGlpG into liposomes, the liposomes were next analyzed under a fluorescence microscope for their morphology (Figure 20).
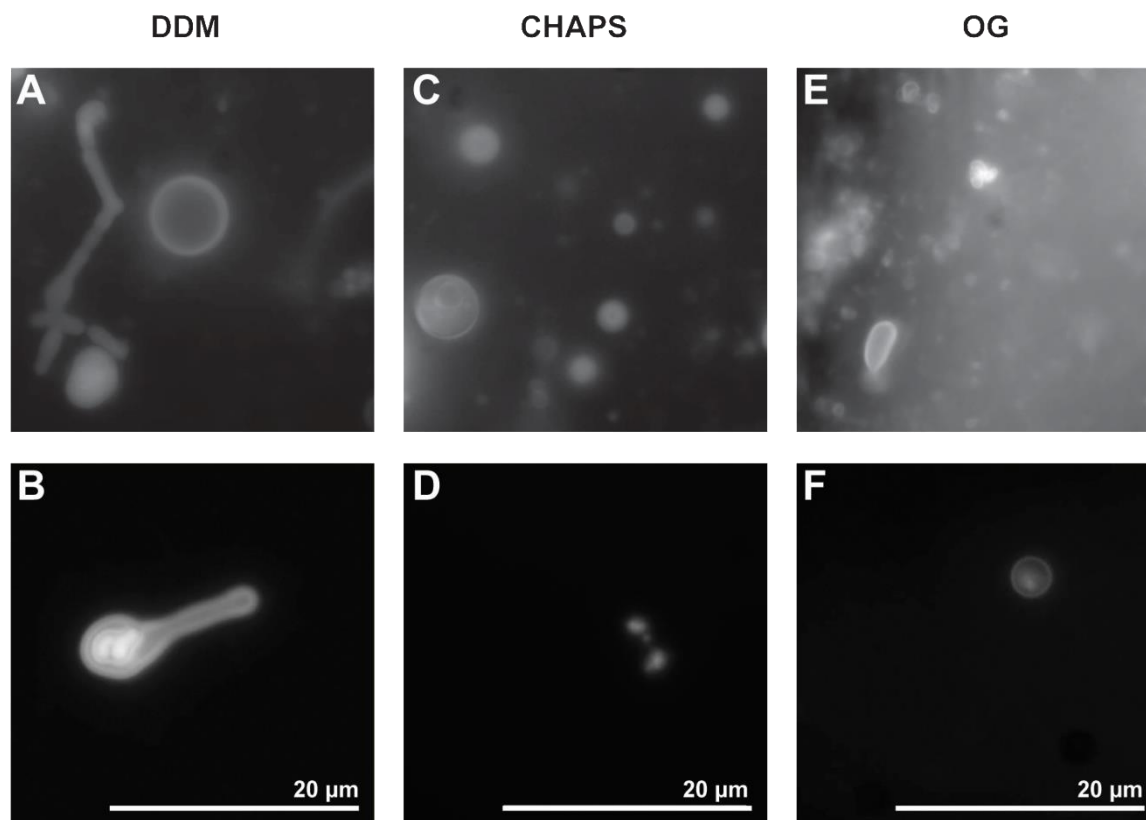
**Figure 20 Fluorescence microscopy of LUVs containing EcGlpG from different detergent environments.** The liposome samples were visualized under a fluorescence microscope with 100 x magnification and excitation of the dansyl fluorophore which is attached to the PE-lipid. Overview of the sample containing LUVs with reconstituted EcGlpG from DDM micelles (A,B), CHAPS micelles (C,D) and OG micelles (E,F).

Liposomes are spheres consisting of a lipid bilayer shell and a buffer-filled lumen. Under the fluorescence microscope unilamellar liposomes should thus appear as a single ring (the fluorophore-labeled lipid shell) with a darker inside (the lumen).

The DDM sample (Figure 20A) contained multiple proper liposomes, but also various cylindrical and globular lipid aggregates. The structures often contained inclusions of other membranes, resulting in multilamellar vesicles rather than unilamellar vesicles (Figure 20B). While the CHAPS sample formed globular spheres (Figure 20C), they were not dark inside but seemed to be rather solid and were additionally often very small (Figure 20D).

The OG sample produced by far the largest amount of liposomes, with the whole field of vision filled with liposomes of various sizes, which were often assembling into large clusters (Figure 20E). Almost all liposomes in this sample were unilamellar with a well visible lipid shell and dark center (Figure 20F).

Due to the lipid composition and the reconstitution method used, the resulting curvature should create mostly large unilamellar vesicles (LUVs) [155, 156]. In order to check the average vesicle size, the three different liposome samples made from DDM, CHAPS and OG purified EcGlpG were analyzed by dynamic light scattering (Figure 21).
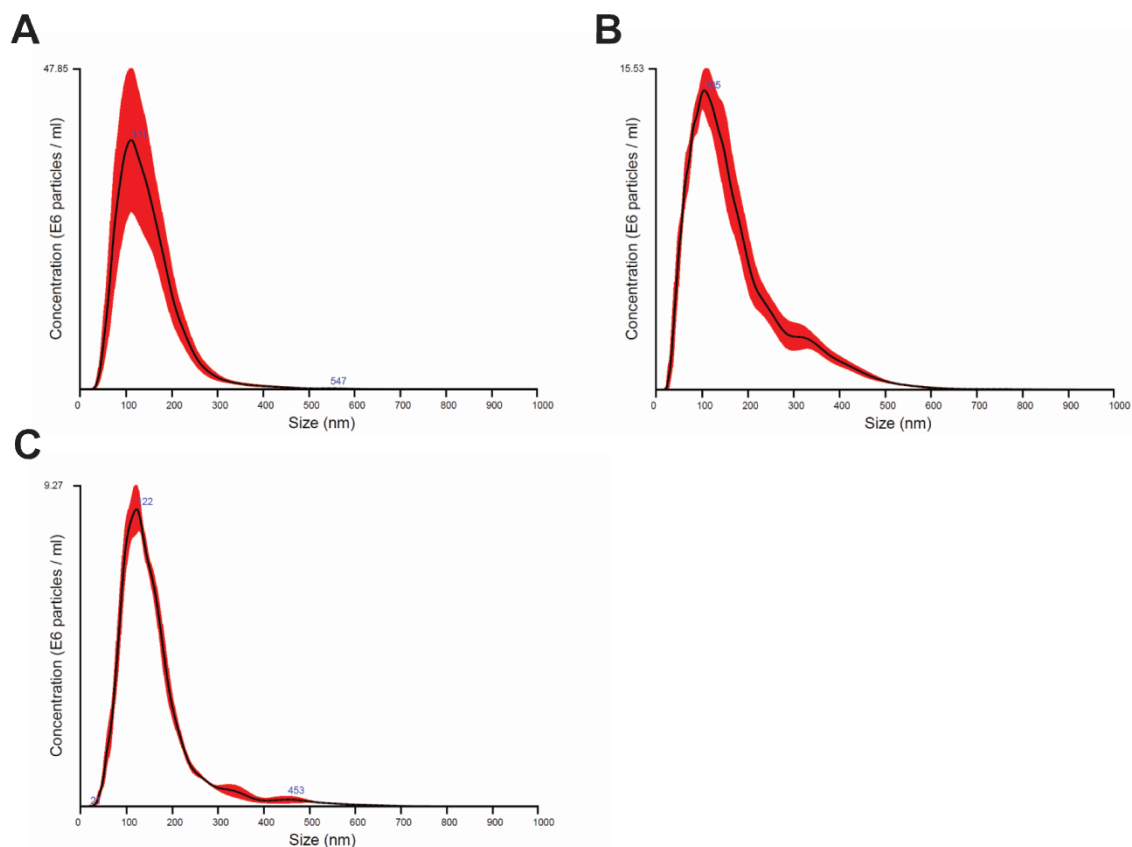


**Figure 21 Dynamic light scattering data of LUVs for size determination.** Dynamic light scattering data measured in the NanoSight to determine the average size distribution of the LUVs with incorporated EcGlpG made from (A) DDM micelles (B) CHAPS micelles and (C) OG micelles.

The light scattering data confirmed that the average size of all three liposome samples was between 100 and 200 nm, liposomes of this size are defined as LUVs [157]. While all three detergents resulted in liposomes of LUV-ranged sizes (Figure 21) with incorporated active EcGlpG (Figure 19), the liposomes made from OG were qualitatively the best as judged from fluorescence microscope pictures (Figure 20).

Additionally, the liposomes made from DDM were possibly mixed micelles and as such not the desired pure-lipid liposomes. Because of this OG was used as detergent for solubilization and reconstitution in all subsequent experiments.

While the 100 to 200 nm large LUVs were visible under a fluorescence microscope, visualization was still challenging so that the question arose, whether for future imaging studies, the LUVs could be used for the generation of giant unilamellar vesicles (GUVs). GUVs range in size from 1 to 100 µm and are easily visible under a fluorescence microscope [157, 158]. To test whether GUVs containing active EcGlpG (or EcGlpG S201A mutant as a control) can be created, the LUVs were subjected to the dehydration-rehydration method [157, 158]. For this, one volume LUVs were dried on glass slides in a desiccator and the lipid film was then rehydrated by addition of one volume buffer. After 2 h the GUVs were transferred to a reaction tube. To test whether EcGlpG was still active after this procedure, LUV and GUV samples were first treated for 30 min with DMSO or the inhibitor **97** and then labeled with FP-R or DMSO and visualized on a fluorescent gel (Figure 22).
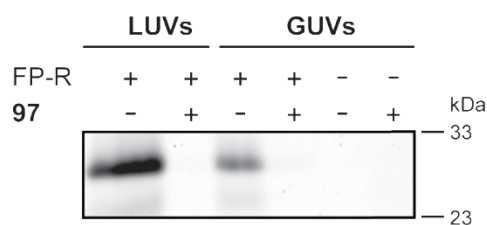


**Figure 22 ABPP of EcGlpG in LUVs and GUVs.** One volume of LUVs containing EcGlpG was dried to a lipid film in a desiccator o/n at RT and rehydrated in one volume of buffer for 2 h at RT to create GUVs. 20 µl of either LUVs or GUVs were incubated with 100 µM **97** or an equal volume of DMSO for 30 min at 37 °C and then labeled with 1 µM FP-R or an equal volume of DMSO for 2 h at 37°C. For all samples the whole 20 µl were loaded and visualized on a fluorescent gel.

Labeling could be achieved for uninhibited EcGlpG in both LUVs and GUVs, but not for inhibited samples or samples labeled with DMSO instead of FP-R. While the EcGlpG band was well visible in the uninhibited GUV sample, the corresponding band in the LUV sample is much stronger. Since equal amount were loaded, this indicates that not all LUVs could be rehydrated from lipid films and formed into GUVs. Additionally it seems very likely that a fraction of the EcGlpG lost its activity during the process. Both proposed reasons for a lower labeling intensity in the GUV sample could be expected, and since the GUV-EcGlpG sample gave a satisfying activity-dependent labeling, the GUV creation was deemed successful.

Having created GUVs with incorporated active EcGlpG, the next experiment aimed to further characterize them. Due to the expected GUV size of 1-100 μm, dynamic light scattering for size determination was not possible using the NanoSight which is designed for samples ranging up to hundreds of nm. Since GUVs are large enough to be easily visualized under a microscope, visual size-determination were performed.

First, the morphology of GUVs and LUVs with EcGlpG WT and S201A mutant was analyzed by transmission electron microscopy (Figure 23). Both LUVs and GUVs clearly showed single boundaries representing lipid bilayers around their lumen in the TEM, confirming that they were indeed unilamellar vesicles. Furthermore, although the liposome were deflated during the mounting procedure, a size estimation by eye could me made showing that the GUVs were approximately ten times larger than the LUVs, which had been sized to be around 100 to 200 nm by dynamic light scattering.
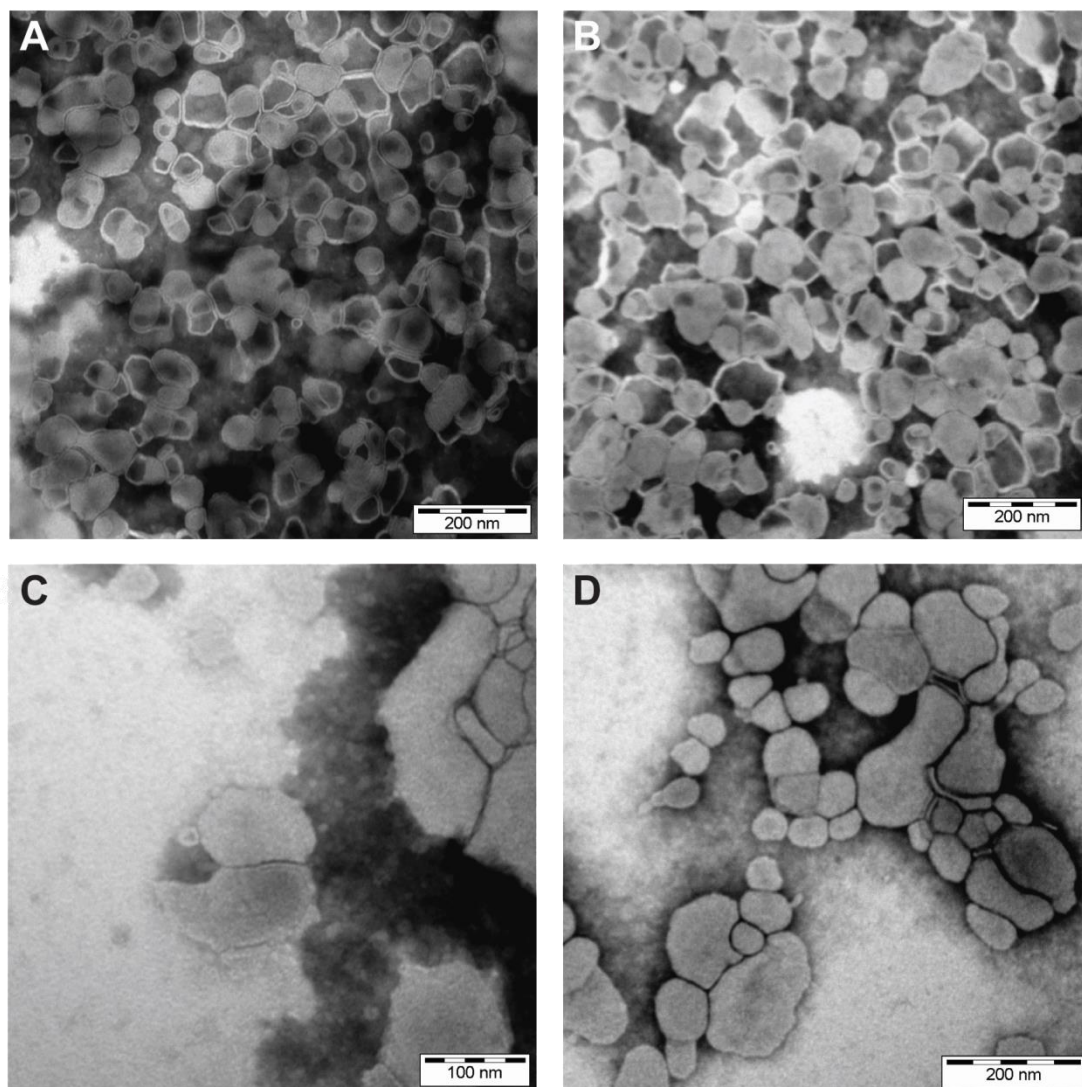
**Figure 23 LUVs and GUVs in electron microscopy.** All images were taken with a transmission electron microscope and 80x magnification. (A) LUVs with EcGlpG WT. (B) LUVs with EcGlpG S201A. (C) GUVs with EcGlpG WT. (D) GUVs with EcGlpG S201A. Note that probably due to the mounting and staining procedures, liposomes are smaller than expected [179].

With the LUVs and GUVs thus characterized, the next experiment was designed to test whether the GUVs can be used for imaging. To this end, GUV samples containing either EcGlpG WT or S201A mutant were incubated with either DMSO or the β-lactone **48** for 30 min and then labeled with EK2 for 2 h. EK2 was used instead of the promiscuous FP-R, since its inhibitor-based structure is more selective for EcGlpG.

Unbound EK2 was then removed by dialysis o/n and the GUVs visualized under a fluorescence microscopy in a Dansyl-channel (for the lipids) and the TAMRA channel (for the bound probe EK2) (Figure 24).

In all samples the GUVs could be seen as large, spherical vesicles with a dark interior lumen with a diameter of around 1 to 10 μm, showing they were truly GUVs.

The DMSO-treated EcGlpG WT GUVs (positive control) could be visualized in both the lipid and the probe channel since the EcGlpG was active in the GUVs and could be labeled with the probe EK2. The overlay shows co-localization of the fluorescence (Figure 24A). For the β-lactone **48** treated EcGlpG WT GUVs, fluorescence could be only detected in the lipid, but not in the probe-channel (Figure 24B). The overlay emphasizes that only the lipid channel gave a signal. This was to be expected since the β-lactone **48** inhibited EcGlpG in the GUV, so that the probe EK2 later could not react with the enzyme and was dialyzed away. The red spots in the background are small lipid aggregates that due to their hydrophobicity unspecifically bind the equally hydrophobic probe EK2. The negative control, EcGlpG S201A mutant in GUVs could not be labeled with EK2 and was only visible in the lipid, but not the probe-channel, similar to the inhibited sample (Figure 24C).

Taken together, these experiments confirmed that it is indeed possible to create GUVs with active EcGlpG from LUVs using the rehydration-dehydration method. These GUVs have the right size in the μm-range and can be used for inhibition studies and imaging, as shown the simple inhibition experiment presented here.

| Lipid | Probe EK2 | Overlay |
|-------|-----------|---------|
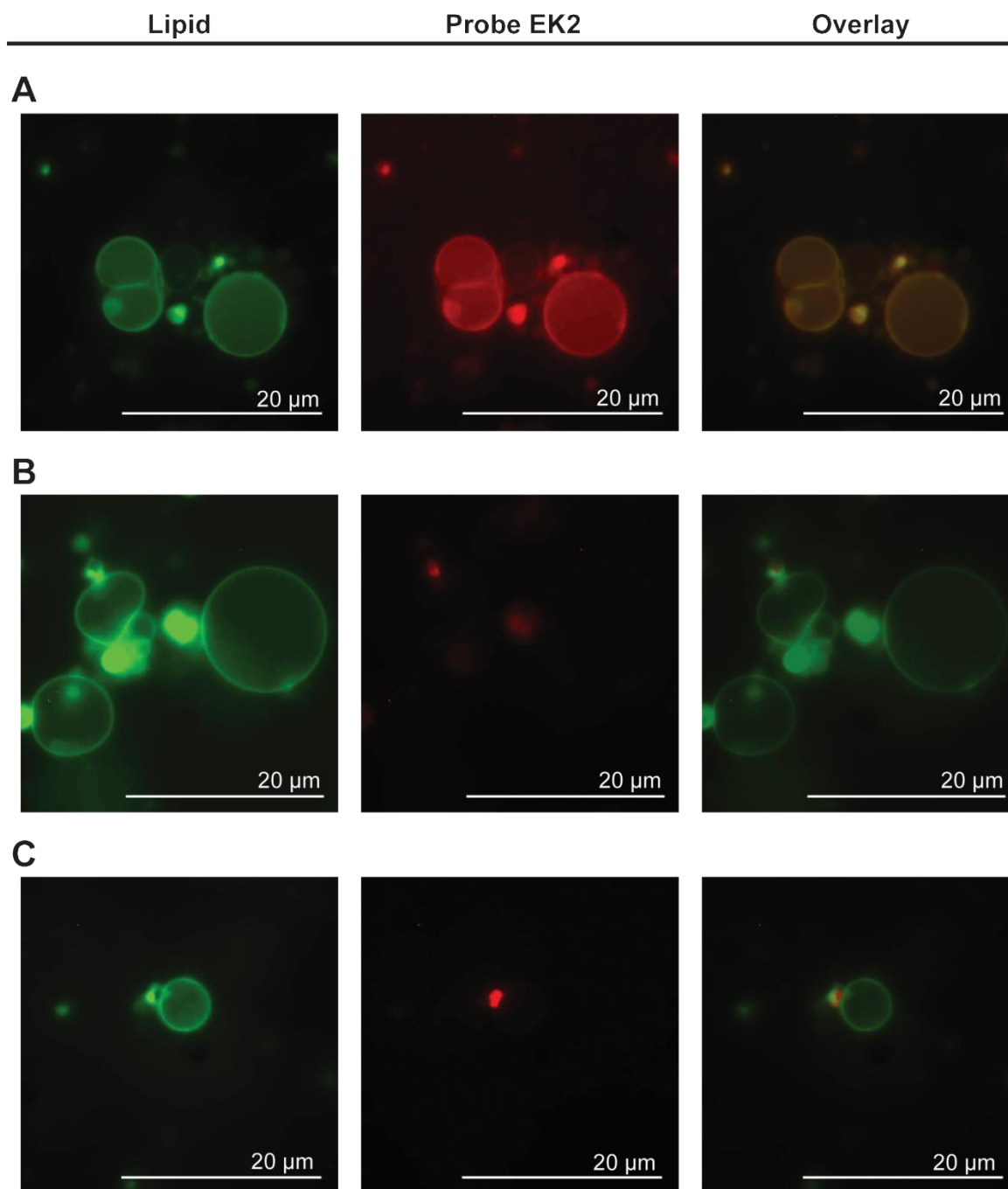


**Figure 24 Fluorescence imaging of GUVs containing EcGlpG.** (A) GUVs with EcGlpG WT incubated with EK2 and visualized in the Dansyl channel (360-370/420 nm) for lipid visualization and the TAMRA channel (530-550/590 nm) for visualization of EK2 probe-labeled active EcGlpG. (B) GUVs with EcGlpG WT inhibited with the β-lactone **48** prior to labeling with EK2 probe and visualized as before. (C) GUVs with (inactive) EcGlpG S201A mutant labeled with EK2 and visualized as before.

Having successfully established the reconstitution of EcGlpG in LUVs and GUVs, the question arose if also other rhomboid proteases could be reconstituted into LUVs using the same procedure and lipid composition as EcGlpG, or if more optimization is needed in the future. To this end, rhomboid proteases of various origins were reconstituted as described above for EcGlpG and 20 µl of each LUV sample reacted with FP-R and visualized on a fluorescent gel (Figure 25).
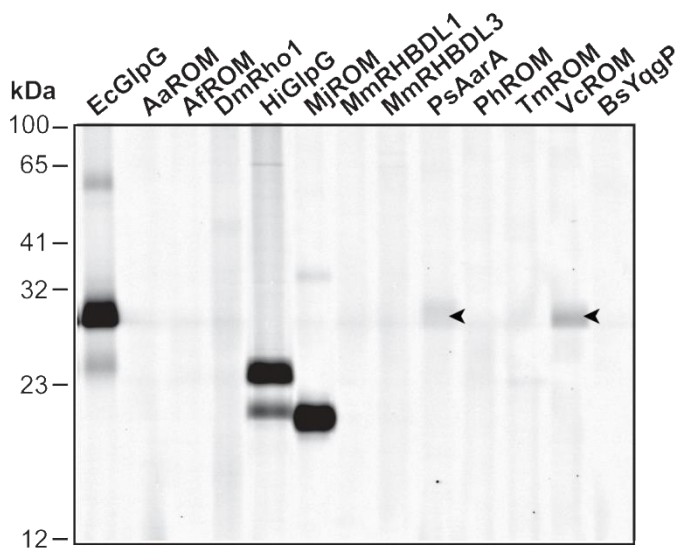


**Figure 25 ABPP of LUVs containing reconstituted rhomboid proteases of various origins.** 200 µg detergent solubilized rhomboid were used for the creation of LUVs. Each LUV sample was incubated with 1 µM FP-R for labeling of active rhomboid proteases. 20 µl of each sample was visualized on a fluorescent SDS-polyacrylamide gel. Arrowheads indicate faintly visible bands of active rhomboid.

Without optimizing any conditions, it was possible to reconstitute HiGlpG (from *Haemophilus influenza*) and MJROM (from *Methanococcus jannaschii*) on the first try. Both actively reconstituted rhomboids showed a strong labeling with FP-R in gel, comparable in intensity to the labeling of EcGlpG. For two other rhomboids, PsAarA (from *Providencia stuartii*) and VcROM (from *Vibrio cholera*) faint fluorescent bands were visible. This indicates that at least a tiny fraction of those rhomboids was successfully reconstituted into LUVs. For all other rhomboids, no definite bands above the background signal were visible. It is unclear at this point whether this was due to failed reconstitution or inactivity of the rhomboids in the reconstituted liposomes.

### 4.2.2. Competitive ABPP of EcGlpG in liposomes

The successful reconstitution of EcGlpG into LUVs was the prerequisite for the following experiments, which aimed to answer the question whether the environment has an influence on inhibitor screening results. Since screening in micelles is far easier than screening in the less artificial but more laborious liposomes, all inhibitors screens (including the Rhomboid FluoPol ABPP) had so far been conducted in micelles. While it can be reasonable assumed that a lipid environment might influence the inhibition results to some extend compared to a detergent environment, it is unclear whether compounds might qualify as rhomboid inhibitors in a detergent but not a lipid environment. Since lipid and detergent molecules might interact with individual inhibitors differently based on the inhibitor's structure and hydrophobicity, more than a couple of inhibitors needed to be analyzed in both environments to observe whether the environment had a severe effect on inhibition results. To this end, EcGlpG in either DDM micelles or reconstituted in LUVs was screened against 51 small molecules in a gel-based ABPP (Figure 26A). The gel data of duplicate experiments was additionally quantified densitometrically and the averages plotted with the standard error into a bar graph (Figure 26B).

The gel band pattern of the 51 small molecules appeared similar in both micelles and liposomes. While band intensities varied to a small degree between the two environments, they did not substantially differ. The bar graph representation confirmed this observation: Compounds that act as EcGlpG inhibitors in micelles are also inhibitors in liposomes. Only the observed potency of the inhibitors varied based on the environment, answering the question, whether it might be necessary to conduct future inhibitor screenings in liposomes: for the identification of inhibitors simple micelle-environments seem to be sufficient.
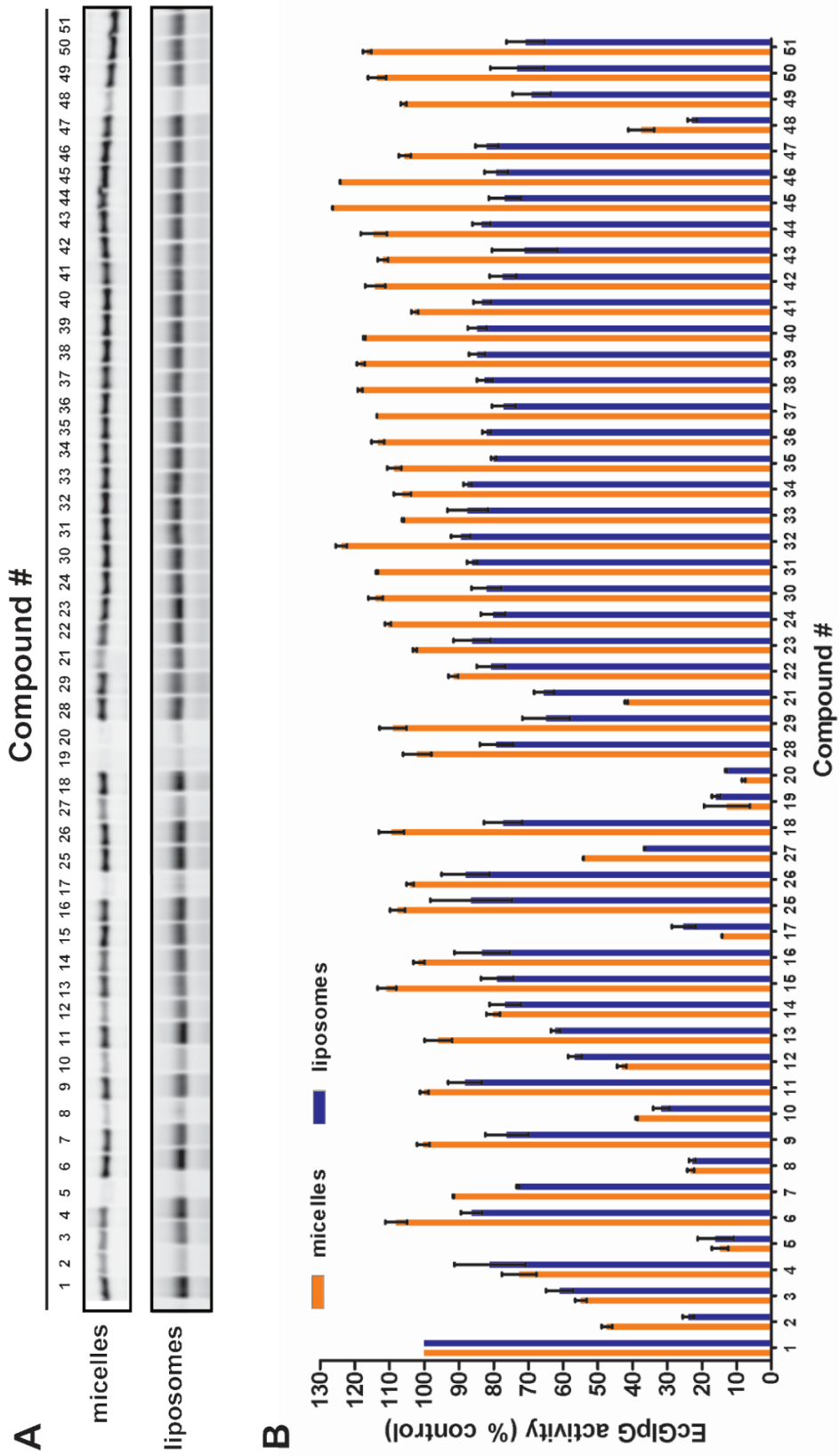
**Figure 26 Inhibitory profile of EcGlpG WT in micelles and liposomes.** (A) Panel of 51 compounds screened against EcGlpG in DDM micelles and in liposomes (LUVs) visualized with FP-R in a fluorescent SDS–polyacrylamide gel. (B) Bar graph representation of duplicate measurements of the inhibition pattern of 51 compounds against EcGlpG WT in DDM micelles and liposomes (LUVs). Shown are the averages with standard errors.

While basic "inhibitor / no inhibitor" determinations seemed to be independent on the environment, the question remained, to what extend the potency of the inhibitors is affected by the environment. In order to further investigate this question, the apparent $IC_{50}$ of three selected inhibitors was determined in both DDM micelles and LUVs (Table 7). EcGlpG in DDM micelles and LUVs was incubated with a range of concentrations of inhibitors **2**, **5** or **48** and incubated for 30 min. The samples where then labeled for 2 h with 1 µM FP-R and visualized on a fluorescent gel. Gel band intensities were determined densitometrically and used for apparent $IC_{50}$ determination.

**Table 7 Apparent $IC_{50}$s of three small molecules against EcGlpG in DDM micelles and large liposomes.**

| | Apparent $IC_{50}$ [µM] | |
|:---:|:---:|:---:|
| **Cmpd** | **Micelles** | **Liposomes** |
| **2** | $19 \pm 4$ | $5.6 \pm 0.8$ |
| **5** | $5.6 \pm 1.8$ | $9.3 \pm 1.0$ |
| **48** | $44 \pm 6$ | $29 \pm 4$ |

The apparent $IC_{50}$ of the three different inhibitors differed when measured in either micelles or liposome. Depending on the inhibitor, the determined apparent $IC_{50}$ was either higher or lower in micelles in contrast to liposomes. An environment-dependent effect on the inhibitor potency could not be observed, i.e. inhibitors were not generally determined to be more potent in a micelle-environment. The determined apparent $IC_{50}$ values differed by about a factor of 2 for the two environments, showing that environment effects were present but not very pronounced. Taken together, the inhibitor experiments in micelles and liposomes showed that for screening inhibitors, it does not matter if micelles or liposomes are used – inhibitors will always be identified as inhibitors. Having determined that the environment effect on the rhomboid inhibitor screening results is negligible, all future experiments were conducted in micelles, which were more ready accessible.

## 4.3. Gel-based activity-based protein profiling of rhomboid inhibition

### 4.3.1. Gel-based competitive ABPP fingerprinting

In a previous MALDI-based rhomboid inhibitor screen, the two studied rhomboids PsAarA and EcGlpG showed differences in their inhibitory profile when screened against a set of structurally diverse isocoumarins [97]. It was thus reasoned that different rhomboids might show different profiles when assayed against a collection of potential inhibitors, and that such a 'fingerprint' might be useful to delineate similarities among them. Furthermore, a comprehensive analysis of the inhibition of various rhomboids is a reliable way to identify novel inhibitors and possibly also ABPs for hitherto not well studied rhomboids.

While in principle various rhomboid inhibition screening assays can be used for such an experiment, a gel-based ABPP seemed especially suitable in this context, as no universal rhomboid substrate is available and a general ABP would allow for substrate-free inhibitor profiling of the various rhomboids. Furthermore a gel-based format allows for immediate read-out of inhibition and a relatively easy experimental set-up: The inhibition is assayed by competitive ABPP and visualized in fluorescence SDS-polyacrylamide gels, and the inhibition patterns of different rhomboids then analyzed visually or by further data analysis.

The commercially available FP-R probe was successfully used for labeling of EcGlpG in both FluoPol as well as gel-based ABPP experiments. FP-R is a general and promiscuous serine hydrolase probe, so it stood to reason that also rhomboid proteases from other origins should be labeled with it. To test this, 13 different rhomboid proteases from *Aquifex aeolicus* (AaROM), *Archaeoglobus fulgidus* (AfROM), *Methanocalcococcus jannaschii* (MjROM), *Pyrococcus horikoshii* (PhROM), *Thermotoga maritima* (TmROM), *Vibrio cholera* (VcROM), *Providencia stuartii* (PsAarA), *Escherichia coli* (EcGlpG), *Haemophilus influenzae* (HiGlpG), *Bacillus subtilis* (BsYqgP), *Mus musculus* (MmRHBDL1 and MmRHBDL3) and *Drosophila melanogaster* (DmRho1) (see also Table 3, page 26) were recombinantly expressed and purified. The purified rhomboids were then incubated for 2 h with 1 μM FP-R and visualized on a fluorescent 15% SDS-polyacrylamide gel (Figure 27).
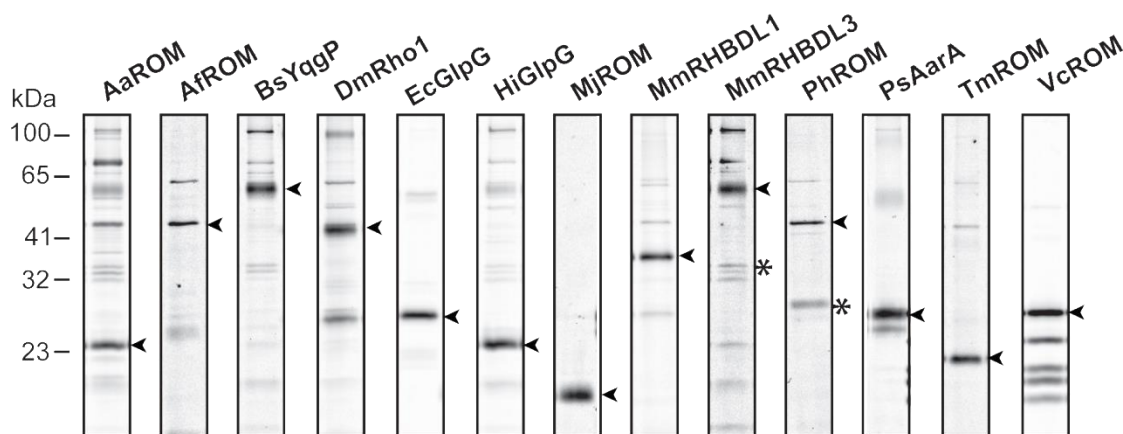
**Figure 27 Labeling of active rhomboids of prokaryotic, eukaryotic and archaean origins using the probe FP-R.** Thirteen rhomboids of different origins were labeled with 1 µM FP-R and visualized on the same fluorescent gel and scanned at the same intensity. Due to differences in reactivity with the probe, fluorescence intensities varied between the rhomboids. For better visualization, contrasts were enhanced for weaker labeling rhomboids. All rhomboids could be labeled with FP-R. The arrowheads indicate the expected monomeric molecular weights of the rhomboids which were also the most strongly labeled bands, with the exception of MmRHBDL3 and PhROM, where the most strongly labeled band corresponds to the dimer. The expected monomeric size of these two rhomboids has been indicated with a star. For further analysis of inhibition of rhomboids, only the bands indicated with arrowheads were used.

For all rhomboid samples fluorescent gel bands were detected at the expected mass of the monomer or dimer. This proved that all rhomboid proteases studied can be labeled with FP-R, meaning that all samples contained an active serine hydrolase of the expected molecular weight.

Most rhomboid samples showed some additional background labeling: active degradation products, multimers of the rhomboids, or contaminations with other active serine hydrolases. The sample purity is important for experiments like FluoPol or other fluorescence-based assays, where the output und subsequent data analysis is based on the whole sample and might be influenced by contamination. An advantage of gel-based ABPP experiments over substrate-based experiments is that only the band of interested is included in the data analysis, so that a minor background in the sample is not an issue. Since the strongest labeled bands were of the molecular weights (or corresponding to the dimer) expected for the corresponding rhomboids, the samples were deemed pure enough and the expression in *E.coli* and purification considered successful.

Consequently, for all subsequent experiments, only the fluorescent bands corresponding to the expected molecular weights of the monomers or, for MmRHBDL3 and PhROM the dimers, were used for data evaluation.

With 13 eukaryotic, archaean, and prokaryotic rhomboid proteases available, their activity and inhibition was further investigated in order to obtain an inhibition fingerprint profile.

In a competitive ABPP set-up, the rhomboids were first incubated with 100 µM of the small molecule for 30 min, followed by labeling with 1 µM FP-R and visualization on a fluorescent SDS-polyacrylamide gel (Figure 28).
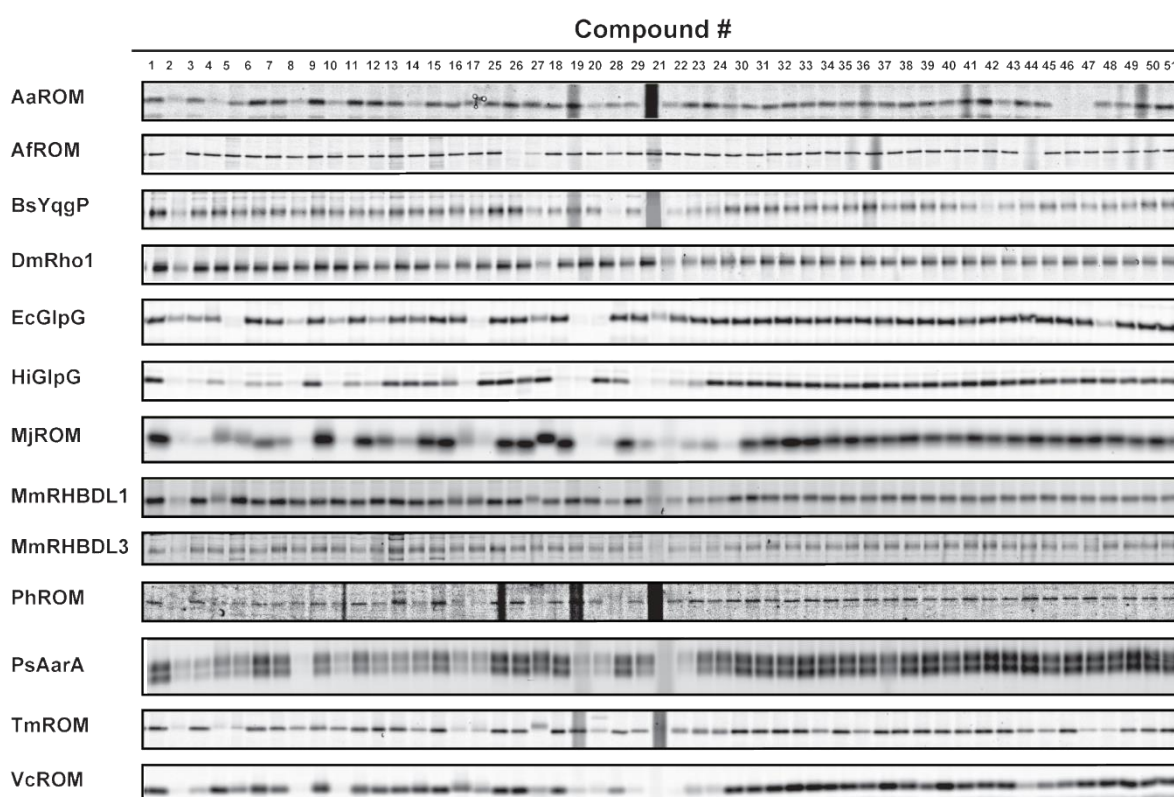


**Figure 28 Inhibitor screening panel of 51 small molecules against 13 different rhomboid proteases.** Thirteen different rhomboid proteases from various organisms were incubated in duplicates for 30 min with 100 µM of 51 different small molecules and then probed for 2 h with 1 µM FP-R. The samples were visualized on fluorescence SDS-polyacrylamide gels. Shown here is one representative gel picture for each rhomboid, duplicates were made and analyzed densitometrically.

For all rhomboids, the gel band corresponding to the expected molecular weight was used for the measurement of activity and inhibition.

From the raw gel data, it was already possible to identify inhibitors: active and uninhibited rhomboids were labeled by FP-R and appeared as fluorescent gel bands, while inhibited rhomboids did not show a fluorescent band.

In addition to the identification of rhomboid-specific inhibitors, comparing the inhibition patterns of the 13 rhomboids allowed one further observation: among the 51 compounds were selective inhibitors like for example **48** (inhibiting only one or two rhomboids), as well as pan-inhibitors (inhibiting a majority of the rhomboids), for example **2** and **21**. Furthermore, through comparing the inhibition patterns, it was possible to identify rhomboids sharing similar inhibitory patterns like AaROM and EcGlpG, which were both inhibited by **48**.

In order to further investigate possible similarities between different rhomboids and also better visualize the selective and pan inhibitors, the gel bands were quantified densitometrically and their numerical values color-coded with black tiles for 0% inhibition and bright red tiles for 100% inhibition (Figure 29A).

The numerical data was clustered for rhomboid similarity as well as compound similarity and visualized in a heat map (Figure 29B). Through this visual representation the pan-inhibitors **2** and **21** as well as more selective inhibitors, for example **26**, **44**, **47**, and **48** were easily identifiable.

Furthermore due to the double-clustering of both rhomboids and compounds, black and red areas could be detected that allowed further conclusions for both the inhibitors as well as the rhomboids.

The inhibitors clustered in a way that allowed for subdivision into four categories: (1) inhibitors without selectivity, consisting of mostly isocoumarin, where all compounds inhibit at least one but often multiple rhomboids, (2) bad inhibitors that only weakly or not at all inhibit only a few rhomboids, (3) pan inhibitors that inhibit (almost) all rhomboids relatively strongly, and (4) inhibitors with selectivity, containing mostly β-lactones, where a single inhibitor inhibits not more than two of the 13 rhomboids. Taken together these observations indicated that the isocoumarin scaffold yields more promiscuous inhibitors that label a lot of different rhomboids, while β-lactone based inhibitors are more selective, but react with less rhomboids.
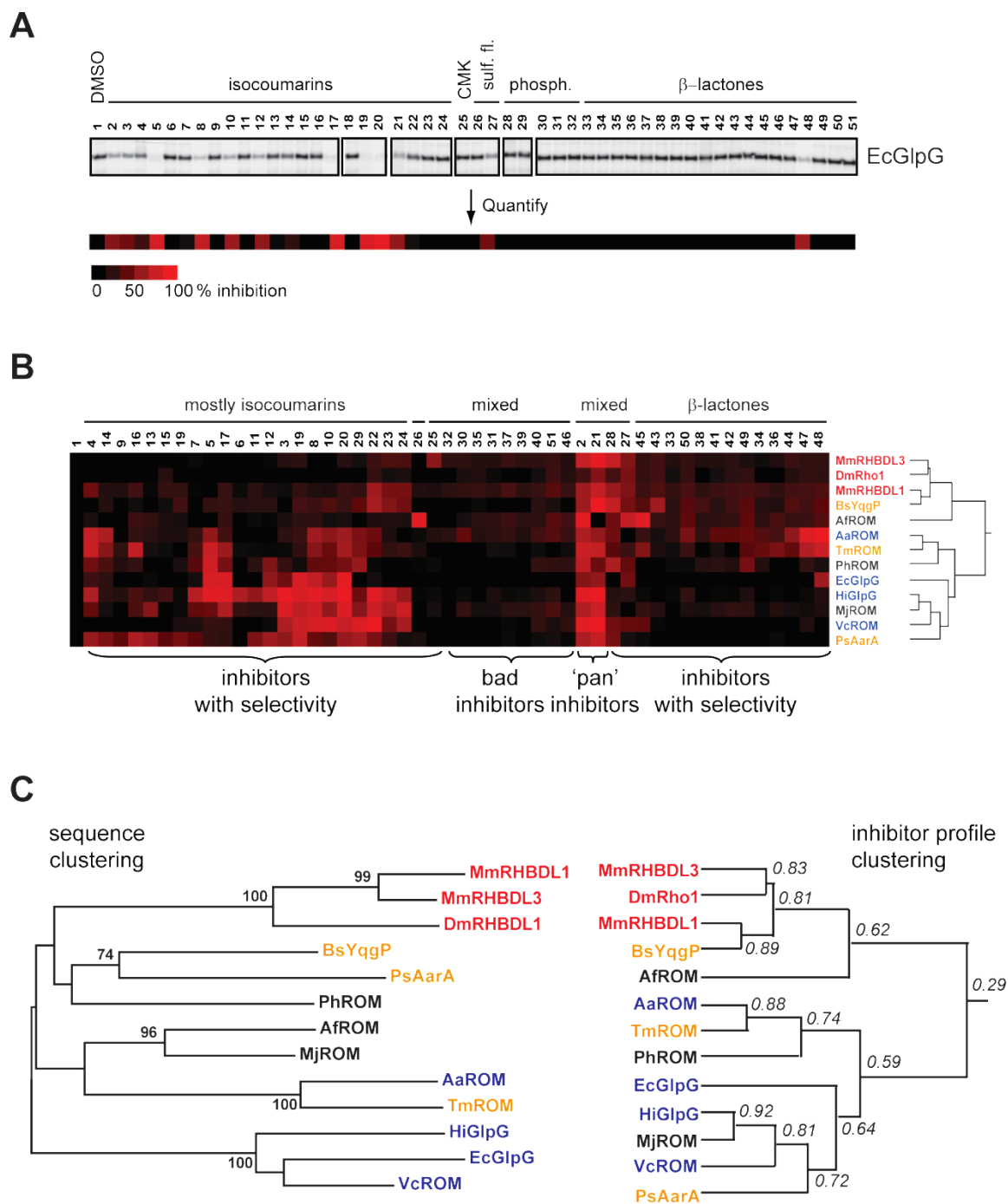
**Figure 29 The inhibitor screening data as basis for a heat map and clustering.**
(A) Inhibition data from the fluorescent gels was densitometrically quantified and converted into a heat map ranging from black tiles (0% inhibition) to bright red tiles (100% inhibition). The structural classes of screened small molecules have been indicated. (B) Heat map of the screening data of 51 small molecules and 13 rhomboid proteases clustered for both compounds as well as rhomboids. Eukaryotic rhomboids are marked in red, archaean rhomboids in dark grey, and prokaryotic rhomboids in blue (6 TM helices) and in yellow (7 TM helices).

The structural class of the small molecules has been indicated were possible. Based on the amount of red tiles in neighboring rows, areas have been indicated containing inhibitors with selectivity, bad inhibitors, and pan inhibitors.
(C) Left side: Phylogenetic analysis of the rhomboid sequences using MEGA6 software [164]. The numbers at the nodes represent the percentage of replicate trees in which the associated taxa clustered together in the bootstrap test. Right side: Inhibitor screening data clustered for similar inhibition pattern and visualized in a tree. The numbers at the nodes represent the correlation of the members within the node.

In the clustering for the rhomboids, altogether three groups could be observed in the heat map: Rhomboids inhibited almost exclusively by pan inhibitors **2** and **21** and a few selective inhibitors (AfROM, BsYqgP, DmRho1, MmRHBDL1 and MmRHBDL3), rhomboids inhibited by β-lactones and the pan inhibitors (AaROM, TmROM, PhROM and EcGlpG), and rhomboids inhibited by many different isocoumarins in addition to the pan inhibitors (HiGlpG, MjROM, VcROM and PsAarA).

In order to see if the rhomboid clustering based on the inhibitory profile is similar to a clustering based on the sequence, both types of clusterings were depicted as hereditary trees for easy comparison (Figure 29C). The inhibitory profile-based clustering did not match the sequence-based clustering, indicating that the active site environment probed by the various potential inhibitors does not correlate to the overall amino acid sequence. This indicates that sequence similarities do not imply susceptibility for the same inhibitor structures and therefore a similar architecture of the active site. It should be noted however, that all rhomboids investigated are so distantly related, that even the closest clustering rhomboids, MmRHBDL1 and MmRHBDL2, share a sequence identity of only 52%. Hence it seems unlikely, that such distantly related proteins cluster similarly based on their inhibitor profile. At the same time the three eukaryotic rhomboids MmRHBDL1, MmRHBDL3 and DmRho1 clustered together in both trees, indicating there might be a weak correlation between sequence and active site structure amongst the eukaryotic rhomboids, but the overall correlation is not strong enough to allow for definitive conclusions.

In the end, the fingerprinting data showed that by using a universal ABP, different rhomboids can be profiled for their inhibitory pattern, and that the resulting data can be used to group the rhomboids as well as the inhibitors to gain further insight into the inhibition itself. A correlation between inhibitory profile and sequence similarity could meanwhile not be observed.

### 4.3.2. Further investigations on the inhibitors of different rhomboids

Among the inhibitors identified in the panel screen, some inhibited almost all rhomboids, while some reacted with only one or two rhomboids. The pan-inhibitor **2**, the well-known rhomboid inhibitor DCI, inhibited all rhomboids except DmRho1. To assess if **2** inhibited all rhomboids equally well, the apparent $IC_{50}$ was determined for all rhomboids by gel-based competitive ABPP and the $IC_{50}$ curves plotted (Figure 30).
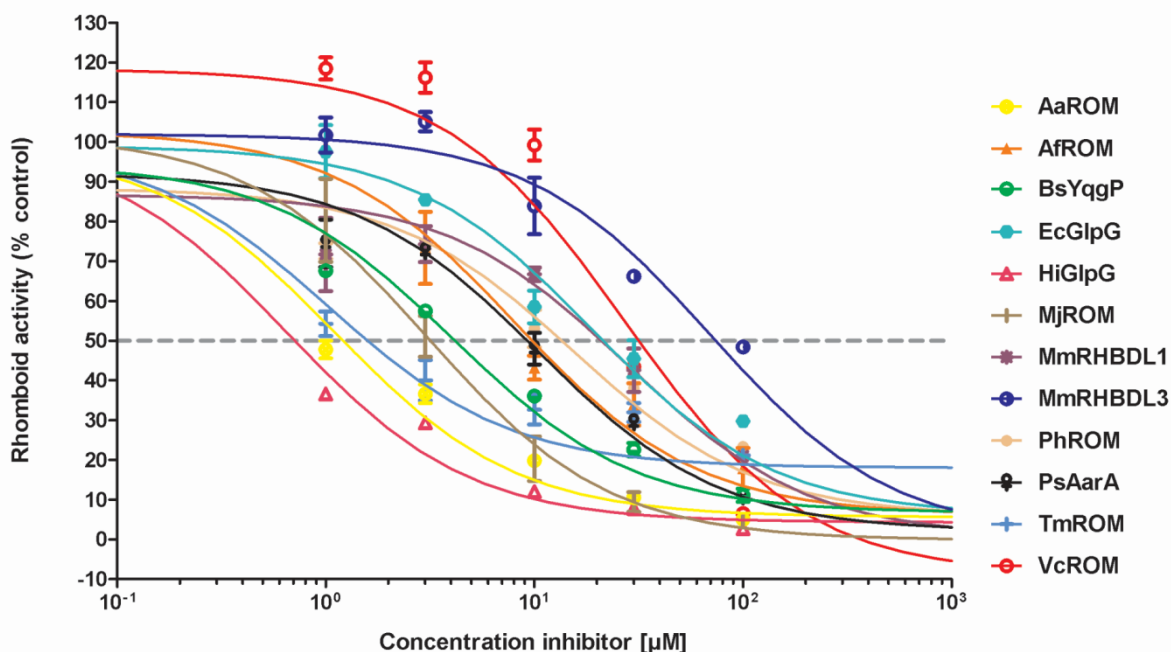


**Figure 30 Apparent $IC_{50}$ curves of the pan inhibitor 2 (DCI) against 12 rhomboids.** The pan inhibitor **2** inhibits 12 out of 13 tested rhomboids. Depicted here are the percentages of rhomboid activity at different inhibitor concentration with $IC_{50}$ regression curves. The grey dashed line indicates 50% rhomboid activity for easy estimation of the apparent $IC_{50}$ values. The apparent $IC_{50}$ value of **2** is between 1 and 100 μM for all 12 rhomboids.

All rhomboids were inhibited by **2** with $IC_{50}$s ranging within two orders of magnitude, from 1 μM up to 100 μM. Considering the tested rhomboids are from origins as diverse as archaea, prokaryotes and eukaryotes, the relatively $IC_{50}$ range determined seemed relatively small.

For further characterization of the pan-inhibitors and some selective inhibitors identified through the gel-based competitive ABPP screen, the apparent $IC_{50}$s of some selected compounds were determined using the same method and ABP as for the fingerprint itself (Table 8 and Table 9).

**Table 8 Apparent $IC_{50}$ values for the pan rhomboid inhibitors 2 and 21.**
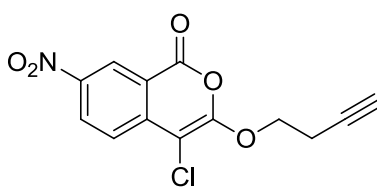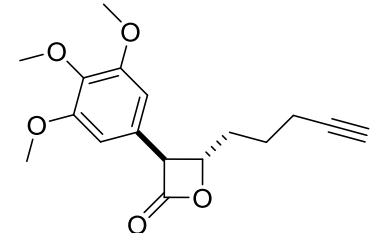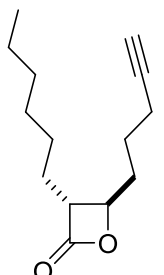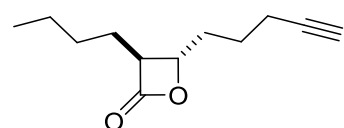
| Rhomboid | Apparent $IC_{50}$ [µM] | |
| --- | --- | --- |
| | 2 | 21 |
| AaROM | $1.1 \pm 0.2$ | $1.7 \pm 0.2$ |
| AfROM | $8 \pm 2$ | N.D. |
| BsYqgP | $4.1 \pm 0.9$ | $25 \pm 6$ |
| EcGlpG | $19 \pm 4$ | N.D. |
| HiGlpG | $0.7 \pm 0.1$ | $4.6 \pm 1.0$ |
| MjROM | $3.1 \pm 0.5$ | $9.7 \pm 1.6$ |
| MmRHBDL1 | $28 \pm 9$ | $39 \pm 6$ |
| MmRHBDL3 | $70 \pm 13$ | $24 \pm 3$ |
| PhROM | $16 \pm 5$ | $25 \pm 10$ |
| PsAarA | $10 \pm 2$ | $10.4 \pm 0.8$ |
| TmROM | $1.0 \pm 0.4$ | $28 \pm 7$ |
| VcROM | $27 \pm 9$ | $76 \pm 28$ |

The apparent $IC_{50}$ values for the two pan-inhibitors **2** and **21** varied a lot between the individual compounds, so that rhomboids were inhibited in different magnitudes. In most cases **2** seemed to be a better inhibitor with a lower apparent $IC_{50}$ than **21**. The selective β-lactone inhibitors were weaker inhibitors compared to the isocoumarins, with an apparent $IC_{50}$ approximately one order of magnitude higher (Table 9).

The apparent $IC_{50}$ values of both the pan and selective inhibitors give a first indication on the potency against rhomboids. For many rhomboids, the molecules characterized here are the first reported inhibitors for that particular rhomboid.

Excitingly, the newly identified β-lactone rhomboid inhibitors from the Rhomboid FluoPol screen also inhibit rhomboids beside EcGlpG, namely TmROM and AfROM (Table 9).

**Table 9 Apparent IC$_{50}$ values for some selective rhomboid inhibitors.**

| Compound | Rhomboid / Apparent IC$_{50}$ [μM] |
|---|---|
| **6**  | HiGlpG   58 ± 7 |
| **45**  | AfROM   5.0 ± 0.9 |
| **47**  | TmROM   27 ± 6 |
| **48**  | EcGlpG   44 ± 6<br>TmROM   48 ± 10 |

Some of the compounds carried an alkyne handle, making them applicable to tandem labeling with a fluorophore by azide-alkyne cycloaddition. Seven different rhomboids were incubated with 100 μM inhibitor or DMSO for 30 min and then subjected to the copper-mediated click-reaction in order to functionalize the alkyne handle with a TAMRA-fluorophore and then visualized on a fluorescence SDS-polyacrylamide-gel (Figure 31).
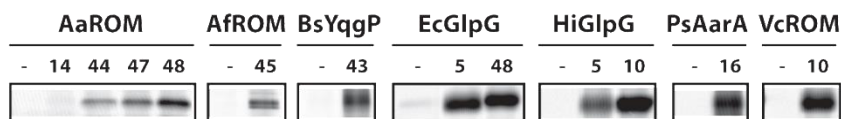
**Figure 31 Tandem labeling of rhomboids with selected inhibitors.** For seven of the screened rhomboid proteases, identified inhibitors carried an alkyne handle for tandem labeling. Rhomboids were first incubated with the inhibitor or DMSO and then subjected to the azide-alkyne cycloaddition to attach a TAMRA-fluorophore to the alkyne handle. Samples were analyzed on a fluorescence SDS-polyacrylamide gel.

With the exception of one rhomboid-inhibitor combination (**14** with AaROM), two step labeling using the different inhibitors worked on all rhomboids. This showed that not only were the reactions with the inhibitors covalent, but also that they could be used as novel activity-based probes for these rhomboids. Together with the FP-R used in the labeling experiments, the TAMRA-functionalized inhibitors are the first ABPs reported for the rhomboids AaROM, AfROM, BsYqgP, HiGlpG and VcROM.

Most of the selective inhibitors included in the heat map were β-lactones. These compounds had been for the first time identified as rhomboid inhibitors in the Rhomboid FluoPol ABPP in part one of the results section. The β-lactones are structurally related to the known β-lactam rhomboid inhibitors [82]. Both molecule classes are based on a four-membered rings, with the β-lactones oxygen in the 1-position being replaced by a nitrogen in the β-lactam structure. For the β-lactam inhibitor L29 a crystal structure of the rhomboid-inhibitor complex has been reported [82]. Due to the localization of the substituent on the 1-position of the lactam-ring in the proposed P2'-pocket, this particular group has been indicated in the literature to be responsible for selectivity [82] (Figure 32A). In contrast to this, the β-lactones identified to inhibit different rhomboids in the gel-based ABPP fingerprint, contain a substituent in the 3-position, that might be responsible for selectivity (Figure 32A). Both compounds react with the active site serine leading to a ring opening.

Crystallization experiments with β-lactones conducted by a collaborating scientist had so far not resulted in crystals usable for x-ray structure analysis. In order to still be able to speculate on the orientation of the β-lactones in the active site, both the β-lactam L29 and the β-lactone **48** were docked into the active site of EcGlpG (Figure 32B).
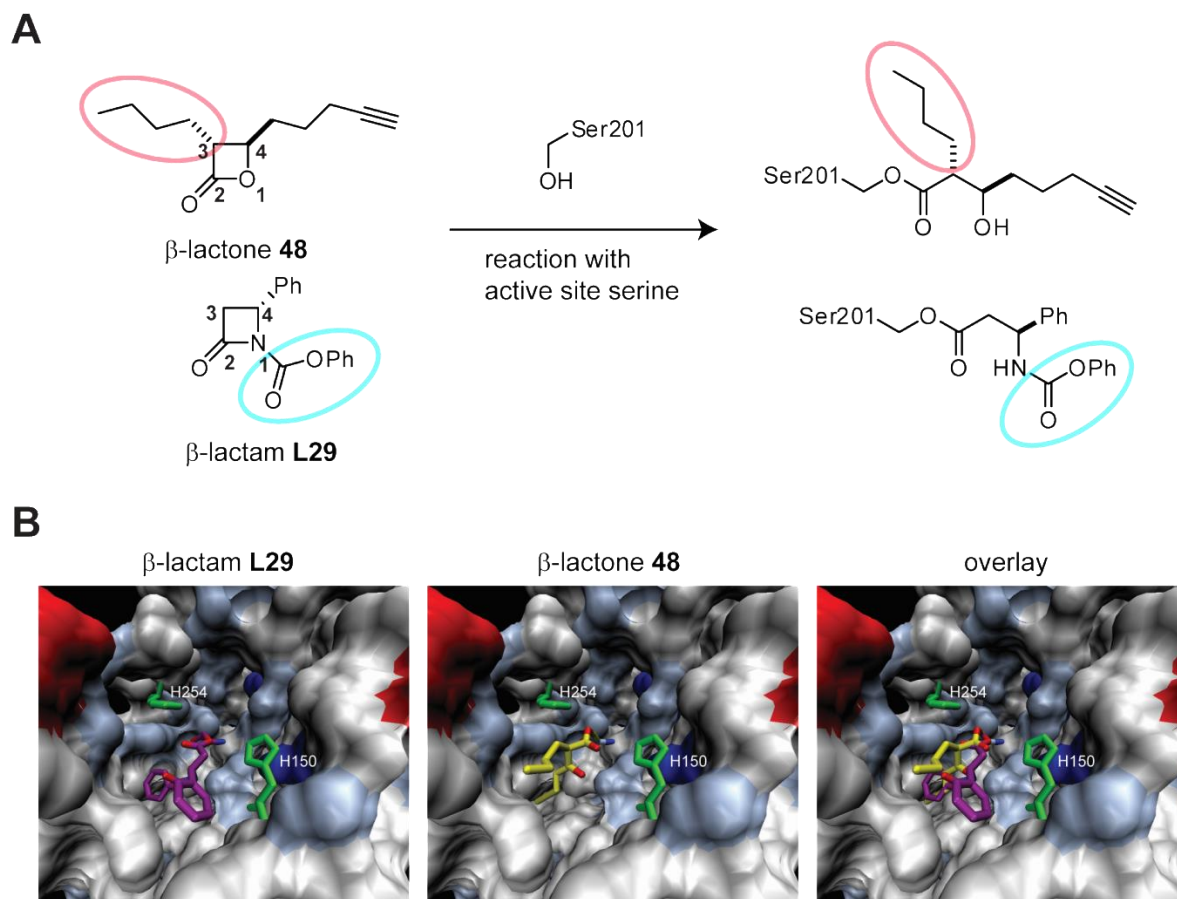
**Figure 32 Docking of LacG2 into the EcGlpG active site.** (A) The hit compound **48** from both the FluoPol and the fingerprint screen is a β-lactone, and structurally related to the known rhomboid inhibitor L29, a β-lactam, for which a crystal structure in EcGlpG has been published. Both react covalently with the active site serine of the rhomboid protease, leading to a ring opening of the structure. Indicated in blue for L29 and red for **48** are the side chains, that might be the selectivity elements. (B) Docking of the inhibitor into the active site of the rhomboid EcGlpG using AutoDock Vina. For L29, the 1-substituent interacts with the proposed S2' pocket. Note that the carbonyl group is pointed away from the oxyanion hole. **48** is positioned in the active site so that the 4-substituent interacts with the proposed S2' pocket. Note that in this structure the carbonyl group points towards the oxyanion hole, like the substrate would. While the 4-subsitutent of L29 protrudes between TM2 and TM5, the 3-subsitutent of **48** points towards a small hydrophobic patch on TM5.

Satisfyingly, the docked β-lactam L29 had the same orientation as in the crystal structure, indicating that the docking itself worked. When docking the β-lactone **48** into the active site, a couple of differences compared to the orientation of L29 were noticeable.

The β-lactam's carbonyl group, which resembles the acyl intermediate formed during substrate cleavage, was pointing away from the oxyanion hole, formed by several residues including H150 (in green). In contrast to this the β-lactone's carbonyl group was pointing towards the oxyanion hole, much like a substrate would.

Furthermore in L29, the phenyloxycarbonyl substituent at the 1-position of the lactam ring, which was suggested to be responsible for the inhibitor selectivity, interacted with a pocket that is proposed to be the S2' cavity [96]. The β-lactone **48** lacks this substituent, as it has an oxygen instead of a nitrogen at the 1-position in its ring structure. This is why for **48** the alkynyl substituent at the 4-position fills the S2' cavity, overlaying for most parts with the phenyloxycarbonyl group of the β-lactam. The second substituent on the 3-position of the β-lactone, that might be responsible for the selectivity of the compound as discussed above, points towards a small hydrophobic patch on TM5. In contrast, the second substituent of the β-lactam, a phenyl group at the 4-position, protrudes through between TM2 and TM5 (Figure 32B). The β-lactones seem to be flexible enough to adopt a conformation more similar to a substrate, despite their lack of a substituent at the 1-position.

### 4.3.3. Auto-processing of PsAarA and VcROM

During the course of the fingerprinting experiments, a recurring phenomenon was observed: multiple bands for the rhomboids PsAarA and VcROM (see also Figure 27, page 76). The observed bands had lower molecular weights than the expected full length rhomboids, but where still labeled by FP-R. A similar occurrence had been reported previously for the rhomboid EcGlpG with the probe EK2, which caused a rhomboid cross-link resulting in a double band in the gel [97]. In order to test whether also in this case the multiple bands were caused by the probe, PsAarA and VcROM were incubated with DMSO or FP-R and visualized by both fluorescence (for activity) as well as a by western blot or Coomassie stain respectively, for the overall detection of rhomboid (Figure 33A and B). The double band for PsAarA and the multiple bands for VcROM were visible in both detection methods, indicating that the multiple bands were not caused by reaction with the FP-R probe.
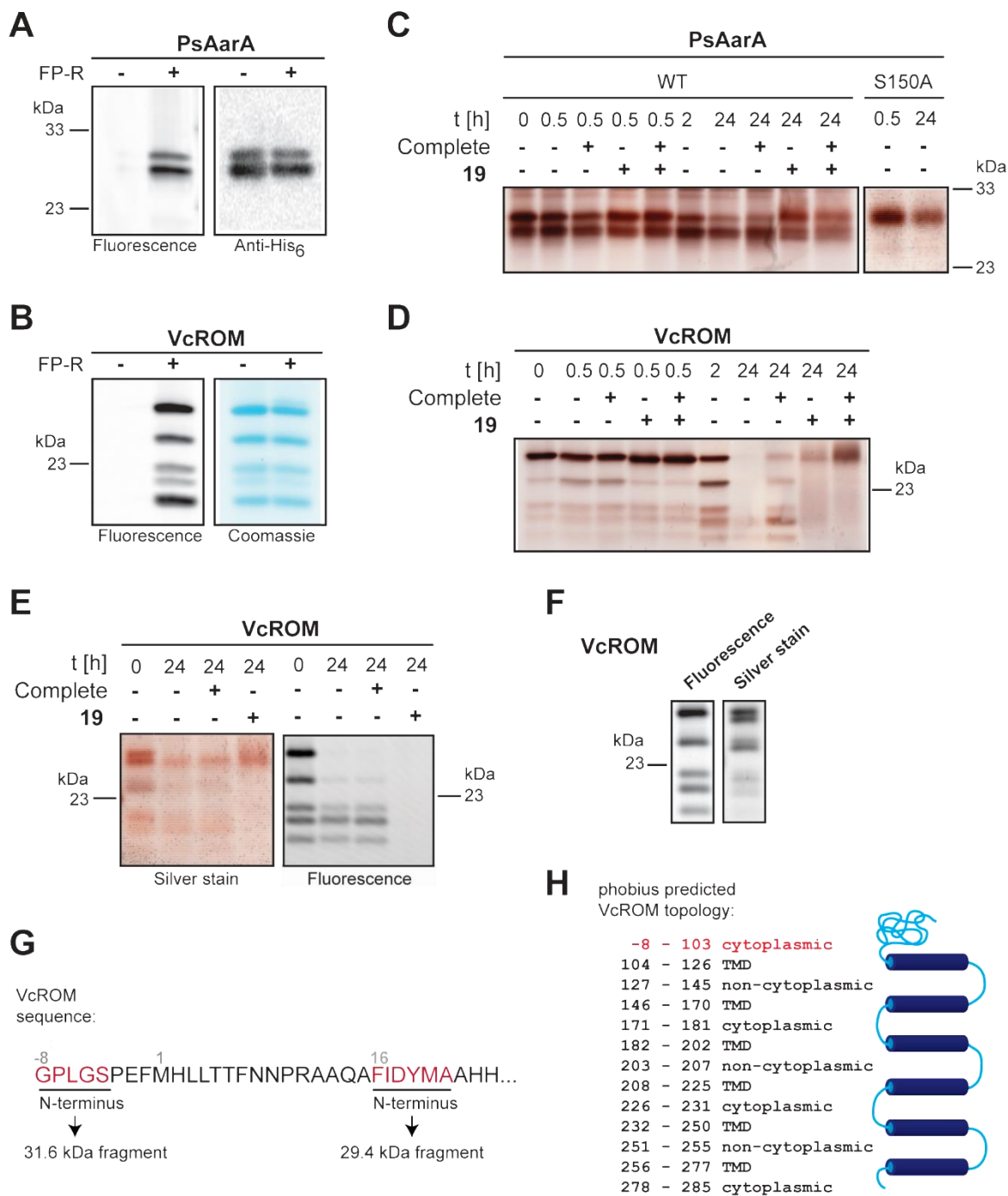
**Figure 33 Investigation of the lower bands observed for PsAarA and VcROM.** (A,B) The rhomboids PsAarA and VcROM were reacted with DMSO or FP-R and visualized on a fluorescent gel as well as with western blot or Coomassie stain respectively. Catalytically active bands were detected that ran lower than the bands containing the full-length rhomboids. (C) PsAarA WT and its S150A mutant were incubated at 37 °C with DMSO, complete protease inhibitor tablet, or the rhomboid specific inhibitor **19** for different times and visualized on a gel by silver stain. (D) VcROM was incubated at 37 °C with DMSO, complete protease inhibitor tablet, or the rhomboid specific inhibitor **19** for different times and visualized on a gel by silver stain.

87

(E) VcROM was incubated at 37 °C with DMSO, complete protease inhibitor tablet, or the rhomboid specific inhibitor **19** for 0 or 24 h, and subsequently labeled with FP-R for 2 h, and visualized on a gel by fluorescence and silver stain (F) VcROM was incubated at 37 °C for 2 h with FP-R and visualized on a gel by fluorescence and silver stain. (G) Overview of the N-termini identified by Edman-degradation. (H) The topology of the recombinantly expressed VcROM predicted by Phobius [151, 180].

Another possible explanation for additional lower gel bands could be (self-) digestion of the rhomboids leading to active truncated forms. To test this hypothesis, PsAarA and VcROM were incubated for different times at 37 °C in the absence or presence of a general complete protease inhibitor tablet (labeled "complete") and the rhomboid specific inhibitor **19** (Figure 33C and D). It is known that rhomboids are not inhibited by the complete protease inhibitor tablet, so it was reasoned that they would make a good control for non-rhomboid background-protease cleavage. Since a mutant version of PsAarA was available, it was included in this experiment.

For PsAarA WT (Figure 33C), double bands were visible as expected. The upper gel band corresponded to the full length PsAarA and was growing weaker over incubation time in samples not inhibited or inhibited only with the "complete" tablet. The lower (truncated) bands gained intensity where the upper bands lost intensity. Addition of the PsAarA-inhibitor **19** could in contrast completely inhibit truncation over time, indicating that the effect observed was indeed auto-digestion. Notably, all 24 h samples showed an overall weaker gel band intensity, probably due to protein aggregation by prolonged heat exposure. In contrast to the PsAarA WT, the PsAarA S150A mutant showed only the upper gel band and did not change in appearance after a 24 h incubation except loosing overall intensity, again probably due to prolonged heat exposure. This shows that PsAarA is produced as the full length form (upper band), and only gains the truncated form over time through auto-catalysis, as evidenced by the lack of truncation in **19**-inhibited and S150A mutant samples. The truncation probably already takes place during expression and purification, as the lower band is absent from the mutant sample.

In order to further pinpoint the location of the cleavage, the molecular weight of the two PsAarA bands in the SDS-PAGE gel was analyzed by ImageJ. These bands were calculated at 33.1 kDa (upper band) and 30.2 kDa (lower band), the expected size for the full length PsAarA was 33.5 kDa.

The difference of 2.9 kDa between the upper (full length) band and the lower (truncated) band amounts to about 26 amino acids, calculated with an average molecular weight of 110 Da per amino acid. The C-terminal $His_6$-tag could be visualized with an Anti-$His_6$-antibody in gel in both bands, which showed that the C-terminus is unprocessed, meaning that processing must have taken place at the N-terminus (Figure 33A). Taken together with the calculated difference of about 26 amino acids, this would mean that cleavage took place N-terminal, somewhere in the first TMD, as predicted by Phobius.

For VcROM, a similar pattern compared to the PsAarA could be observed (Figure 33D): Uninhibited samples or samples with the tablet showed an increased loss in the uppermost band, while the lower bands gained in intensity, with an almost complete loss of all bands after 24 h. Only the VcROM-inhibitor **19** inhibited degradation, and even after 24 h the inhibited sample still only showed a top band, although weakened by prolonged exposure to an elevated temperature.

First, to test whether indeed already truncated but still active rhomboid was labeled and not alternatively the labeled full-length rhomboid was truncated by unlabeled rhomboids, a time course experiment was set up, this time visualized by silver stain as well as fluorescence (Figure 33E): VcROM was incubated at 37 °C for 0 or 24 h and then labeled for 2 h by FP-R. After 24 h the full length species had completely disappeared in both fluorescence and silver stain, indicating there was no active, full length species left. Lower molecular weight bands containing truncated rhomboid meanwhile were still being labeled, and thus not only visible in the silver stain but also the fluorescence scan, indicating that these truncated rhomboids still contained an active serine-histidine dyad despite the processing.

Next, a fluorescent gel showing the active truncated bands of VcROM was additionally visualized by a very sensitive silver stain (Figure 33F). In the silver stain, it was possible to observe two inactive bands, not visible in the fluorescence scan. While the lower one was very weak, the upper one was clearly visible, situated underneath the topmost band. Comparison of the fluorescent gel and the silver stain showed that the topmost band visible in the silver stain contained active rhomboid, and was therefore also visible in the fluorescent gel. The band a little lower was not visible in the fluorescence, indicating that this truncated form is inactive.

In order to further elucidate whether the processing might have happened at the N-terminus, Edman degradation was conducted in collaboration with Kvido Strisovsky and co-workers in order to identify the N-termini of the two bands (Figure 33G). The identified termini corresponded to the expected N-terminus, eight amino acids prior to the starting methionine, and a phenylalanine, at amino acid 16, approximately 2.5 kDa further into the protein sequence. This experiment confirmed the suspicion that the lower bands might be truncated form, since it showed a truncated N-Terminus for the first lower band. The molecular weights of the various VcROM gel bands were calculated using ImageJ to be from the top: 31.6 kDa, 26.6 kDa, 22.2 kDa, 20.5 kDa, and 18.3 kDa. The expected molecular weight of the full length VcROM was 31.9 kDa, matching the calculated molecular weight of the topmost band. The difference between the topmost and the bottommost bands was calculated to be 13.3 kDa, indicating that all the truncations had happened within the N-terminal cytosolic domain and for the bottommost band, within the first TM helix. C-terminal cleavage would not explain the calculated numbers, since truncation of up to 13.3 kDa would cleave off the TM helix containing the catalytic histidine, meaning that the lower bands would lack the catalytic residues responsible for labeling by FP-R (Figure 33A).

The reason why N-terminal truncations might not affect VcROM activity can be better understood by looking at the topology: The recombinantly expressed VcROM protein was predicted to have a relatively long N-terminal cytoplasmic domain (Figure 33H). Analogous to EcGlpG which has been reported many times to be functional without its cytosolic domain [72], it seemed reasonable to assume that VcROM might likewise be unaffected by a truncation in that particular region. At the same time, it is puzzling that two of the truncations yield inactive rhomboid: two of the lower gel bands could not be visualized with the FP-R probe and are therefore inactive. The question why some truncations have no effect on the activity of the rhomboid, while others do, remains unclear at the moment and requires more investigations in the future.

Nevertheless, the experiments conducted here showed auto-catalysis of rhomboids into active and inactive truncated forms for the first time and provided evidence that this digest is caused by the rhomboids themselves.

## 5. Discussion

## 5.1. Rhomboid FluoPol ABPP assay

The Rhomboid FluoPol ABPP presented in this thesis, was adopted from the FluoPol ABPP assay developed by Cravatt and co-workers. In the past this assay has been successfully used with various soluble enzymes [143, 144, 146-149, 170]. The assay is in principle applicable to any enzyme that is targetable with an ABP. For the rhomboid protease EcGlpG, the best studied member of this family, two ABPs were reported by another group and the Verhelst group [97, 110]: The commercially available fluorophosphonate probe FP-R and the isocoumarin probe EK2, which was created by Cu(I)-mediated azide-alkyne cycloaddition of an isocoumarin inhibitor with the TAMRA fluorophore.

For both ABPs, activity-based labeling of EcGlpG was shown in this work (Figure 10), in agreement with already published work [97, 110]. EcGlpG WT activity-based labeling with EK2 led to a double band in fluorescent gel. This phenomenon has been described before in the literature [97]: the attack by the active site Ser201 on the isocoumarin's carbonyl carbon in combination with a secondary attack by His150 on the 4-position carbon leads to a doubly bound inhibitor and thus a crosslinking of the rhomboid, creating a faster migrating species in the SDS-polyacrylamide gel. Once the Ser201 hydrolyzes off, the rhomboid is no longer cross-linked but only singly bound to the inhibitor, and the relaxed protein structure gives rise to a slower migrating species. This lower migrating species also consists of rhomboid which is singly bound through Ser201 to the isocoumarin. Thus two species can be seen in the SDS-polyacrylamide gel. Despite this more complex gel band pattern, EK2 showed only labeling for uninhibited, active WT EcGlpG and as such was shown to be a suitable ABP for EcGlpG. FP-R showed a much stronger activity-based labeling of EcGlpG compared to EK2, as can be expected due to the much more reactive fluorophosphonate warhead. In the end both ABPs could be confirmed as suitable probes for EcGlpG, that only label active but not inactivated or inactive rhomboid species.

91

In principle both ABPs were suitable for the FluoPol ABPP, with the freedom to choose the one that gave the best signal-to-noise ratio in the FluoPol, and the other ABP for secondary confirmation experiments in SDS-polyacrylamide gels. Comparison of both ABPs in the Rhomboid FluoPol ABPP showed that FP-R gave rise to a more robust and stable polarization signal, probably due to its higher potency and reactivity. It was thus decided to use FP-R for the FluoPol assay, and the other ABP, EK2, for the secondary confirmation experiments in gel. Having a second ABP available was insofar fortunate, as utilization of two structurally different probes for screening and confirmation experiments eliminates false positives due to probe effects. This is why for the confirmed hits from the Rhomboid FluoPol ABPP a bias due to the probes can be disregarded.

Up to the start of this work the assay had never been used on membrane proteases, but only on soluble enzymes [143, 144, 146-149, 170]. Membrane proteases are more challenging to work with, as they require solubilization by a detergent, which complicates this highly sensitive assay: as it turned out during the optimization experiments for the Rhomboid FluoPol ABPP in this work, the FluoPol measurements are highly sensitive towards the detergent and its concentration. The detergent DDM for example, which is with few exceptions the detergent of choice for any rhomboid experiments, disrupted the polarization signal so much that positive and negative controls were indistinguishable.

As a consequence the first optimization steps were aimed to find the ideal detergent and concentration that would create a stable polarization signal. While lowering the detergent concentration in general improved the polarization curves (Figure 11), addition of a non-ionic copolymer surfactant, Pluronic F-127, always greatly improved the polarization signals. This was probably due to the fact that this surfactant helps solving the hydrophobic ABP in the polar buffer solution, thus preventing unspecific sticking of the ABP to either well walls, other ABP molecules or the enzyme. Even with soluble enzymes, it is routinely used in the standard FluoPol ABPP, and because of its positive impact during the optimization experiments, has also been included in the Rhomboid FluoPol ABPP.

Further improvement to the polarization curves could be achieved by switching from the detergent DDM to Triton X-100. The latter has been used with rhomboids before and greatly improved the polarization signals, especially when lowering its concentration to around the CMC. While Triton X-100 was the detergent of choice for the Rhomboid FluoPol ABPP buffer, rhomboid purification was still performed with DDM, as this detergent gives excellent yield and a high percentage of active enzyme during rhomboid purification.

The remaining DDM in the purified rhomboid sample was then diluted 20-100 times below the CMC in the Triton X-100 containing FluoPol buffer. It thus had not observable negative impact on the polarization signal.

The test screen with known rhomboid inhibitors and non-inhibitors validated the ability of the optimized assay to correctly identify covalent rhomboid inhibitors (Figure 12). In principle both the ABP-binding curves as well as endpoint measurements can be used to identify inhibitors. For covalent irreversible inhibitors simple endpoint measurements are sufficient, while such an endpoint measurement, due to the utilization of an ABP, is not very suitable for reversible covalent and allosteric inhibitors: in order to prevent ABP-binding, inhibitors need to block the active site until the measurement is performed. Consequently, in order to detect such reversible covalent or instable inhibitors, the time-curve of the ABP-binding needs to be analyzed instead of only the end-point. This could be shown for compound **2** (Figure 12): in the beginning this compound blocked the active site and therefore binding of FP-R, but over time hydrolyzed off enabling FP-R binding to EcGlpG and thereby raising the polarization signal. This is an advantage of the Rhomboid FluoPol ABPP over a gel-based approach: The kinetics of probe binding can be observed in real time during the measurement, and difference in the binding kinetics of the probe to different enzymes can be observed in the slope development. For the purpose of finding irreversible and stable binding inhibitors, as was the case in this work, it is sufficient to analyze the polarization value at a given time point to distinguish between positive and negative samples. While the incubation can be performed in the POLARstar plate reader and the reaction monitored online, this step can as easily be performed in an incubator and only the single point measurement has to be conducted in the plate reader.

The optimal time point for evaluating the polarization results, 4 h for the Rhomboid FluoPol ABPP, was determined by quantifying the assay window, i.e. the space between the positive and the negative samples. This distance, quantified by the so-called Z'-factor (a parameter published by Zhang et al. that shows the suitability of an assay for HTS [153]), confirmed that the Rhomboid FluoPol ABPP was very robust and reliable, as indicated by the calculated Z'-value of 0.8 - 0.9 at the 4 h time point (Figure 13). As defined by the authors Zhang et al., any assay with an Z'-value above 0.5 can be considered to be an excellent assay, with a perfect assay with an ideal separation of negative and positive samples reaching 1.0. The calculated 0.8 - 0.9 of the Rhomboid FluoPol ABPP can be therefore considered to testify that this is an excellent assay for the screening of rhomboid inhibitors.

Due to these excellent Z'-values, the optimization of the Rhomboid FluoPol ABPP was halted at this point, as the conditions were suitable for an actual inhibitor screening. While in principle this assay can be automated and run as a HTS with tens of thousands of compounds, for this work a focused library consisting of isocoumarins [172], phosphonates, phosphoamidates, β-lactones [127, 173], β-sultams, epoxides, and thiiranes [174] was used, in which the compounds were likely to yield rhomboid inhibitors, due to fact that all structures contained an electrophile and some had previously been reported as serine hydrolase inhibitors. Indeed nine of a total of 85 compounds, corresponding to 11% of screened compounds, were identified as primary hits (Figure 14). Seven compounds could be confirmed in the secondary gel-based ABPP with the ABP EK2 and a fluorescent TatA substrate and shown to irreversibly bind to the rhomboid (Figure 15 and Figure 16). The two false positives were phosphonates that had in other studies already given false positive signals [181]. This illustrates how important a secondary confirmation of hits is.

The seven confirmed inhibitors contained isocoumarins, which are known rhomboid inhibitors, but also β-lactones, which are serine hydrolase inhibitors, but had never been described to also inhibit rhomboids (Figure 17). They therefore represent a novel structural group of rhomboid inhibitors, adding to the already known rhomboid inhibitor scaffolds: chloromethylketones [19, 72], 4-chloroisocoumarins [19, 71, 97], fluorophosphonates [69, 94, 110] and N-sulfonylated β-lactams [82]. The β-lactones are structurally related to the β-lactams, but possess an oxygen instead of a nitrogen at their 1-position.

This has implications on the substitution pattern: In β-lactones there can be no substituent at the 1-position (the oxygen), but at the 3- and 4-positions (see Figure 32A).

In order to roughly characterize their potency, an "apparent" $IC_{50}$ was determined using the Rhomboid FluoPol ABPP (Table 5). Ideally for inhibitor characterization, a substrate and not an ABP is used for kinetic determinations, with a $K_i$ determined for reversible inhibitors, and a $K_{obs}/[I]$ determined for irreversible inhibitors [182, 183]. In this work only limited amounts of rhomboid and inhibitor were available, and the only available substrate was cleaved very inefficiently. This is why it was decided that the determination of an apparent $IC_{50}$ by Rhomboid FluoPol ABPP would be a sufficient first estimation to quantify the potency of the inhibitors. In order to verify that the determined $IC_{50}$ values were not too far from values determined in another study that utilized substrates for the determination [97], an already characterized inhibitor was included as a positive control. This compound, **97**, inhibited within the same order of magnitude as in the reference assay, confirming that the apparent $IC_{50}$ values determined here are valid for a first impression of the potency. The isocoumarins were determined to inhibit in the low μM-range, as has also been reported in the literature for other isocoumarins against rhomboids [97]. The two β-lactones were one order of magnitude weaker than the isocoumarins, inhibiting in the same range as the structurally related rhomboid inhibitors, the β-lactams [82].

While isocoumarins are so far the most potent rhomboid inhibitors, they are also known to be non-selective, inhibiting multiple targets. The β-lactones in contrast, although weaker in potency, seemed to be more selective towards rhomboids in this work: Their potency against the two canonical serine proteases, bovine chymotrypsin and bovine trypsin, was much lower than against EcGlpG, with higher apparent $IC_{50}$s. As such while isocoumarins are more potent but less selective, β-lactones may prove to be the more selective and might therefore be more useful study tools, despite their lower potencies. Ideally in the future, a combination of the strengths of both inhibitors scaffolds may provide a selective and potent rhomboid inhibitor. For the moment though, despite their lower potencies, the two novel β-lactones can already be used as research tools, for use in regular ABPP and even as novel ABPs in the Rhomboid FluoPol ABPP:

Due to their alkyne handle, the β-lactones could be used successfully as ABPs in a tandem labeling experiment (Figure 18), further confirming that their binding to the catalytic site is indeed a covalent mechanism (Figure 34).
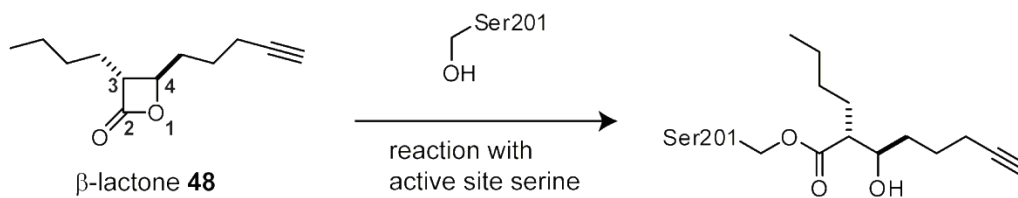


**Figure 34 Mechanism of β-lactone-binding to the rhomboid.** The reaction of the β-lactone **48** with the active site residue Ser201 of the rhomboid EcGlpG leads to a ring-opened structure.

As a whole, the work presented here illustrates that the Rhomboid FluoPol ABPP is a powerful, HTS-compatible new screening assay that does not require a substrate, but can identify irreversible active site inhibitors. It has already been optimized for use with the rhomboid EcGlpG and can easily be adjusted for the screening of other rhomboids in the future. Of the inhibitors found with this assay, two belonged to a novel structural class, adding the β-lactones to the small selection of already known rhomboid inhibitors. Due to their alkyne handles they also represent novel ABPs that can be added to the rhomboid experimenter's toolkit.

## 5.2. Inhibitor screening in proteoliposomes

The proteoliposomes were created in this study to investigate the influence of the rhomboid environment on the inhibitor screening results. The first hurdle was to create proper proteoliposomes of defined compositions, consisting only of a selection of lipids and active rhomboids. The lipids were chosen according to experiments in the literature, which showed that while surprisingly EcGlpG is inactive in its own membrane, it is active in a selection of other lipids [107]. The lipids chosen for this work, POPC, Soy-PI and DOPE, are a compromise between a composition somewhat resembling the *E.coli* membrane and lipids reported to result in rhomboid activity. Only recently, and after this work had been almost completed, the same group reported data which showed that EcGlpG is after all active in the *E.coli* membrane [64].

While rhomboid-containing liposomes have been reported in the literature, the preparation method did not seem ideal for investigating environmental effects on rhomboid inhibition: The previously reported method employs rapid dilution of mixed micelles to below the CMC of the detergent DDM [64, 107]. While this is a valid method, it does not guarantee that all detergent molecules are removed from the liposome: not only might there be still detergent molecules left in the proteoliposomes, but they might also preferentially localize next to the reconstituted rhomboid, as has been observed for reconstituted y-secretase (personal communication, Prof. Dr. Harald Steiner, DZNE, Germany). If this were indeed the case, effects observed on rhomboid inhibition might be due to a detergent belt surrounding the rhomboid within the liposome, and not due to the lipids themselves. This is why it was essential to choose a liposome preparation method that would as completely as possible remove the detergent from the mixed-micelles.

One well established method is the removal of detergent by dialysis. For the successful dialysis the detergent in question must be dialyzable, which is not the case for the routinely used detergent DDM. Experiments performed in this work showed that alternatively also CHAPS and OG can be used as detergents (Figure 19): while both render the rhomboid EcGlpG inactive in their micelles, these detergents are able to produce liposomes with actively reconstituted EcGlpG.

Indeed the fact that the rhomboids regain activity during reconstitution, confirms that most detergent is successfully removed during dialysis, as otherwise the rhomboid would be still inactive in the detergent-containing liposomes.

Of the two dialyzable detergents, OG was shown to produce the best looking liposomes, as estimated by fluorescence microscopy, and was thus used for the liposome preparation in this work (Figure 20). It should be noted here that DDM can be used for liposome experiments, in which potentially remaining detergents are of no relevance. It produced proper liposomes, although the sample itself seemed to be quite heterogeneous with many lipid aggregates in addition to the liposomes. CHAPS on the other hand produced solid spheres instead of lumen-containing liposomes, so that it is not advisable to use this detergent for liposome generation.

Most LUVs produced in this work ranged between 100 and 200 nm in size, independent of the detergent used for their generation, indicating that the lipid composition influences the curvature and ultimately size of the particles (Figure 21). While most liposomes in the sample were LUVs, some were larger and can be considered already as GUVs, which made it possible to assess them properly in the fluorescence microscope in the first place. Since these few giant liposomes were so much easier to visualize under the microscope, a fraction of the LUV sample was used for the generation of a whole GUV population by the dehydration-rehydration method. While there are more sophisticated GUV generation methods available, the ultimate reason for choosing this method was the straightforward procedure and requirement for only the most basic laboratory equipment. Indeed it was shown that GUVs produced with this method from the LUV sample contained active rhomboid (Figure 22), were surrounded by only one bilayer and thus unilamellar (Figure 23), ranged in the µm-size of giant liposomes and enabled activity-based profiling and inhibitor testing (Figure 24). These tests showed that GUVs containing active EcGlpG can be produced with this simple method and used for future visualization experiments by fluorescence microscopy.

Furthermore it was shown that the LUV-generation method is not limited to the *E.coli* rhomboid EcGlpG, but can also be used for four other rhomboids (Figure 25). For all other rhomboids, which did not reconstitute in an active form in this brief scouting experiment; future adjustments of the lipid composition may also enable their active reconstitution.

For the purpose of the work presented here, LUVs with reconstituted active EcGlpG were sufficient, and used in the following experiments.

Due to the rhomboid's hydrophobicity, inhibitor screenings must always be conducted in some sort of hydrophobic environment, which may be a micelle, a liposome, or a membrane. Most rhomboid studies and inhibitor screens have been performed in a micelle environment in the past, as the experimental setup is very easy and rhomboids can be directly purified into the micelles. While rhomboid-containing liposomes have been used a few times in the literature, their production is more laborious and a lot of rhomboid is lost during the procedure, which is why most often micelles are the environment of choice.

Despite the wide popularity of the micelle approach in the rhomboid field, it must be questioned whether this very artificial environment - compared to the natural membrane environment - alters results gained from experiments performed in micelles. While this might be true for all kinds of experiments performed in micelles, for this work, due to the focus on inhibitor screening assays, the influence of the hydrophobic environment on screening results was in the focus, i.e.: are the same inhibitors identified in a micelle and in a liposome environment? This question was addressed here using LUVs produced as discussed above and standard DDM micelles, in a gel-based ABPP assay (Figure 26). Comparison of the densitometrically estimated fluorescent gel band intensities of duplicate experiments showed that the rhomboid environment influenced the potency of inhibition, but not the inhibition itself: compounds that acted as inhibitors in a micelle environment also acted as such in liposomes and vice versa. This means that the environments influenced only the degree of inhibition.

The question whether this result is surprising or not is debatable: There is no doubt that the environment that surrounds an enzyme influences its structure, behavior and activity [184, 185]. This can also be seen in the results obtained here: The inhibitors behaved slightly differently in micelle and liposome environments, sometimes being more potent in the one or the other. The question here is, if these differences are due the rhomboid behaving differently in the two environments, or if these environments directly influence the inhibitors.

One indication in favor of the latter theory is that apparent $IC_{50}s$ determined for three exemplary inhibitors showed that there was no general preferable environment: While one inhibitor was more potent in micelles (**5**, Table 7), the other two were more potent in liposomes (**2** and **48**, Table 7). This might reflect interaction of the detergent or lipids with different structural properties in the inhibitors, making some more potent in one environment, and the others more potent in the other environment. If the environment caused the rhomboid itself to behave differently, for example rendering the rhomboid more active in micelles, inhibitors would be expected to behave the same in the same environment, i.e. all inhibitors should be more potent in liposomes.

Fully understanding this complex mechanism certainly exceeds the limitations of the method employed, and requires further work in the future. However, the experiments nicely show that inhibitors are correctly identified as such in both micelles and in liposomes, so that for the purpose of rhomboid inhibitor screening, the environment the assay is performed in is irrelevant. This finding can be confirmed by the fact that two separate recent rhomboid kinetic studies, performed either in liposomes or in micelles, were generally in very good agreement, further illustrating that the influence of the environment on rhomboid activity might be less important for crude laboratory studies [64, 102]. This does of course not state anything about the influence of the lipid environment on rhomboid activity in vivo, which might be quite substantial and an important regulation mechanism. The experiments performed here show that inhibitor screenings will offer qualitatively the same results whether performed in micelles or in liposomes.

As a word of caution it should be noted, that for the correct assessment of the inhibitor potency, special care needs to be taken in regard to the environment as well as the kinetic measurement technique. But again as in this work only a crude estimation of inhibitor potency was desired in addition to the identification of inhibitors, the much easier to handle micelle environment seems to be quite sufficient for these purposes. As such both Rhomboid FluoPol ABPPs, as well as regular gel-based ABPPs, can be performed in micelles without any negative impact on the screening results.

## 5.3. Gel-based ABPP of rhomboid inhibition

The initial purpose of the inhibitor fingerprinting in this thesis was to create a rhomboid fingerprint panel, in which the inhibitor profiles of various rhomboids of prokaryotic, eukaryotic, and archaean origins can be easily compared.

The basis of such a comparative gel-based competitive ABPP study was the ability to label all 13 recombinantly expressed and solubilized rhomboids with an ABP (Figure 27). While it seems little surprising that a serine hydrolase-reactive probe such as FP-R would label not only EcGlpG, but also 12 other rhomboids from various organisms, the implications of this seemingly trivial experiment are more profound. It nicely demonstrates the power of ABPs as research tools: At this point there is no other method available - no substrate, antibody or similar entities - that would allow probing the activity of 13 different rhomboids with one and the same testing system. ABPs are presently the only way to assess the activity of rhomboids that do not cleave known substrates.

With the aptitude of FP-R to label all 13 rhomboids demonstrated, the next step was the competitive ABPP of 51 small molecules against the rhomboids in duplicate measurements (Figure 28). While more laborious compared to the Rhomboid FluoPol ABPP, the experiments were quite straightforward and the results already visible from the raw gel data.

For easier data analysis, the fluorescent gel band intensities were quantified densitometrically, normalized against the WT signal and visualized in a heat map (Figure 29). The advantage of transforming the gel data into numerical values was that this enabled a simple sorting and clustering of the inhibitors and rhomboids respectively in the heat map.

Interestingly, the inhibitors, sorted based on their inhibition pattern, grouped according to their chemical scaffold into isocoumarins and β-lactones, and furthermore into groups of inhibitors with selectivity, without selectivity (bad inhibitors) and into pan inhibitors (inhibiting almost all rhomboids) (Figure 29B). The sorting illustrates which chemical properties promote selectivity in rhomboid inhibitors, since most selective inhibitors were either isocoumarins or β-lactones. Especially noteworthy here are the two pan inhibitors, **2** and **21**, that are able to inhibit almost all rhomboids.

Further investigation into common structural properties may elucidate some common architectural properties in the rhomboids - especially when contrasted to features in selective inhibitors, which direct them towards only one or two targets, as this might help future efforts in the development of selective rhomboid inhibitors.

The clustering of the rhomboids based on their inhibitory profile showed that while the eukaryotic rhomboids share a more similar inhibition pattern, the overall similarity of the inhibitor pattern between all rhomboids is low. This indicates that rhomboids have different preferences for inhibitors, and may be a good sign for the future development of highly selective inhibitors: Since rhomboids seem to be very specific in their susceptibility towards different inhibitors, it is reasonable to assume that inhibitors can be targeted towards a single rhomboid in the future.

The comparison of the inhibitor profile clustering with a phylogenetic clustering illustrates that there is no correlation between sequence similarity and similarity in the active site architecture, as indicated by a similar inhibition pattern (Figure 29C). This is not very surprising, as the overall sequence identity of all rhomboids in this screen is low, and conserved active site architecture over such an evolutionary distance would be surprising. Nevertheless, the three eukaryotic rhomboids cluster together in both trees, showing that they are not only related more closely, but are also susceptible to similar inhibitors. In conclusion the comparison shows that no deductions based on the inhibition profile can be made on evolutionary relationships - especially the prokaryotic rhomboids cluster differently in both trees.

The fingerprint itself identified multiple novel inhibitors, which is especially noteworthy for the not well studied rhomboids. Comparison of the pan inhibitor **2** apparent $IC_{50}$s showed that while this compound inhibits 12 out of 13 studied rhomboids, the potency ranges within two orders of magnitude, between 1-100 µM, proving that the susceptibility of the rhomboids to one and the same inhibitor differs (Figure 30). Both pan inhibitors **2** and **21** were shown to inhibit within the same order of magnitude, although in almost all cases, **2** was estimated to be more potent, as indicated by a lower apparent $IC_{50}$ (Table 8).

Four selective inhibitors, one isocoumarin and three β-lactones, were more closely analyzed (Table 9). Each inhibits only a single rhomboid, with the exception of **48**, which inhibits EcGlpG and TmROM with about the same potency. The fact that EcGlpG and TmROM are inhibited by the same β-lactone to about the same degree is noteworthy, since their overall inhibitor profile similarity is relatively low (Figure 29B). As such it might be interesting to investigate in the future, why these seemingly different rhomboids share a preference for this particular inhibitor structure.

Another interesting finding of the apparent $IC_{50}$ determination is that the selective isocoumarin inhibitor **6**, which inhibits HiGlpG, inhibits within the same order of magnitude as β-lactone and β-lactam rhomboid inhibitors, and not one order of magnitude lower, in the single digit μM range, as is common for isocoumarin rhomboid inhibitors. This phenomenon will certainly require more experiments, but it is interesting to speculate if the higher selectivity of this particular isocoumarin comes at the cost to its potency.

Yet another noteworthy apparent $IC_{50}$ value is that of the β-lactone **45** which inhibits AfROM at only 5 μM, a value common for isocoumarins. It seems that this particular β-lactone is as potent as the most potent rhomboid inhibitors, the isocoumarins, and as such may offer insights into how β-lactones can be made more portent in the future.

Many of the inhibitors identified for the various rhomboids could be turned into ABPs by tandem labeling of their alkyne handle with a TAMRA azide (Figure 31). This shows that tandem labeling is a powerful technique that can be used on various rhomboids and might be a helpful method in future research. Furthermore, this experiment confirms almost all of the alkyne-containing inhibitors as ABPs, which for many of the studied rhomboids, are the first ABPs reported for them – besides the FP-R probe.

The docking experiment performed with both the β-lactone **48** and the structurally related β-lactam L29 provided a first insight into the inhibitor binding of the β-lactone to the active site (Figure 32): While the β-lactam was docked exactly as in the reported crystal structure, with an "unnatural" conformation of the carbonyl group which is turned away from the oxyanion hole, the β-lactone docked in a more substrate-like conformation, with the carbonyl group pointing towards the anion hole.

One might speculate that this more "natural" binding, that more closely resembles the substrate, could be utilized in future studies that employ "substrate-like" inhibitors instead of a real substrate for rhomboid-substrate crystal structures.

In conclusion the inhibitor fingerprint ABPP uncovered novel inhibitors and ABPs for many poorly studied rhomboids. The newly discovered rhomboid inhibitors, the β-lactones, are mostly less potent compared to isocoumarin inhibitors, but as a whole seem to be much more selective. Docking of a β-lactone into the EcGlpG structure revealed that these inhibitors, unlike the related β-lactams, bind in a conformation more closely resembling the proposed binding of the natural substrate.

During the course of the experiments, lower molecular weight gel bands were observed: one for PsAarA, and multiple for VcROM. Closer analysis of this phenomenon revealed that these lower gel bands represent truncated forms of the full length rhomboid (Figure 33). These gel bands are not only visible in western blot and Coomassie or silver stain, but also in a fluorescent gel, due to activity-based labeling with fluorescent ABPs. The important issue here is, whether the truncation happens before or after activity-based labeling: if the truncation happens prior to the activity-based labeling, this means that the truncated rhomboid fragments are still catalytically active. On the other hand it is also conceivable that the full length form gets labeled and only then truncated; so that all truncated forms inheritably carry the ABP fluorescent label.

For VcROM, the question can already be answered: Samples that are already completely truncated, i.e. in which no full length rhomboid is present anymore, can still be labeled with the ABP. They show the same labeling pattern of the four lower gel bands as can be observed in a sample that is immediately labeled with the ABP, while there is still full length rhomboid present. This proves that the truncated forms of VcROM are still catalytically active.

For PsAarA, further experiments are required, but there is already one observation that points toward the fact that also the lower, truncated rhomboid band is active: PsAarA is already a double band prior to labeling, and both bands get strongly labeled by the probe, indicating that truncation does not impair rhomboid activity. Future experiments will completely settle this matter.

One statement that can already be made about PsAarA truncation is that it happens N-terminally, as the truncated form can be visualized on a western blot using the C-terminal His-tag.

For VcROM, the question whether truncations happen N- or C-terminally could at least be partially addressed through the Edman degradation experiment: For the second to top gel band, corresponding to the longest truncation product, an N-terminus 23 amino acids further into the protein could be identified. Because of this it stands to reason that all other truncations also happen at the N-terminus. Furthermore, when looking at the VcROM topology, it makes sense that truncations would happen N-terminally, as there is a 111 amino acid large extra membranous domain on the N-terminus, in which also large truncations could happen without reaching vital areas in the rhomboid core.

Experiments presented here on both PsAarA and VcROM have shown that this truncation is susceptible to rhomboid-specific inhibition, but not to general protease inhibitors, that are known to be ineffective with rhomboids. This clearly illustrates that the truncation is caused by the rhomboid itself as a form of auto-cleavage, and not by other proteases that have been accidently co-purified.

The exact process of the truncation remains elusive: Is the truncation performed by the rhomboid protease on its own N-terminus or by a sister-rhomboid? And how is this achieved with the N-terminal domain localized on one site of the membrane, and the active site oriented towards the other site of the membrane? It is not clear at this point, whether in vivo and also during overexpression all rhomboids are oriented in the same direction, or if they have a random orientation. Only a presumed random orientation would easily explain how the N-terminal domain can be cleaved by sister-rhomboids, as this would put the N-terminal domains and active sites of other rhomboids on the same side of the membrane.

If the orientation were uniform, it would require some complex translocation of the N-terminal domain through the membrane to reach the active site for truncation. Unfortunately there is no experimental evidence what orientations the different rhomboids have in vivo. The topology prediction software Phobius predicts the N-termini of all 13 rhomboids of this work to be cytoplasmic.

While rhomboid auto-processing has never been described in the literature before, it is not an entirely new phenomenon: an in vivo truncation has been described for HsRHBDL2, which is required for rhomboid activity [186]. Additionally, searching through experimental documentation of multiple rhomboid researchers revealed that PsAarA appears as a double band during expression on most western blots and also in purified samples. This indicates that - at least for PsAarA - the truncation is not an in vitro effect of the experiment, but happens already during overexpression. If it is also a naturally occurring effect is unclear at this moment. Clearly, investigations into the auto-processing of rhomboids are only at the beginning.

# 6. Conclusions and Outlook

### *Rhomboid FluoPol ABPP*

In the work described in this thesis, a novel rhomboid inhibitor screening assay was developed: the Rhomboid FluoPol ABPP. In contrast to all other rhomboid screening assays, this assay is substrate-free and requires only an ABP for enzymatic activity probing. This is especially advantageous for rhomboids that do not - or only weakly - cleave the few available rhomboid substrates. The Rhomboid FluoPol ABPP has been adapted for use with rhomboids from an already published assay developed for soluble proteases. This was done by adjusting the detergent and its concentration, as these two factors are critical for the workings of the polarization measurements. The validity and robustness of this new assay was confirmed and determined to be very good. Furthermore in a mock-screen all tested known inhibitors were identified correctly. The assay was then employed for screening a small focused library consisting of 85 compounds. Potential hits were confirmed by gel-based competitive ABPP and substrate cleavage assay, and their binding mode confirmed to be irreversible.

As a result of the screen and confirmations, a couple of new inhibitors were discovered, among these an entirely novel structural class of rhomboid inhibitors: the β-lactones. These compounds, structurally related to the known rhomboid β-lactam inhibitors, showed similar potency as estimated from an apparent $IC_{50}$ determination. Utilizing their alkyne handles, they could be successfully used for tandem labeling by Cu(I)-mediated azide-alkyne cycloaddition. Taken together, these ABPs can be used as valuable research tools for various rhomboid experiments ranging from simple gel-based activity assays to localization experiments.

The Rhomboid FluoPol ABPP itself can easily be further adjusted in the future: while it has been established and optimized with the rhomboid EcGlpG, preliminary experiments have shown that for reliable and robust screening with other rhomboids, further optimization of the screening conditions and especially the rhomboid purification is needed. The most critical factor for a successful Rhomboid FluoPol ABPP is a high rhomboid concentration and large active fraction, so it is likely that the assay itself will not need many adjustments, but rather the rhomboid expression and purification - especially for the eukaryotic rhomboids.

At this moment, the Rhomboid FluoPol ABPP is ready for use with EcGlpG in an automated high-throughput set-up. Once other rhomboids give robust signals in the Rhomboid FluoPol ABPP, they can also be screened against large compound libraries. In contrast to the HTS-compatibility of the Rhomboid FluoPol ABPP, the secondary confirmation assays, by competitive ABPP and substrate cleavage, are at the moment gel-based and therefore low-throughput.

In order to establish a secondary confirmation assay amendable for HTS, the assaying platform has to be changed from SDS-polyacrylamide gel to a fluorescence reader: a known rhomboid Förster resonance energy transfer (FRET)-substrate [82] was synthesized using different fluorophores, and tested in a preliminary fluorescence experiment against bovine trypsin and 10 rhomboid proteases used in this work (Figure 35).
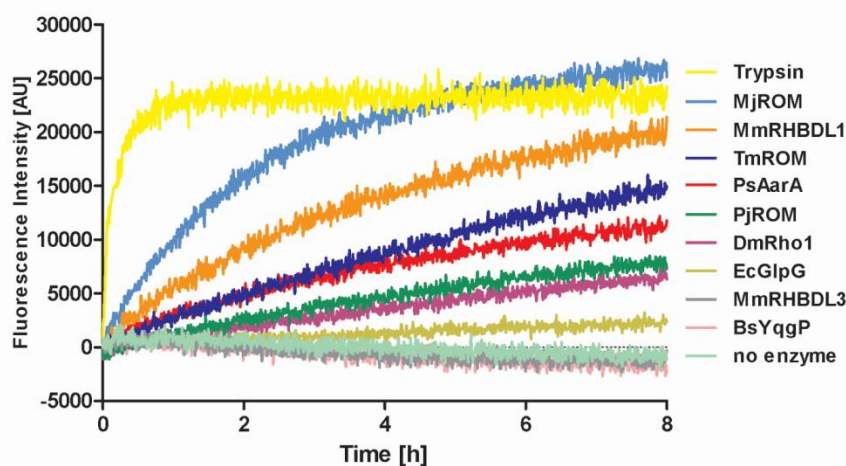


**Figure 35 Cleavage of a FRET-peptide by bovine trypsin and 10 different rhomboid proteases of prokaryotic, archaean, and eukaryotic origin.** 100 nM bovine trypsin or 1 µM of rhomboid protease was added to 70 nM FRET-peptide in FluoPol buffer. The cleavage reaction was monitored for 8 h at 37 °C. During cleavage, the fluorophore and the quencher on the FRET-peptide are separated, leading to a regain of fluorescence and thus an increase in overall sample fluorescence, which can be observed in a fluorescence plate reader.

Many rhomboids were able to at least weakly cleave this substrate, as indicated by an increase in fluorescence. Apart from the positive control bovine trypsin, MjROM and MmRHBDL1 were able to cleave the substrate relatively well, while MmRHBDL3 and BsYqgP could not cleave the substrate at all.

While this preliminary experiment shows that creating a substrate-based secondary confirmation assay is not an easy feat and will likely require work in the future, it also proves the underlying assertion of this work: most rhomboids do not - or if so only weakly - cleave available substrates, and as a consequence, a substrate-free screening assay - the Rhomboid FluoPol ABPP – is a valuable asset for future investigations of rhomboids other than the one or two well-studied members.

*Influence of the rhomboid environment on inhibitor screening*

In the second part of this thesis, the influence of the rhomboid environment on inhibitor screening results was investigated, by comparison of inhibitor screens performed in detergent micelles and liposomes. In order to create suitable proteoliposomes for this experiment, a tertiary lipid composition resembling the natural *E.coli* membrane was chosen. For proper removal of the detergent from the mixed-micelles by dialysis, OG was determined to be the most suitable detergent. The liposomes were determined to be LUVs of proper morphology by dynamic light scattering, TEM and fluorescence microscopy. The activity of the reconstituted rhomboids in the LUVs was successfully confirmed by gel-based competitive ABPP.

In preliminary experiments other rhomboids were reconstituted into LUVs as well, some of which were shown to be active. This is remarkable, as the conditions were not adjusted for the individual rhomboids, but the standard conditions optimized for EcGlpG were employed. For the rhomboids that could not be reconstituted in an active form into LUVs, it seems reasonable to assume that future optimizations of the lipid composition will enable successful reconstitution, as also other intramembrane proteases are influenced by the lipid composition [184, 185, 187]. Once reconstitution of active rhomboid is achieved, future experiments on rhomboids can - where needed - be performed in a lipid environment of controlled composition, which is more natural than a micelle.

For even better imaging of the liposomes by fluorescence microscopy, the dehydration-rehydration method was successfully used for the creation of GUVs. The morphology and size of the GUVs was analyzed by TEM and fluorescence microscopy, and the activity of the reconstituted rhomboid confirmed by gel-based competitive ABPP.

Using these GUVs, both rhomboid labeling with an ABP and inhibition by a β-lactone could be easily visualized under the fluorescence microscope. This has shown that the GUV preparation method employed here can be used in the future for experiments, in which the liposomes should have a size and curvature comparable to a cell.

For the investigation of the screening environments, EcGlpG was screened against 51 small molecules in either DDM micelles or LUVs. The screening data showed no dramatic difference in the results: all small molecules were identified as either inactive or inhibitors in both assays, and only the degree of inhibition differed between the environments. There was also no apparent environmental effect on the overall degree of inhibition: some inhibitors appeared more potent in micelles, while other inhibitors showed stronger inhibition in liposomes.

In conclusion the results of the environment experiments indicate that the environment of rhomboid inhibitor screening has no influence on the correct identification of inhibitors. The small differences in determined apparent $IC_{50}s$ for a single inhibitor are probably due to interactions between lipid and detergent molecules and the inhibitor itself. Due to this it can be assumed that rhomboid inhibitor screening assays can safely be performed in micelles, and no false positive - or negative - identification of inhibitors, compared to a screen performed in liposomes, is to be expected.

In the future, a comparison of these findings to screening data from a membrane environment will further elucidate if micelles can replace even a natural environment for fast and easy inhibitor screening. Such an experiment will require elaborate controls, as probe-penetration effects into the cell will have to be excluded from the screening results.

While not at all a complete investigation into this matter, a preliminary screening of EcGlpG in lysed *E.coli* membranes against 51 compounds has provided a first glimpse into the inhibition pattern in the natural *E.coli* environment (Figure 36).

**Figure 36 Heat map of the inhibitory profile of EcGlpG in three different environments.** EcGlpG in lysed *E.coli* membranes was screened against 51 compounds in a competitive ABPP. The fluorescent gel bands were densitometrically determined and normalized to 0% WT inhibition. Shown here is a heat map of the data obtained for the membranes and additionally for the micelles and liposomes as shown in figure 26. All three screens were performed in duplicates.

The heat map showed that most inhibitors were identified correctly in all three environments, with the exception of compounds **16** and **27**. These two were identified as inhibitor and inactive compound respectively by the membrane environment screen alone, in contrast to both the micelle and liposome screen, which determined the opposite for both compounds. At this point it is unclear whether this effect is truly due to the membrane environment or simply an effect of the membrane preparation method.

The preliminary experiment shown here indicates that the effects, if at all present, are minor, so that inhibitors that are identified in micelles are most likely also valid in a membrane environment. As such it seems irrelevant in which environment the inhibitor screen is performed in, as long as the identified inhibitors are afterwards tested rigorously in a more natural context. Future investigations into this may uncover not only more insights into the effect of the environment on inhibitor screening, but by proxy also into the effect the environment has on rhomboid activity. This may then lead to a better understanding of how rhomboid activity may be regulated in vivo.

*Rhomboid fingerprint and auto-cleavage*

The third part of this work aimed to create inhibitory fingerprints of 13 rhomboids from prokaryotic, archaean and eukaryotic origin. Due to the fact that not all of these rhomboids are able to cleave available substrates well, the usage of an ABP was the only way to conduct such an experiment. It was shown here for the first time that the ABP FP-R is able to label all 13 investigated rhomboids in an activity-dependent manner. The comprehensive screen in duplicates of these 13 rhomboids against 51 small molecules has not only provided an overview of the individual inhibition patterns, but has also identified new inhibitors and the first ABPs for many of the less well studied rhomboids. The fingerprint has furthermore uncovered the existence of rhomboid pan-inhibitors, compounds **2** (commonly known as DCI) and **21**. It was shown that the potency of these inhibitors ranges between two orders of magnitude for the different rhomboids, and that β-lactones generally, but not always, show potency comparable to β-lactams. As such they are often less potent than isocoumarins, but - based on the fingerprint - seem to be more selective towards individual rhomboids.

A simple docking experiment has shown that the β-lactones bind in a more natural manner in the active site compared to the β-lactams. This binding mode more closely resembles the assumed binding of a substrate, so that β-lactones might prove to be valuable scaffolds for creating crystal structures of rhomboid with pseudo substrate in the future.

While most β-lactones are not very potent at present, changing their substituents might make them more potent, while retaining their selectivity. Another interesting approach for future experiments could be the addition of the 3-substituents from the β-lactones to the 3-position of the β-lactams, thereby creating hybrid inhibitors with substituents at all three positions, which can be tuned for high potency and selectivity. If successful, such compounds would be the first selective and potent rhomboid inhibitors and undoubtedly valuable research tools and may further along even be used as lead structures for drug development.

The phenomenon of rhomboid auto-catalysis, which was discovered during the course of this work, might offer novel insights into rhomboid catalysis and regulation of activity. While investigations on this matter are still at the beginning, the first experiments conducted in this work have shown that rhomboid auto-catalysis is a cleavage reaction by rhomboids.

This cleavage reaction can be inhibited with rhomboid inhibitors and can lead to the progressive N-terminal truncation of rhomboids. The experiments presented here indicate that the truncated rhomboids are still active, proving that the N-terminal extra membranous rhomboid region is not required for rhomboid activity. Future experiments should be aimed to elucidate if this truncation happens also in vivo without overexpression, how the rhomboids are orientated in vivo, and if rhomboids cleave themselves or only sister rhomboids.

Future investigations will not only shed more light onto this exciting new phenomenon for rhomboids, but might even provide more insight into rhomboid cleavage, activity and regulation. More speculatively, it might turn out that not all rhomboids are produced in their active form, as has already been shown for HsRHBDL2 [186], but that a zymogen form could exist after all, regulating this highly versatile enzyme family.

### *Further directions from this work*

The rhomboids investigated in this study have been kindly provided by various labs and expressed recombinantly in *E.coli*. While rhomboid expression and purification is generally challenging, especially the eukaryotic rhomboids are very hard to produce. This is why only three eukaryotic rhomboids, DmRho1, MmRHBDL1 and MmRHBDL3, were investigated here. Ideally even more diverse rhomboid proteases should be subjected to inhibitor screening, fingerprinting and auto-cleavage analysis, as rhomboids from all origins might be relevant in understanding the mechanism and purpose of these unique family of enzymes. Eukaryotic and especially the human rhomboids are - due to their direct implications for human health - probably the most interesting rhomboids to study. This pertains certainly also to the non-protease human rhomboids, but from an inhibitor-centered point of view, the five human active rhomboids, HsRHBDL 1-4 and PARL, might be ideal candidates for the further continuation of the projects presented in this thesis.

While the function of HsRHBDL1 and 3 remain hitherto unknown, HsRHBDL2 has been implicated in wound healing through RIP of thrombomodulin [188], cell-adhesion modulation by ephrin cleavage [189], EGF activation [117], as well as down-regulation of the EGF receptor ErbB-1 by shedding [190].

HsRHBDL4 is involved in endoplasmatic reticulum-associated degradation (ERAD) through recognition of substrate ubiquitinylation and subsequent clipping within TM helices or luminal loops [77]. PARL, as explained in the introduction, is thought to be implicated in Parkinson's disease [60, 61, 113].

Clearly the discovery of inhibitors and the study of regulation and inhibition of these rhomboids would be beneficial and medically relevant. Inhibitors and ABPs which might be obtained through future experiments will serve as study tools and can help to uncover the biological function and mechanism of HsRHBDL1 and 3.

Since their discovery in 2001, many experiments have been conducted that have slowly started to unravel the function and implications of rhomboid proteases. In the next decade, the rhomboid field will probably move towards the potentially medically relevant rhomboids, by trying to further elucidate if and by which exact mechanisms rhomboids are involved in diseases, and how they might be used as potential drug targets. Simultaneously the focus will likely shift from the few well studied rhomboid proteases to other members of this family, including the inactive rhomboids, in the hopes of better understanding their overall functions and importance. Conducting experiments in liposomes or other environments will likely become more relevant, until research tools are available that allow studying rhomboids in vivo. As such it is important to provide highly potent and selective research tools to the rhomboid community, which can only be accomplished through continued work on rhomboid assays, inhibitors, ABPs, and other such tools. The next years will probably see great advancements in these areas.

# Appendix

## *Rhomboid fingerprint*

The gel-based competitive ABPP was performed in duplicate measurements and used as a basis for the heat map and clustering. The measurement data for each individual rhomboid are depicted below (Figure 37).
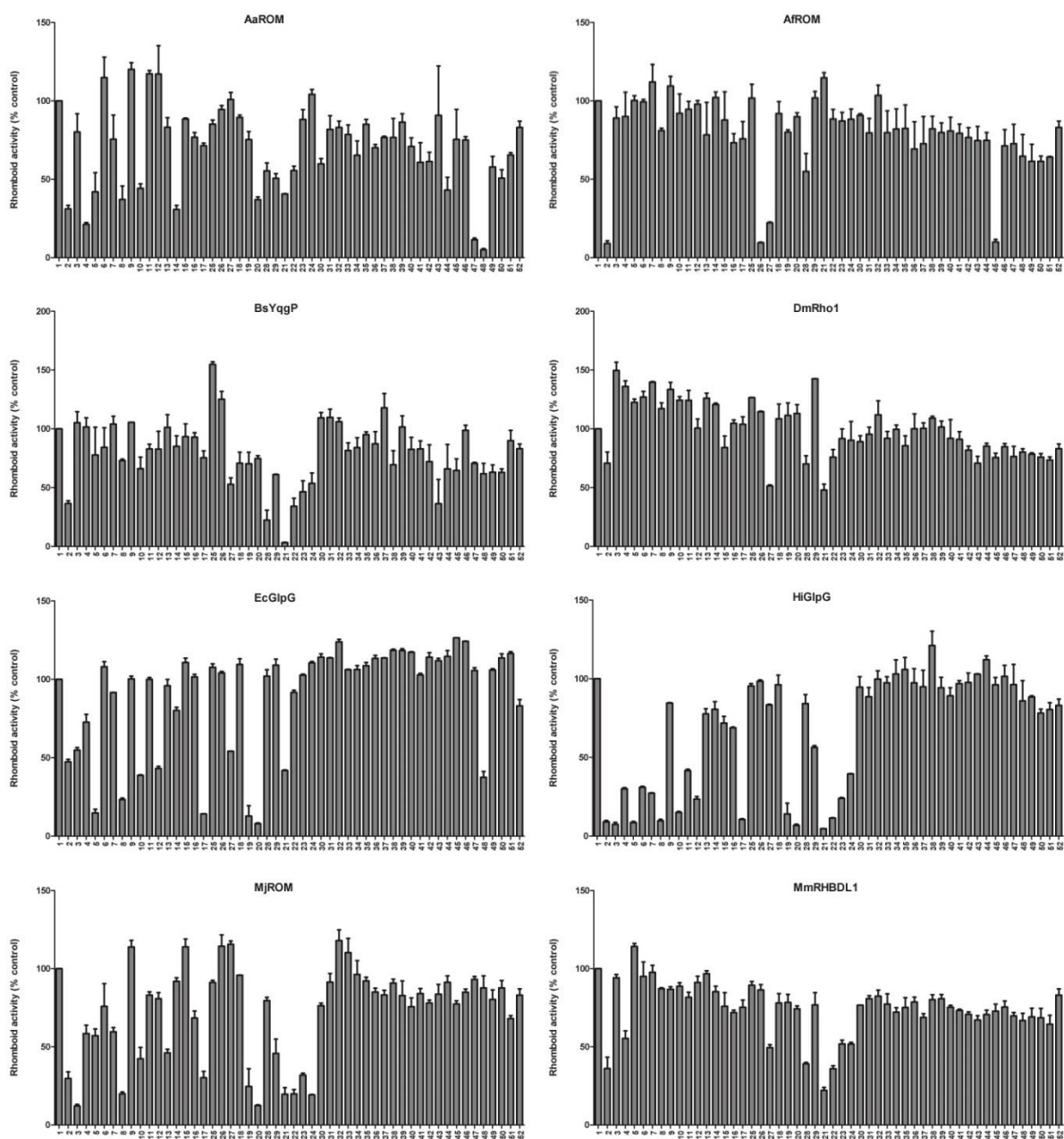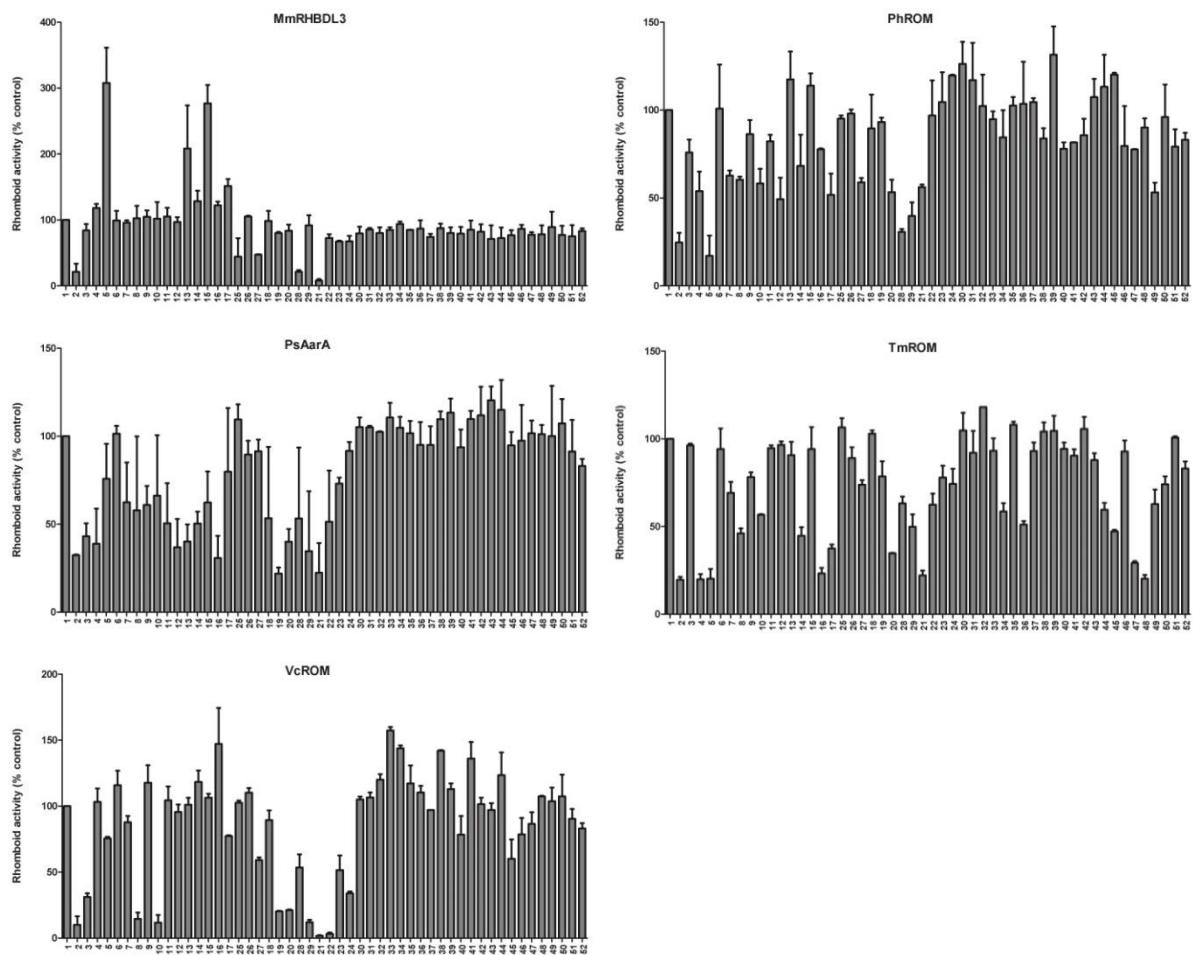
**Figure 37 Duplicates of inhibitor screens of 51 small molecules against 13 different rhomboids.**
Rhomboids were first incubated with 100 μM small molecule for 30 min and then with 1 μM FP-R for 2 h. The samples were visualized on a fluorescence SDS-polyacrylamide gel and the bands densitometrically evaluated with ImageJ. The intensity of the DMSO-incubated rhomboid sample (**1**) was set as the 100% reference. The average of duplicate measurements and the standard error are plotted in the graphs.

*Edman degradation*

For determination of the N-termini of VcROM, Edman degradation experiments were performed by Dr. Kvido Strisovsky and co-workers at the Institute of Organic Chemistry and Biochemistry AS CR in Prague, Czech Republic (Figure 38).
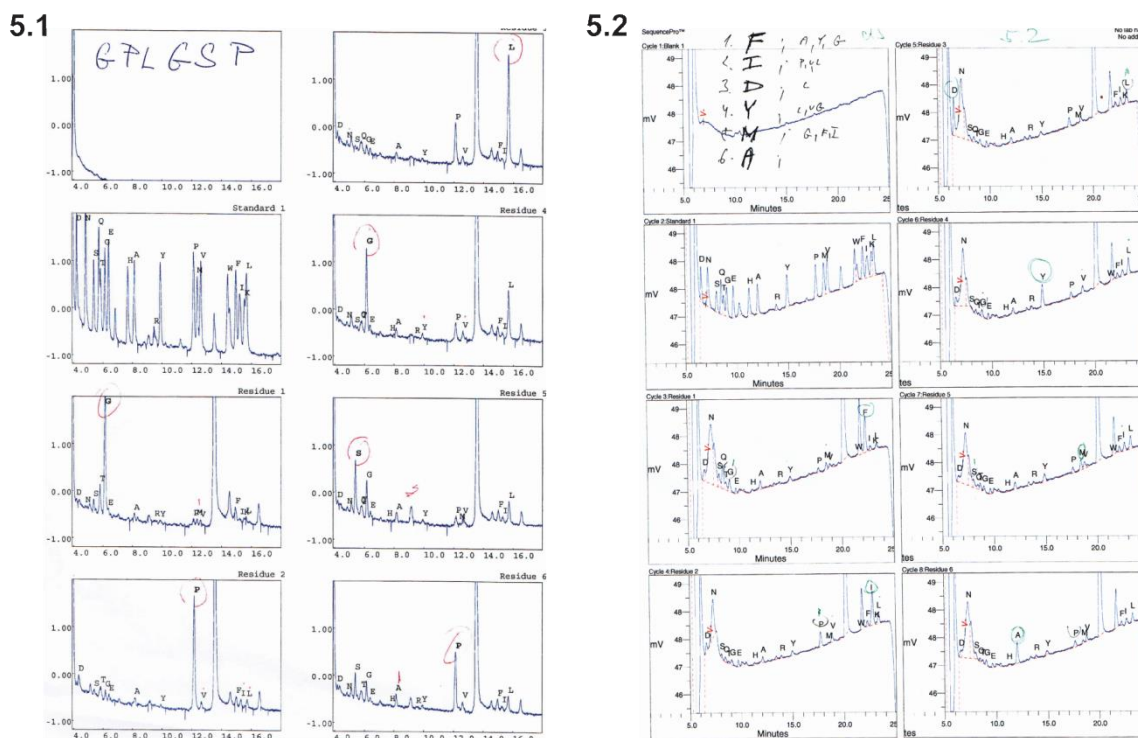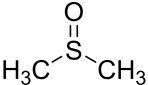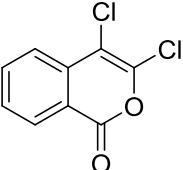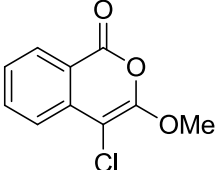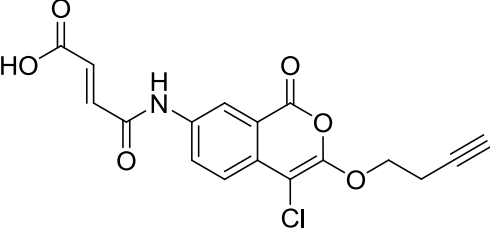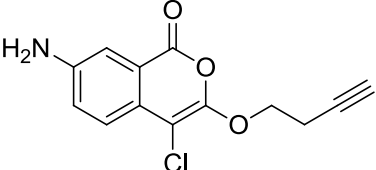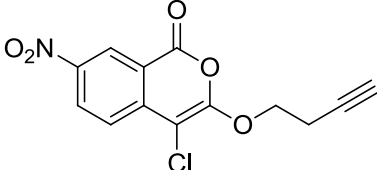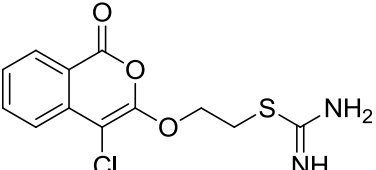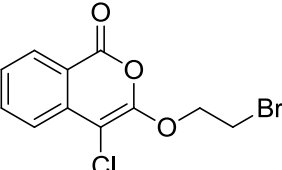


**Figure 38 Raw data of the Edman degradation of two VcROM samples.** The samples (5.1. and 5.2. correspond to the first and the second gel band from the top respectively) were reacted with phenylisothiocyanate and the stepwise fragmented N-terminal amino acids analyzed using the Procise Protein Sequencing System.

## Small molecules investigated in this thesis

The chemical structures and identification numbers of all molecules investigated in this thesis are depicted below (Table 10).

**Table 10 Chemical structures of all compounds used in the screens.**

| # (ID) | Structure | # (ID) | Structure |
|--------|-----------|--------|-----------|
| **1** (DMSO) | | **2** (DCI) | |
| **3** (S004) | | **4** (S005) | |
| **5** (S006) | | **6** (S007) | |
| **7** (S008) | | **8** (S009) | |

118

**9** (S119)
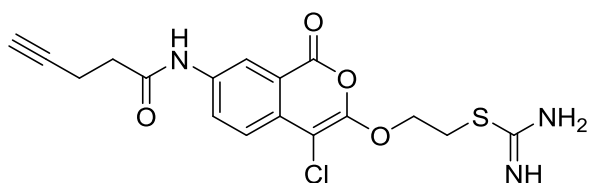
**10** (S011)
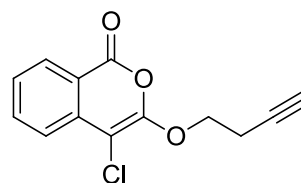
**11** (S012)
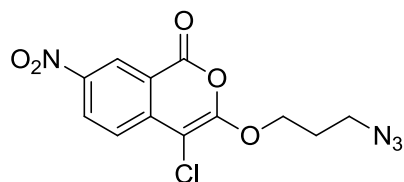
**12** (S013)
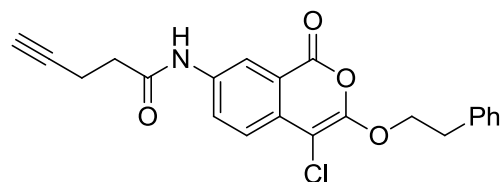
**13** (S014)
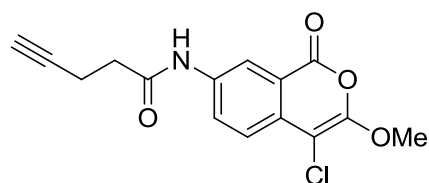
**14** (S015)
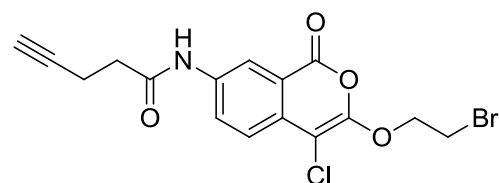
**15** (S017)
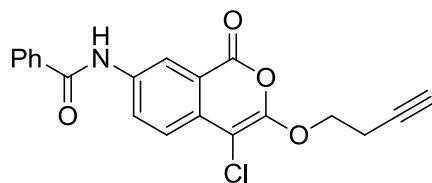
**16** (S019)
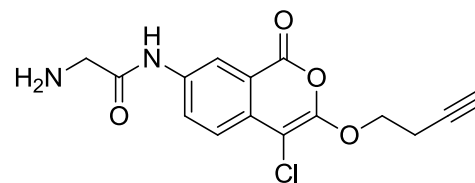
**17** (S020, JLK-6)

**18** (S035)

119
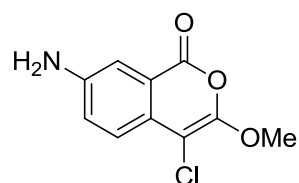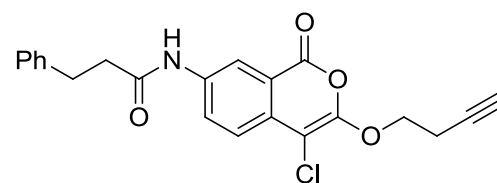
**19** (S036)
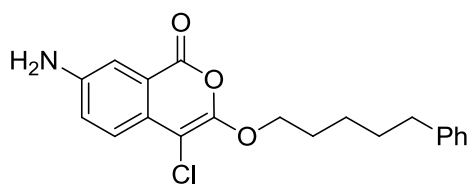
**20** (S037)
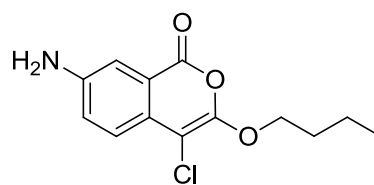
**21** (S044)
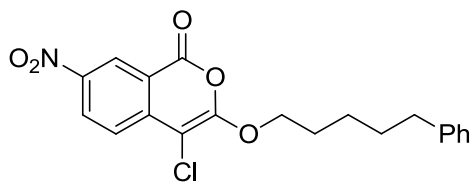
**22** (S045)
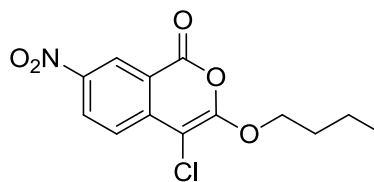
**23** (S046)
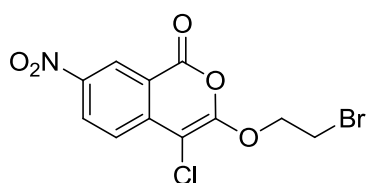
**24** (S047)
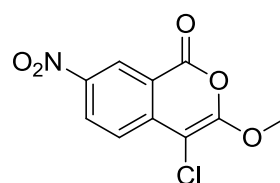
**25** (S025, TLCK)
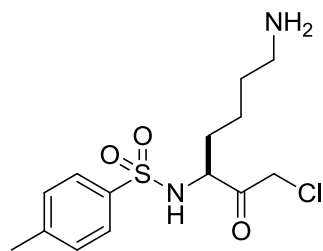
**25** (S029)
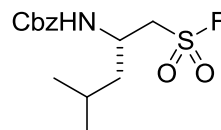
**27** (S032)
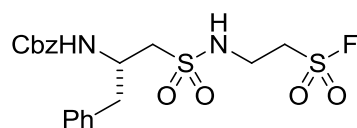
**28** (S038)
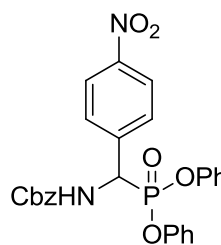
**29** (S043)
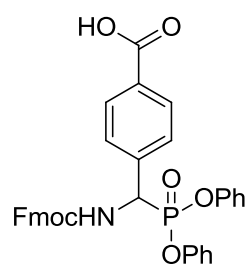
**30** (S052)
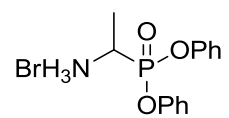
**31** (S063)
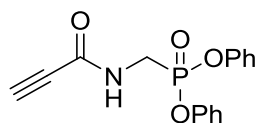
**32** (S065)
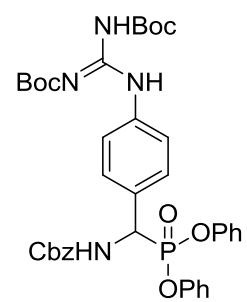
**33** (D3cis)
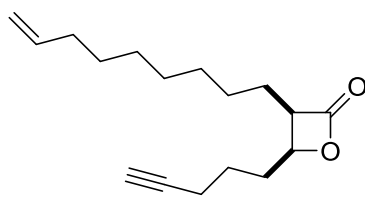
**34** (D3)
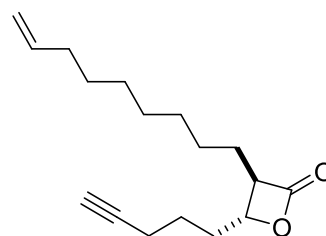
**35** (LT1)
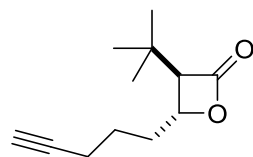
**36** (R1)
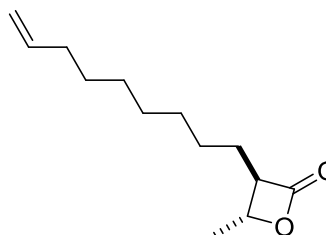
**37** (A1)
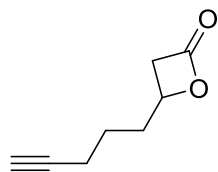
**38** (P1)
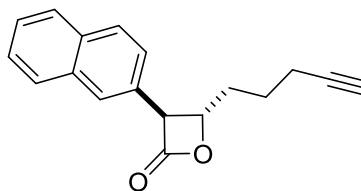


**39** (N1)
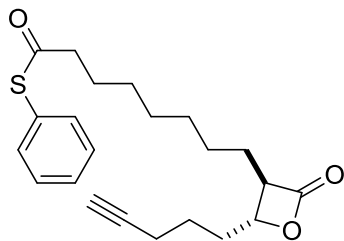
**40** (S1)
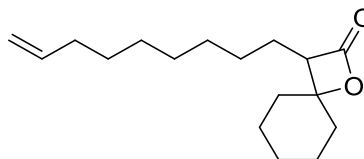


**41** (U1)
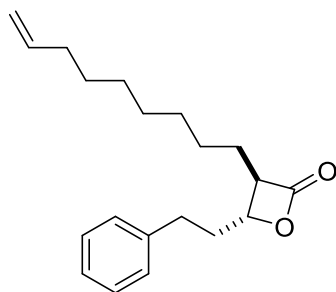
**42** (T1)
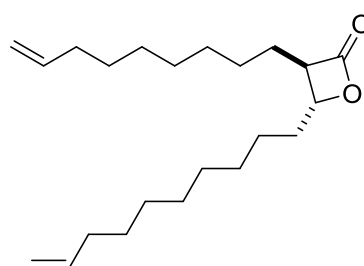


**43** (O1)
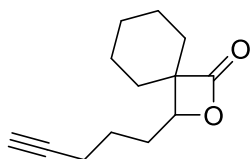
**44** (U1S)
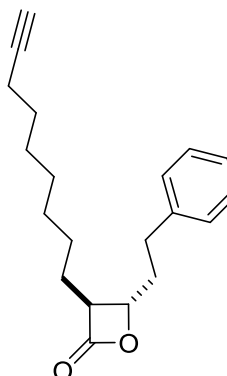
**45** (Q1)
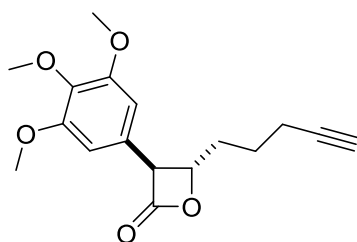
**46** (L1)
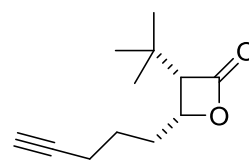
**47** (B1)
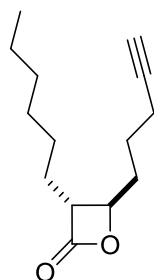
**48** (G2)
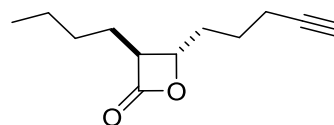
**49** (X1)
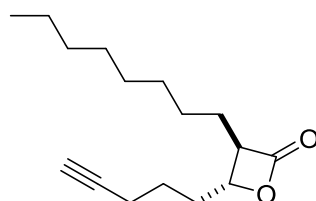
**50** (E2)
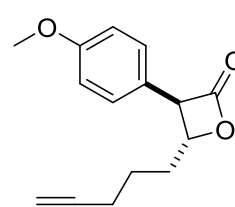
**51** (M1)
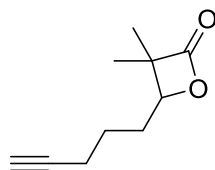
**52** (VlacP)
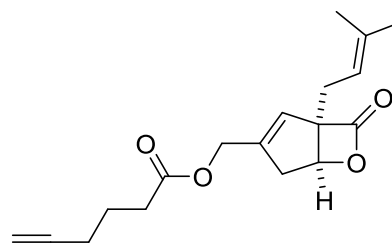
**53** (Vlac)
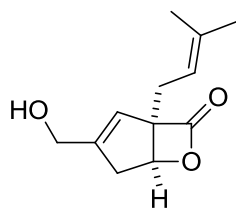
**54** (OXYALL)
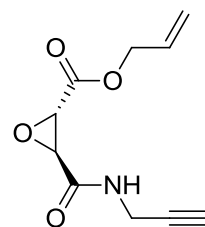
**55** (THIALL)
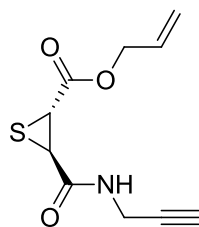
**56** (THIOC)
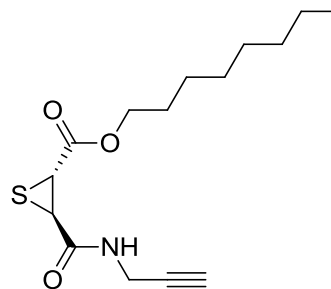
**57** (OXYBOC)
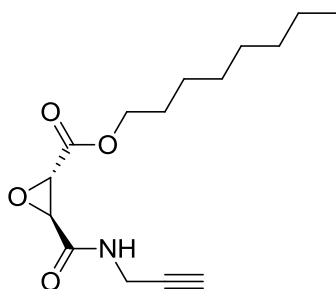
**58** (OXYBENZ)
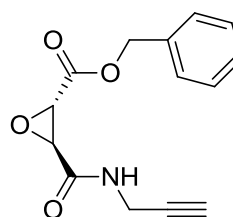
**59** (RKS01)
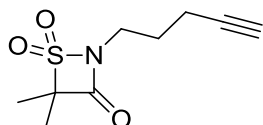
**60** (RKS02)
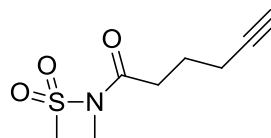
**61** (RKS05)
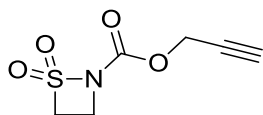
**62** (RKS07)
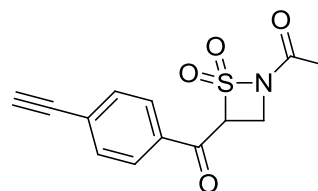
**63** (RKS08)
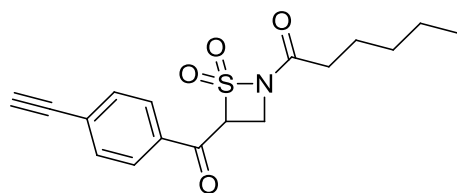
**64** (RKS09)
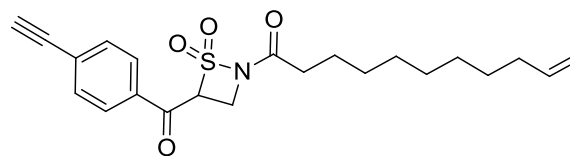
**65** (RKS10)
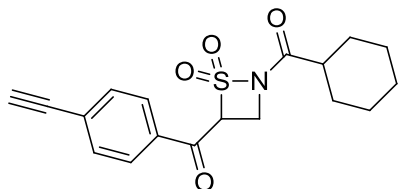
**66** (RKS11)
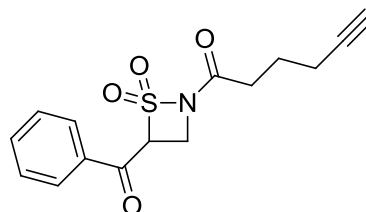
**67** (RKS12)
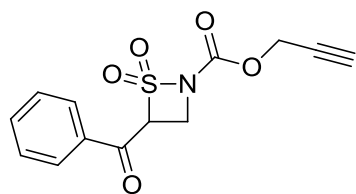
**68** (1.03)
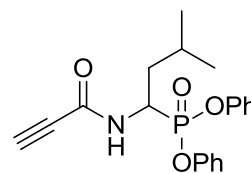
**69** (2.03)
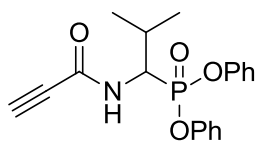
**70** (3.03)
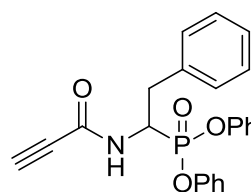
**71** (4.05)
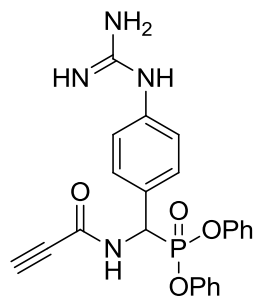
**72** (7.01)
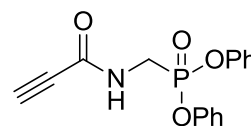
**73** (8.02)
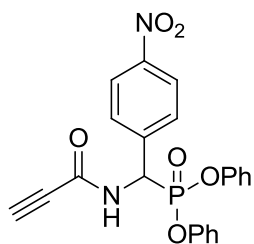
**74** (9.01)
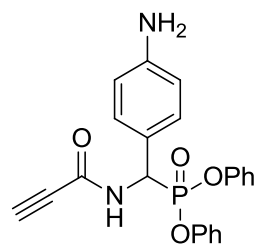
**75** (11.25)
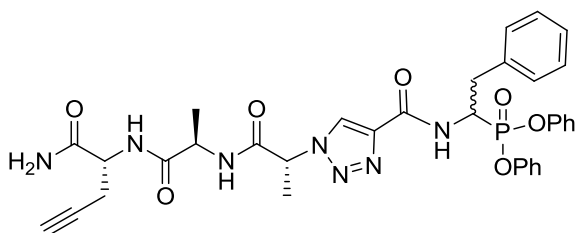
**76** (12.03)
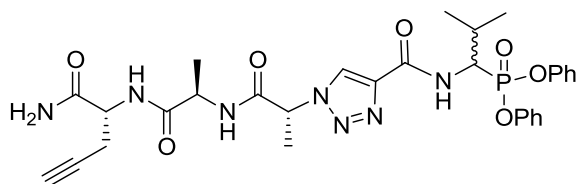
**77** (13.03)
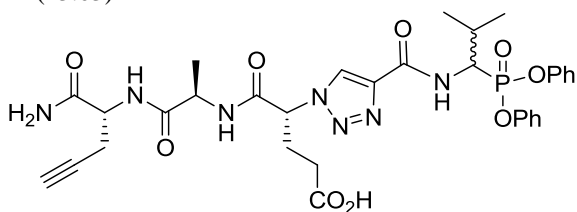
**78** (14.03)
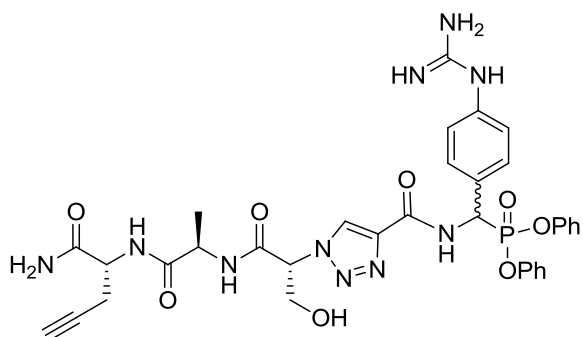
**79** (18.03)
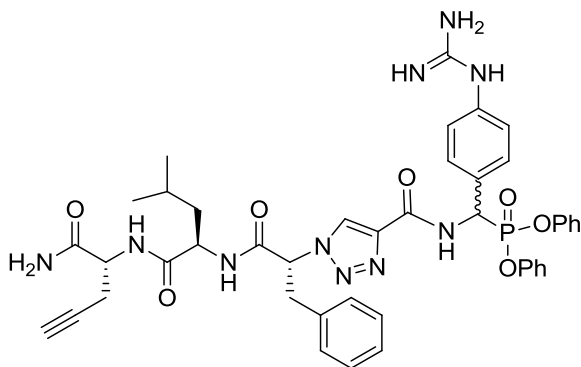
**80** (15.03)
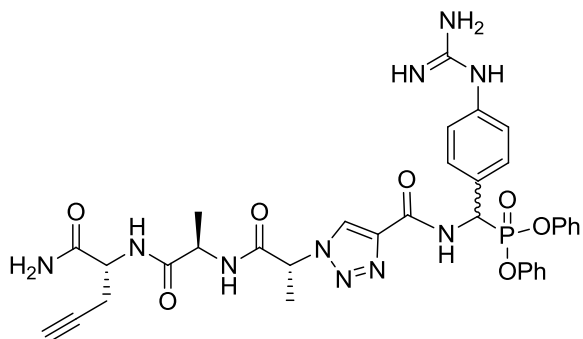
**81** (16.03)
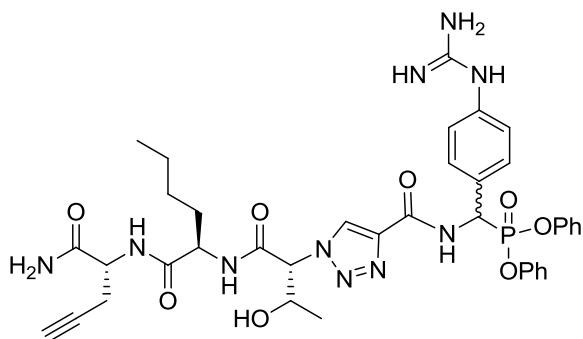
**82** (17.03)
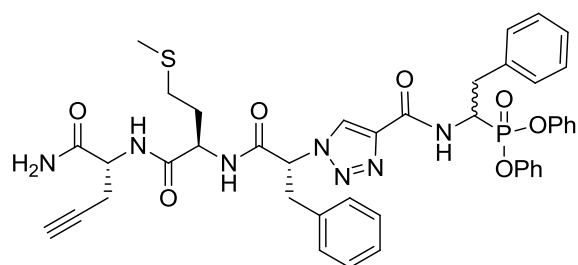


**83** (KPAP)
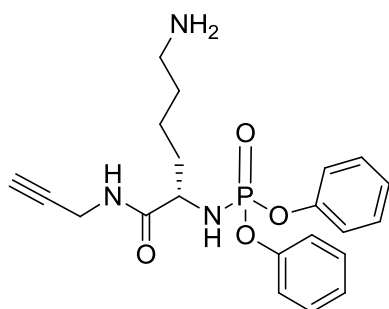
**84** (RPAP)
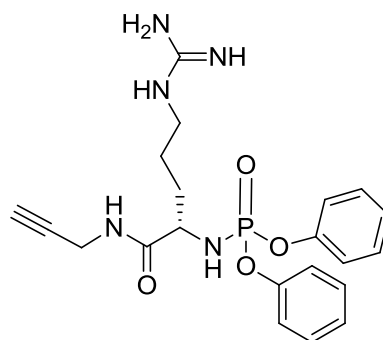


**85** (ArgWLt)
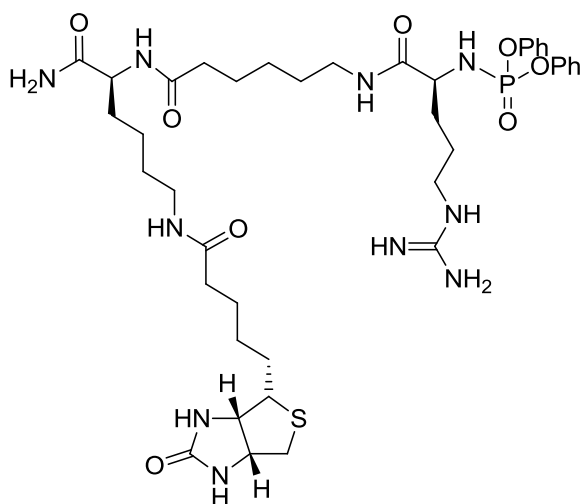
**86** (Cit)
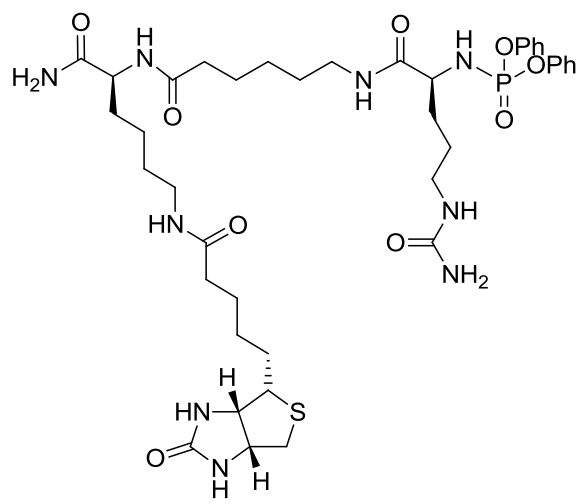
**87 (**biotinKRAP)

**88** (AK)

**89** (AAK)

**90** (KPAP)

**91** (D-Lys)

**92** (Orn)

**93** (Phe)

**94** (Leu)

**95** (S003)

**96** (S010)
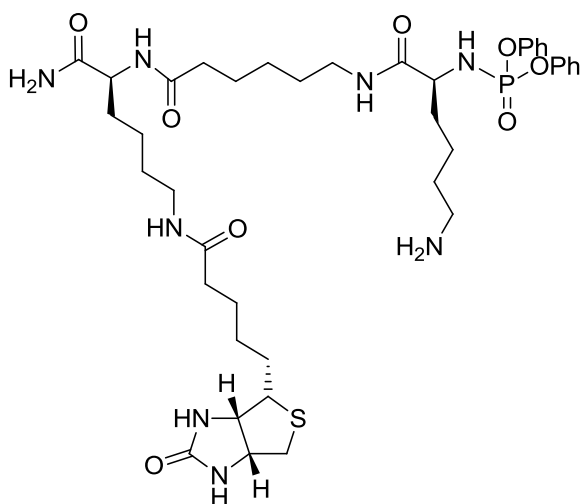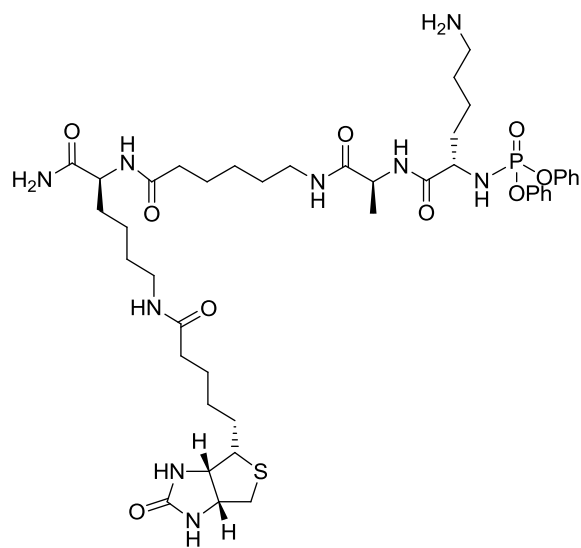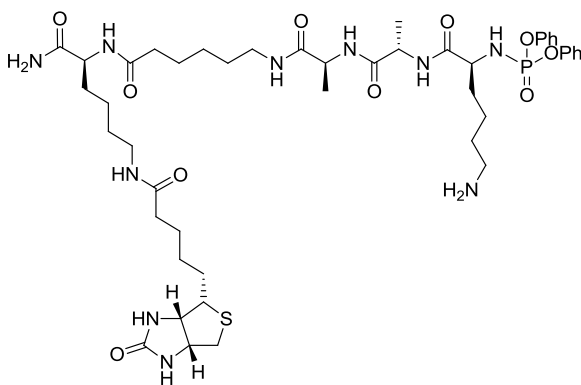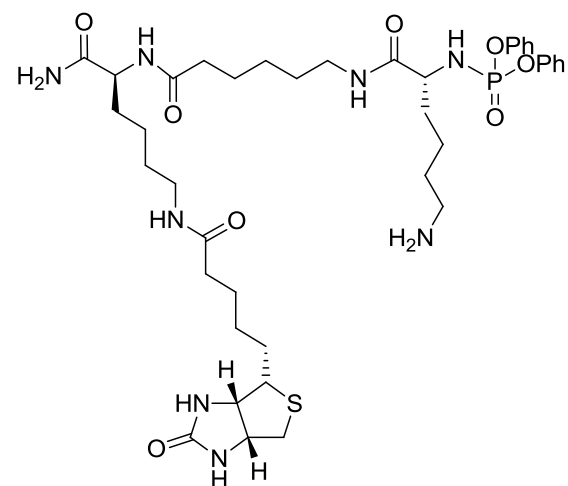
**97** (S016)
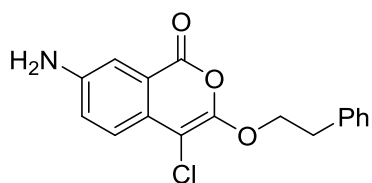
**98** (S021)
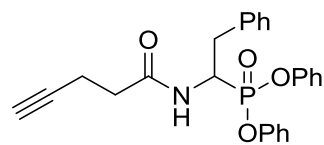
**99** (S024, TPCK)
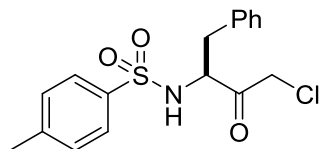
**100** (S039)
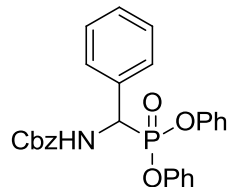
**101** (S040)
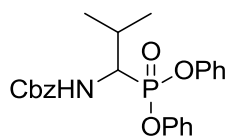
**102** (S041)
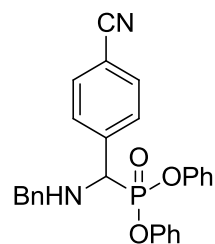
**103** (S042)
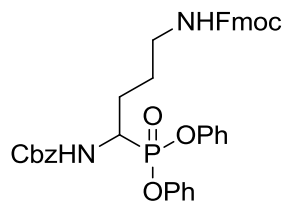
**104** (S048)
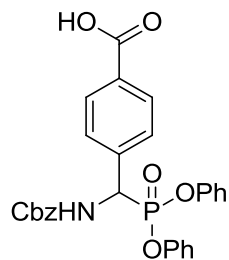
**105** (S049)
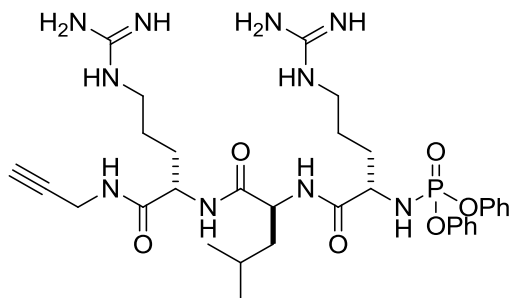
**106** (S050)
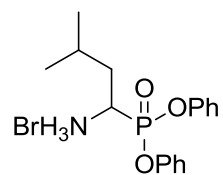
**107** (S051)
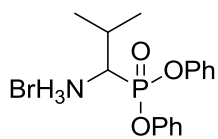
**108** (S053)
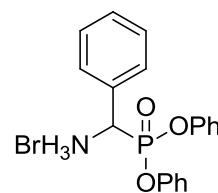
**109** (S054)
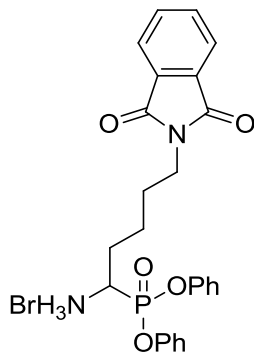
**110** (S055)
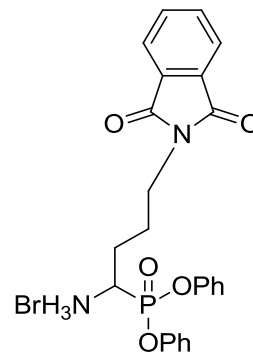
**111** (S056)
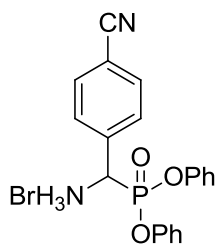
**112** (S057)
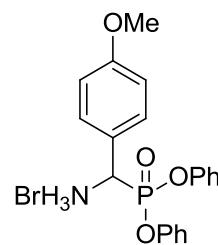
**113** (S058)
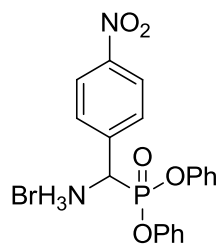
**114** (S059)
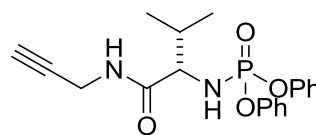
**115** (S060)
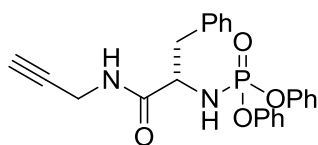
**116** (EK1)
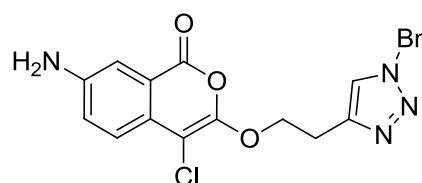
# Abbreviations

| | | | |
|---|---|---|---|
| Å | Ångström, equals 0.1 nm | DCI | 3,4-Dichloroisocoumarin |
| AaROM | Rhomboid from *Aquifex aeolicus* | ddH$_2$O | Double-distilled water or better (Milli-Q preferred) |
| ABP | Activity-based probe | | |
| ABPP | Activity-based protein profiling | DDM | n-Dodecyl β-D-maltoside |
| ACN | Acetonitrile | Derlins | Inactive rhomboids, Der = degradation in the ER |
| AfROM | Rhomboid from *Archaeoglobus fulgidus* | DmRho1 | Rhomboid from *Drosophila melanogaster* |
| APP | Amyloidogenic precursor protein | DMSO | Dimetyl sulfoxide |
| APS | Ammonium persulfate | DOPE | 1,2-Dioleoyl-sn-glycero-3-phosphoethanolamine |
| ATF6 | Activating transcription factor 6 | EcGlpG | Rhomboid GlpG from *Escherichia coli* |
| BACE | β-Secretase | | |
| BsYqgP | Rhomboid YqgP from *Bacillus subtilis* | Edans | (5-((2-Aminoethyl)amino) naphthalene-1-sulfonic acid) |
| CAM | Cerium ammonium molybdate | EGFR | Epidermal growth factor receptor |
| CHAPS | 3-[(3-cholamidopropyl) dimethylammonio]-1-propanesulfonate | eq. | Equivalent |
| | | ER | Endoplasmatic reticulum |
| CMC | Critical micelle concentration | ESI-ToF | Electrospray ionisation-time of flight |
| CNI | Close-Neighbor-Interchange | | |
| complete | Complete EDTA-free protease inhibitor tablet | EtOH | Ethanol |
| | | FA | Formic acid |
| Da | Dalton | FluoPol | Fluorescence polarization |
| Dabcyl | 4-((4-(Dimethylamino) phenyl)azo)benzoic Acid | FluoPol ABPP | Fluorescence polarization activity-based protein profiling |
| Dansyl | 5-(Dimethylamino)naphthalene-1-sulfonyl chloride | FP-R | ActivX TAMRA-FP Serine Hydrolase Probe |
| | | FRET | Förster resonance energy transfer |

| | |
|---|---|
| GUV | Giant unilamellar vesicle |
| HCl | Hydrochloric acid |
| HEPES | 4-(2-Hydroxyethyl)-1-piperazine-ethanesulfonic acid |
| HiROM | Rhomboid GlpG from *Haemophilus influenza* |
| His (H) | Histidine |
| HPLC | High-pressure liquid chromatography |
| HsRHBDL | Rhomboid RHBDL from *Homo sapiens* |
| HTS | High-throughput screen |
| $IC_{50}$ | Half maximal inhibitory concentration |
| IPTG | Isopropyl β-D-1-thiogalactopyranoside |
| IRHD | iRhom homology domain |
| iRhoms | Inactive rhomboids |
| $k_{cat}$ | Turnover number, number of enzymatic reactions catalyzed per second |
| $k_d$ | Dissociation constant |
| $k_i$ | Inhibition constant |
| $k_M$ | Michaelis constant |
| LB | Lysogeny broth |
| LC-MS | Liquid chromatography–mass spectrometry |
| LUV | Large unilamellar vesicle |
| MALDI | Matrix-assisted laser desorption/ionization |
| MeOH | Methanol |

| | |
|---|---|
| MjROM | Rhomboid from *Methanocalcococcus jannaschii* |
| MmRHBDL | Rhomboid RHBDL from *Mus musculus* |
| MW | Molecular weight |
| MWCO | Molecular weight cut-off |
| $N_2$ | Nitrogen |
| NaOH | Sodium hydroxide |
| NTA | Nitrilotriacetic acid |
| o/n | Overnight |
| OD | Optical density |
| OG | Octyl β-D-glucopyranoside |
| PAGE | Polyacrylamide gel electrophoresis |
| PARL | Presenilin associated rhomboid-like |
| PBS | Phosphate buffered saline |
| PBST | Phosphate buffer saline with Tween |
| PC | Phosphocholine |
| PE | Phosphoethanolamine |
| PhROM | Rhomboid from *Pyrococcus horikoshii* |
| PI | Phosphatidylinositol |
| POPC | 1-palmitoyl-2-oleoyl-sn-glycero-3-phosphocholine |
| PPE | Porcine pancreas elastase |
| PsAarA | Rhomboid AarA from *Providencia stuartii* |
| RHBDL1 | Rhomboid-like protein 1 |
| RHBDL2 | Rhomboid-like protein 2 |

| | | | | |
|---|---|---|---|---|
| RHBDL3 | Rhomboid-like protein 3 | | TmROM | Rhomboid from *Thermotoga maritima* |
| RHBDL4 | Rhomboid-like protein 4 | | TNFα | Tumor necrosis factor α |
| RIP | Regulated intramembrane proteolysis | | TPCK | Tosyl phenylalanyl chloromethyl ketone |
| RMSD | root-mean-square deviation | | TRIS | 2-Amino-2-hydroxymethyl-propane-1,3-diol |
| RT | Room temperature | | UV | Ultraviolet |
| S2P | Site-2 protease | | v/v | Volume/volume |
| SDS-PAGE | Sodium dodecyl sulfate polyacrylamide gel electrophoresis | | VcROM | Rhomboid from *Vibrio cholera* |
| Ser (S) | Serine | | w/v | Weight/volume |
| Soy-PI | L-α-phosphatidylinositol from soy | | WT | Wild type |
| SPP/L | Signal peptide peptidase/-like | | | |
| SREBP | Sterol regulatory element-binding protein | | | |
| TAMRA | Tetramethylrhodamine 5-carboxamido-(6-azidohexanyl) | | | |
| TBTA | Tris[(1-benzyl-1H-1,2,3-triazol-4-yl)methyl]amine | | | |
| TEM | Transmission electron microscopy | | | |
| TEMED | Tetramethylethylenediamine | | | |
| TFA | Trifluoroacetic acid | | | |
| THF | Tetrahydrofuran | | | |
| TLC | Thin layer chromatography | | | |
| TLCK | Tosyl-L-lysine chloromethyl ketone | | | |
| TM | Transmembrane | | | |
| TMD | Transmembrane domain | | | |

## List of Tables

## List of Figures

# Bibliography

1. Rawlings, N. D., Barrett, A. J., and Bateman, A. (2010) MEROPS: the peptidase database, *Nucleic Acids Res 38*, D227-233.
2. Schechter, I., and Berger, A. (2012) On the size of the active site in proteases. I. Papain. 1967, *Biochemical and biophysical research communications 425*, 497-502.
3. Strisovsky, K. (2013) Structural and mechanistic principles of intramembrane proteolysis--lessons from rhomboids, *The FEBS journal 280*, 1579-1603.
4. Wang, Y., and Ha, Y. (2007) Open-cap conformation of intramembrane protease GlpG, *Proceedings of the National Academy of Sciences 104*, 2098-2102.
5. Wang, Y., Maegawa, S., Akiyama, Y., and Ha, Y. (2007) The Role of L1 Loop in the Mechanism of Rhomboid Intramembrane Protease GlpG, *Journal of Molecular Biology 374*, 1104-1113.
6. Wang, Y., Zhang, Y., and Ha, Y. (2006) Crystal structure of a rhomboid family intramembrane protease, *Nature 444*, 179-180.
7. Lemieux, M. J., Fischer, S. J., Cherney, M. M., Bateman, K. S., and James, M. N. G. (2007) The crystal structure of the rhomboid peptidase from Haemophilus influenzae provides insight into intramembrane proteolysis, *Proceedings of the National Academy of Sciences 104*, 750-754.
8. Ben-Shem, A., Fass, D., and Bibi, E. (2007) Structural basis for intramembrane proteolysis by rhomboid serine proteases, *Proc Natl Acad Sci U S A 104*, 462-466.
9. De Strooper, B., Saftig, P., Craessaerts, K., Vanderstichele, H., Guhde, G., Annaert, W., Von Figura, K., and Van Leuven, F. (1998) Deficiency of presenilin-1 inhibits the normal cleavage of amyloid precursor protein, *Nature 391*, 387-390.
10. Lee, J. R., Urban, S., Garvey, C. F., and Freeman, M. (2001) Regulated intracellular ligand transport and proteolysis control EGF signal activation in Drosophila, *Cell 107*, 161-171.
11. Rawson, R. B., Zelenski, N. G., Nijhawan, D., Ye, J., Sakai, J., Hasan, M. T., Chang, T. Y., Brown, M. S., and Goldstein, J. L. (1997) Complementation cloning of S2P, a gene encoding a putative metalloprotease required for intramembrane cleavage of SREBPs, *Mol Cell 1*, 47-57.
12. Akiyama, Y., Kanehara, K., and Ito, K. (2004) RseP (YaeL), an Escherichia coli RIP protease, cleaves transmembrane sequences, *The EMBO journal 23*, 4434-4442.
13. Duncan, E. A., Dave, U. P., Sakai, J., Goldstein, J. L., and Brown, M. S. (1998) Second-site cleavage in sterol regulatory element-binding protein occurs at transmembrane junction as determined by cysteine panning, *The Journal of biological chemistry 273*, 17801-17809.
14. Fluhrer, R., Grammer, G., Israel, L., Condron, M. M., Haffner, C., Friedmann, E., Bohland, C., Imhof, A., Martoglio, B., Teplow, D. B., and Haass, C. (2006) A [gamma]-secretase-like intramembrane cleavage of TNF[alpha] by the GxGD aspartyl protease SPPL2b, *Nat Cell Biol 8*, 894-896.
15. Friedmann, E., Hauben, E., Maylandt, K., Schleeger, S., Vreugde, S., Lichtenthaler, S. F., Kuhn, P. H., Stauffer, D., Rovelli, G., and Martoglio, B. (2006) SPPL2a and SPPL2b promote intramembrane proteolysis of TNFalpha in activated dendritic cells to trigger IL-12 production, *Nat Cell Biol 8*, 843-848.
16. Narayanan, S., Sato, T., and Wolfe, M. S. (2007) A C-terminal region of signal peptide peptidase defines a functional domain for intramembrane aspartic protease catalysis, *The Journal of biological chemistry 282*, 20172-20179.

17.    Weihofen, A., Binns, K., Lemberg, M. K., Ashman, K., and Martoglio, B. (2002) Identification of signal peptide peptidase, a presenilin-type aspartic protease, *Science (New York, N.Y.) 296*, 2215-2218.

18.    Wolfe, M. S., Xia, W., Ostaszewski, B. L., Diehl, T. S., Kimberly, W. T., and Selkoe, D. J. (1999) Two transmembrane aspartates in presenilin-1 required for presenilin endoproteolysis and gamma-secretase activity, *Nature 398*, 513-517.

19.    Urban, S., Lee, J. R., and Freeman, M. (2001) Drosophila Rhomboid-1 Defines a Family of Putative Intramembrane Serine Proteases, *Cell 107*, 173-182.

20.    Lemberg, M. K., and Freeman, M. (2007) Functional and evolutionary implications of enhanced genomic analysis of rhomboid intramembrane proteases, *Genome Research 17*, 1634-1646.

21.    Ye, J., Rawson, R. B., Komuro, R., Chen, X., Dave, U. P., Prywes, R., Brown, M. S., and Goldstein, J. L. (2000) ER stress induces cleavage of membrane-bound ATF6 by the same proteases that process SREBPs, *Mol Cell 6*, 1355-1364.

22.    Yang, T., Espenshade, P. J., Wright, M. E., Yabe, D., Gong, Y., Aebersold, R., Goldstein, J. L., and Brown, M. S. (2002) Crucial step in cholesterol homeostasis: sterols promote binding of SCAP to INSIG-1, a membrane protein that facilitates retention of SREBPs in ER, *Cell 110*, 489-500.

23.    Feng, L., Yan, H., Wu, Z., Yan, N., Wang, Z., Jeffrey, P. D., and Shi, Y. (2007) Structure of a site-2 protease family intramembrane metalloprotease, *Science (New York, N.Y.) 318*, 1608-1612.

24.    Bolter, B., Nada, A., Fulgosi, H., and Soll, J. (2006) A chloroplastic inner envelope membrane protease is essential for plant development, *FEBS letters 580*, 789-794.

25.    Levy-Lahad, E., Wasco, W., Poorkaj, P., Romano, D. M., Oshima, J., Pettingell, W. H., Yu, C. E., Jondro, P. D., Schmidt, S. D., Wang, K., and et al. (1995) Candidate gene for the chromosome 1 familial Alzheimer's disease locus, *Science (New York, N.Y.) 269*, 973-977.

26.    Sherrington, R., Rogaev, E. I., Liang, Y., Rogaeva, E. A., Levesque, G., Ikeda, M., Chi, H., Lin, C., Li, G., Holman, K., Tsuda, T., Mar, L., Foncin, J. F., Bruni, A. C., Montesi, M. P., Sorbi, S., Rainero, I., Pinessi, L., Nee, L., Chumakov, I., Pollen, D., Brookes, A., Sanseau, P., Polinsky, R. J., Wasco, W., Da Silva, H. A., Haines, J. L., Perkicak-Vance, M. A., Tanzi, R. E., Roses, A. D., Fraser, P. E., Rommens, J. M., and St George-Hyslop, P. H. (1995) Cloning of a gene bearing missense mutations in early-onset familial Alzheimer's disease, *Nature 375*, 754-760.

27.    Lichtenthaler, S. F., Haass, C., and Steiner, H. (2011) Regulated intramembrane proteolysis-- lessons from amyloid precursor protein processing, *J Neurochem 117*, 779-796.

28.    De Strooper, B., Vassar, R., and Golde, T. (2010) The secretases: enzymes with therapeutic potential in Alzheimer disease, *Nature reviews. Neurology 6*, 99-107.

29.    Kimberly, W. T., LaVoie, M. J., Ostaszewski, B. L., Ye, W., Wolfe, M. S., and Selkoe, D. J. (2003) Gamma-secretase is a membrane protein complex comprised of presenilin, nicastrin, Aph-1, and Pen-2, *Proc Natl Acad Sci U S A 100*, 6382-6387.

30.    Edbauer, D., Winkler, E., Regula, J. T., Pesold, B., Steiner, H., and Haass, C. (2003) Reconstitution of gamma-secretase activity, *Nat Cell Biol 5*, 486-488.

31.    Spasic, D., Raemaekers, T., Dillen, K., Declerck, I., Baert, V., Serneels, L., Fullekrug, J., and Annaert, W. (2007) Rer1p competes with APH-1 for binding to nicastrin and regulates gamma-secretase complex assembly in the early secretory pathway, *The Journal of cell biology 176*, 629-640.

32.    Lemberg, M. K., Bland, F. A., Weihofen, A., Braud, V. M., and Martoglio, B. (2001) Intramembrane proteolysis of signal peptides: an essential step in the generation of HLA-E epitopes, *Journal of immunology (Baltimore, Md. : 1950) 167*, 6441-6446.

33.    Lemberg, M. K., and Martoglio, B. (2002) Requirements for signal peptide peptidase-catalyzed intramembrane proteolysis, *Mol Cell 10*, 735-744.

34. Okamoto, K., Mori, Y., Komoda, Y., Okamoto, T., Okochi, M., Takeda, M., Suzuki, T., Moriishi, K., and Matsuura, Y. (2008) Intramembrane processing by signal peptide peptidase regulates the membrane localization of hepatitis C virus core protein and viral propagation, *Journal of virology 82*, 8349-8361.

35. Li, X., Chen, H., Bahamontes-Rosa, N., Kun, J. F., Traore, B., Crompton, P. D., and Chishti, A. H. (2009) Plasmodium falciparum signal peptide peptidase is a promising drug target against blood stage malaria, *Biochemical and biophysical research communications 380*, 454-459.

36. Koonin, E. V., Makarova, K. S., Rogozin, I. B., Davidovic, L., Letellier, M. C., and Pellegrini, L. (2003) The rhomboids: a nearly ubiquitous family of intramembrane serine proteases that probably evolved by multiple ancient horizontal gene transfers, *Genome biology 4*, R19.

37. Ruohola-Baker, H., Grell, E., Chou, T. B., Baker, D., Jan, L. Y., and Jan, Y. N. (1993) Spatially localized rhomboid is required for establishment of the dorsal-ventral axis in Drosophila oogenesis, *Cell 73*, 953-965.

38. Guichard, A., Biehs, B., Sturtevant, M. A., Wickline, L., Chacko, J., Howard, K., and Bier, E. (1999) rhomboid and Star interact synergistically to promote EGFR/MAPK signaling during Drosophila wing vein development, *Development (Cambridge, England) 126*, 2663-2676.

39. Sturtevant, M. A., Roark, M., and Bier, E. (1993) The Drosophila rhomboid gene mediates the localized formation of wing veins and interacts genetically with components of the EGF-R signaling pathway, *Genes & development 7*, 961-973.

40. Lage, P., Jan, Y. N., and Jarman, A. P. (1997) Requirement for EGF receptor signalling in neural recruitment during formation of Drosophila chordotonal sense organ clusters, *Current biology : CB 7*, 166-175.

41. Golembo, M., Raz, E., and Shilo, B. Z. (1996) The Drosophila embryonic midline is the site of Spitz processing, and induces activation of the EGF receptor in the ventral ectoderm, *Development (Cambridge, England) 122*, 3363-3370.

42. Freeman, M. (1994) The spitz gene is required for photoreceptor determination in the Drosophila eye where it interacts with the EGF receptor, *Mechanisms of development 48*, 25-33.

43. Bang, A. G., and Kintner, C. (2000) Rhomboid and Star facilitate presentation and processing of the Drosophila TGF-alpha homolog Spitz, *Genes & development 14*, 177-186.

44. Mayer, U., and Nusslein-Volhard, C. (1988) A group of genes required for pattern formation in the ventral ectoderm of the Drosophila embryo, *Genes & development 2*, 1496-1511.

45. Dutt, A., Canevascini, S., Froehli-Hoier, E., and Hajnal, A. (2004) EGF signal propagation during C. elegans vulval development mediated by ROM-1 rhomboid, *PLoS biology 2*, e334.

46. Stevenson, L. G., Strisovsky, K., Clemmer, K. M., Bhatt, S., Freeman, M., and Rather, P. N. (2007) Rhomboid protease AarA mediates quorum-sensing in Providencia stuartii by activating TatA of the twin-arginine translocase, *Proc Natl Acad Sci U S A 104*, 1003-1008.

47. Lee, P. A., Tullman-Ercek, D., and Georgiou, G. (2006) The bacterial twin-arginine translocation pathway, *Annual review of microbiology 60*, 373-395.

48. Gohlke, U., Pullan, L., McDevitt, C. A., Porcelli, I., de Leeuw, E., Palmer, T., Saibil, H. R., and Berks, B. C. (2005) The TatA component of the twin-arginine protein transport system forms channel complexes of variable diameter, *Proc Natl Acad Sci U S A 102*, 10482-10486.

49. Dowse, T. J., Pascall, J. C., Brown, K. D., and Soldati, D. (2005) Apicomplexan rhomboids have a potential role in microneme protein cleavage during host cell invasion, *International journal for parasitology 35*, 747-756.

50. Howell, S. A., Hackett, F., Jongco, A. M., Withers-Martinez, C., Kim, K., Carruthers, V. B., and Blackman, M. J. (2005) Distinct mechanisms govern proteolytic shedding of a key invasion protein in apicomplexan pathogens, *Molecular microbiology 57*, 1342-1356.

51. Opitz, C., Di Cristina, M., Reiss, M., Ruppert, T., Crisanti, A., and Soldati, D. (2002) Intramembrane cleavage of microneme proteins at the surface of the apicomplexan parasite Toxoplasma gondii, *The EMBO journal 21*, 1577-1585.

52.     Singh, S., Plassmeyer, M., Gaur, D., and Miller, L. H. (2007) Mononeme: a new secretory organelle in Plasmodium falciparum merozoites identified by localization of rhomboid-1 protease, *Proc Natl Acad Sci U S A 104*, 20043-20048.

53.     Baker, R. P., Wijetilaka, R., and Urban, S. (2006) Two Plasmodium rhomboid proteases preferentially cleave different adhesins implicated in all invasive stages of malaria, *PLoS pathogens 2*, e113.

54.     McQuibban, G. A., Saurya, S., and Freeman, M. (2003) Mitochondrial membrane remodelling regulated by a conserved rhomboid protease, *Nature 423*, 537-541.

55.     Herlan, M., Vogel, F., Bornhovd, C., Neupert, W., and Reichert, A. S. (2003) Processing of Mgm1 by the rhomboid-type protease Pcp1 is required for maintenance of mitochondrial morphology and of mitochondrial DNA, *The Journal of biological chemistry 278*, 27781-27788.

56.     Esser, K., Tursun, B., Ingenhoven, M., Michaelis, G., and Pratje, E. (2002) A novel two-step mechanism for removal of a mitochondrial signal sequence involves the mAAA complex and the putative rhomboid protease Pcp1, *J Mol Biol 323*, 835-843.

57.     Sesaki, H., Southard, S. M., Hobbs, A. E., and Jensen, R. E. (2003) Cells lacking Pcp1p/Ugo2p, a rhomboid-like protease required for Mgm1p processing, lose mtDNA and mitochondrial structure in a Dnm1p-dependent manner, but remain competent for mitochondrial fusion, *Biochemical and biophysical research communications 308*, 276-283.

58.     Chao, J. R., Parganas, E., Boyd, K., Hong, C. Y., Opferman, J. T., and Ihle, J. N. (2008) Hax1-mediated processing of HtrA2 by Parl allows survival of lymphocytes and neurons, *Nature 452*, 98-102.

59.     Martins, L. M., Iaccarino, I., Tenev, T., Gschmeissner, S., Totty, N. F., Lemoine, N. R., Savopoulos, J., Gray, C. W., Creasy, C. L., Dingwall, C., and Downward, J. (2002) The serine protease Omi/HtrA2 regulates apoptosis by binding XIAP through a reaper-like motif, *The Journal of biological chemistry 277*, 439-444.

60.     Shi, G., Lee, J. R., Grimes, D. A., Racacho, L., Ye, D., Yang, H., Ross, O. A., Farrer, M., McQuibban, G. A., and Bulman, D. E. (2011) Functional alteration of PARL contributes to mitochondrial dysregulation in Parkinson's disease, *Human molecular genetics 20*, 1966-1974.

61.     Deas, E., Plun-Favreau, H., Gandhi, S., Desmond, H., Kjaer, S., Loh, S. H., Renton, A. E., Harvey, R. J., Whitworth, A. J., Martins, L. M., Abramov, A. Y., and Wood, N. W. (2011) PINK1 cleavage at position A103 by the mitochondrial protease PARL, *Human molecular genetics 20*, 867-879.

62.     Civitarese, A. E., MacLean, P. S., Carling, S., Kerr-Bayles, L., McMillan, R. P., Pierce, A., Becker, T. C., Moro, C., Finlayson, J., Lefort, N., Newgard, C. B., Mandarino, L., Cefalu, W., Walder, K., Collier, G. R., Hulver, M. W., Smith, S. R., and Ravussin, E. (2010) Regulation of skeletal muscle oxidative capacity and insulin signaling by the mitochondrial rhomboid protease PARL, *Cell metabolism 11*, 412-426.

63.     Wu, Z., Yan, N., Feng, L., Oberstein, A., Yan, H., Baker, R. P., Gu, L., Jeffrey, P. D., Urban, S., and Shi, Y. (2006) Structural analysis of a rhomboid family intramembrane protease reveals a gating mechanism for substrate entry, *Nature structural & molecular biology 13*, 1084-1091.

64.     Dickey, Seth W., Baker, Rosanna P., Cho, S., and Urban, S. (2013) Proteolysis inside the Membrane Is a Rate-Governed Reaction Not Driven by Substrate Affinity, *Cell 155*, 1270-1281.

65.     Lemberg, M. K., Menendez, J., Misik, A., Garcia, M., Koth, C. M., and Freeman, M. (2005) *Mechanism of intramembrane proteolysis investigated with purified rhomboid proteases*, Vol. 24.

66.     Ekici, O. D., Paetzel, M., and Dalbey, R. E. (2008) Unconventional serine proteases: variations on the catalytic Ser/His/Asp triad configuration, *Protein science : a publication of the Protein Society 17*, 2023-2037.

67.     Wang, Y., Zhang, Y., and Ha, Y. (2006) Crystal structure of a rhomboid family intramembrane protease, *Nature 444*, 179-180.

68.     Baker, R. P., Young, K., Feng, L., Shi, Y., and Urban, S. (2007) Enzymatic analysis of a rhomboid intramembrane protease implicates transmembrane helix 5 as the lateral substrate gate, *Proc Natl Acad Sci U S A 104*, 8257-8262.

69.     Xue, Y., and Ha, Y. (2012) Catalytic Mechanism of Rhomboid Protease GlpG Probed by 3,4-Dichloroisocoumarin and Diisopropyl Fluorophosphonate, *Journal of Biological Chemistry 287*, 3099-3107.

70.     Urban, S. (2010) Taking the plunge: integrating structural, enzymatic and computational insights into a unified model for membrane-immersed rhomboid proteolysis, *The Biochemical journal 425*, 501-512.

71.     Vinothkumar, K. R., Strisovsky, K., Andreeva, A., Christova, Y., Verhelst, S., and Freeman, M. (2010) *The structural basis for catalysis and substrate specificity of a rhomboid protease*, Vol. 29.

72.     Zoll, S., Stanchev, S., Began, J., Skerle, J., Lepsik, M., Peclinovska, L., Majer, P., and Strisovsky, K. (2014) Substrate binding and specificity of rhomboid intramembrane protease revealed by substrate-peptide complex structures, *The EMBO journal 33*, 2408-2421.

73.     Zhou, Y., Moin, S. M., Urban, S., and Zhang, Y. (2012) An internal water-retention site in the rhomboid intramembrane protease GlpG ensures catalytic efficiency, *Structure 20*, 1255-1263.

74.     Maegawa, S., Ito, K., and Akiyama, Y. (2005) Proteolytic action of GlpG, a rhomboid protease in the Escherichia coli cytoplasmic membrane, *Biochemistry 44*, 13543-13552.

75.     Daley, D. O., Rapp, M., Granseth, E., Melen, K., Drew, D., and von Heijne, G. (2005) Global topology analysis of the Escherichia coli inner membrane proteome, *Science (New York, N.Y.) 308*, 1321-1323.

76.     Wasserman, J. D., Urban, S., and Freeman, M. (2000) A family of rhomboid-like genes: Drosophila rhomboid-1 and roughoid/rhomboid-3 cooperate to activate EGF receptor signaling, *Genes & development 14*, 1651-1663.

77.     Fleig, L., Bergbold, N., Sahasrabudhe, P., Geiger, B., Kaltak, L., and Lemberg, Marius K. (2012) Ubiquitin-Dependent Intramembrane Rhomboid Protease Promotes ERAD of Membrane Proteins, *Molecular Cell 47*, 558-569.

78.     Lohi, O., Urban, S., and Freeman, M. (2004) Diverse substrate recognition mechanisms for rhomboids; thrombomodulin is cleaved by Mammalian rhomboids, *Current biology : CB 14*, 236-241.

79.     Greenblatt, E. J., Olzmann, J. A., and Kopito, R. R. (2011) Derlin-1 is a rhomboid pseudoprotease required for the dislocation of mutant alpha-1 antitrypsin from the endoplasmic reticulum, *Nature structural & molecular biology 18*, 1147-1152.

80.     Freeman, M. (2008) Rhomboid proteases and their biological functions, *Annual review of genetics 42*, 191-210.

81.     Freeman, M. (2009) Rhomboids: 7 years of a new protease family, *Semin Cell Dev Biol 20*, 231-239.

82.     Pierrat, O. A., Strisovsky, K., Christova, Y., Large, J., Ansell, K., Bouloc, N., Smiljanic, E., and Freeman, M. (2010) Monocyclic β-Lactams Are Selective, Mechanism-Based Inhibitors of Rhomboid Intramembrane Proteases, *ACS Chemical Biology 6*, 325-335.

83.     Strisovsky, K., Sharpe, H. J., and Freeman, M. (2009) Sequence-specific intramembrane proteolysis: identification of a recognition motif in rhomboid substrates, *Mol Cell 36*, 1048-1059.

84.     Urban, S., Schlieper, D., and Freeman, M. (2002) Conservation of intramembrane proteolytic activity and substrate specificity in prokaryotic and eukaryotic rhomboids, *Current biology : CB 12*, 1507-1512.

85. Gallio, M., Sturgill, G., Rather, P., and Kylsten, P. (2002) A conserved mechanism for extracellular signaling in eukaryotes and prokaryotes, *Proc Natl Acad Sci U S A 99*, 12208-12213.

86. Moin, S. M., and Urban, S. (2012) Membrane immersion allows rhomboid proteases to achieve specificity by reading transmembrane segment dynamics, *eLife 1*, e00173.

87. Akiyama, Y., and Maegawa, S. (2007) Sequence features of substrates required for cleavage by GlpG, an Escherichia coli rhomboid protease, *Molecular microbiology 64*, 1028-1037.

88. Urban, S., and Freeman, M. (2003) Substrate specificity of rhomboid intramembrane proteases is governed by helix-breaking residues in the substrate transmembrane domain, *Mol Cell 11*, 1425-1434.

89. Bondar, A. N., del Val, C., and White, S. H. (2009) Rhomboid protease dynamics and lipid interactions, *Structure 17*, 395-405.

90. Vinothkumar, K. R. (2011) Structure of rhomboid protease in a lipid environment, *J Mol Biol 407*, 232-247.

91. Brooks, C. L., Lazareno-Saez, C., Lamoureux, J. S., Mak, M. W., and Lemieux, M. J. (2011) Insights into substrate gating in H. influenzae rhomboid, *J Mol Biol 407*, 687-697.

92. Urban, S., and Baker, R. P. (2008) In vivo analysis reveals substrate-gating mutants of a rhomboid intramembrane protease display increased activity in living cells, *Biological chemistry 389*, 1107-1115.

93. Baker, R. P., and Urban, S. (2012) Architectural and thermodynamic principles underlying intramembrane protease function, *Nat Chem Biol 8*, 759-768.

94. Xue, Y., Chowdhury, S., Liu, X., Akiyama, Y., Ellman, J., and Ha, Y. (2012) Conformational Change in Rhomboid Protease GlpG Induced by Inhibitor Binding to Its S′ Subsites, *Biochemistry 51*, 3723-3731.

95. Xue, Y., and Ha, Y. (2013) Large Lateral Movement of Transmembrane Helix S5 Is Not Required for Substrate Access to the Active Site of Rhomboid Intramembrane Protease, *Journal of Biological Chemistry 288*, 16645-16654.

96. Vinothkumar, Kutti R., Pierrat, Olivier A., Large, Jonathan M., and Freeman, M. (2013) Structure of Rhomboid Protease in Complex with β-Lactam Inhibitors Defines the S2′ Cavity, *Structure 21*, 1051-1058.

97. Vosyka, O., Vinothkumar, K. R., Wolf, E. V., Brouwer, A. J., Liskamp, R. M. J., and Verhelst, S. H. L. (2013) Activity-based probes for rhomboid proteases discovered in a mass spectrometry-based assay, *Proceedings of the National Academy of Sciences 110*, 2472-2477.

98. Herlan, M., Bornhovd, C., Hell, K., Neupert, W., and Reichert, A. S. (2004) Alternative topogenesis of Mgm1 and mitochondrial morphology depend on ATP and a functional import motor, *The Journal of cell biology 165*, 167-173.

99. Wan, C., Fu, J., Wang, Y., Miao, S., Song, W., and Wang, L. (2012) Exosome-related multi-pass transmembrane protein TSAP6 is a target of rhomboid protease RHBDD1-induced proteolysis, *PLoS One 7*, e37452.

100. Erez, E., and Bibi, E. (2009) Cleavage of a multispanning membrane protein by an intramembrane serine protease, *Biochemistry 48*, 12314-12322.

101. Tsruya, R., Wojtalla, A., Carmon, S., Yogev, S., Reich, A., Bibi, E., Merdes, G., Schejter, E., and Shilo, B. Z. (2007) Rhomboid cleaves Star to regulate the levels of secreted Spitz, *The EMBO journal 26*, 1211-1220.

102. Arutyunova, E., Panwar, P., Skiba, P. M., Gale, N., Mak, M. W., and Lemieux, M. J. (2014) Allosteric regulation of rhomboid intramembrane proteolysis, *The EMBO journal 33*, 1869-1881.

103. Brown, M. S., Ye, J., Rawson, R. B., and Goldstein, J. L. (2000) Regulated intramembrane proteolysis: a control mechanism conserved from bacteria to humans, *Cell 100*, 391-398.

104. Urban, S., and Freeman, M. (2002) Intramembrane proteolysis controls diverse signalling pathways throughout evolution, *Current opinion in genetics & development 12*, 512-518.

105. Bier, E., Jan, L. Y., and Jan, Y. N. (1990) rhomboid, a gene required for dorsoventral axis establishment and peripheral nervous system development in Drosophila melanogaster, *Genes & development 4*, 190-203.

106. Brossier, F., Jewett, T. J., Sibley, L. D., and Urban, S. (2005) A spatially localized rhomboid protease cleaves cell surface adhesins essential for invasion by Toxoplasma, *Proc Natl Acad Sci U S A 102*, 4146-4151.

107. Urban, S., and Wolfe, M. S. (2005) Reconstitution of intramembrane proteolysis in vitro reveals that pure rhomboid is sufficient for catalysis and specificity, *Proceedings of the National Academy of Sciences of the United States of America 102*, 1883-1888.

108. Sheiner, L., Dowse, T. J., and Soldati-Favre, D. (2008) Identification of trafficking determinants for polytopic rhomboid proteases in Toxoplasma gondii, *Traffic (Copenhagen, Denmark) 9*, 665-677.

109. Del Rio, A., Dutta, K., Chavez, J., Ubarretxena-Belandia, I., and Ghose, R. (2007) Solution structure and dynamics of the N-terminal cytosolic domain of rhomboid intramembrane protease from Pseudomonas aeruginosa: insights into a functional role in intramembrane proteolysis, *J Mol Biol 365*, 109-122.

110. Sherratt, A. R., Blais, D. R., Ghasriani, H., Pezacki, J. P., and Goto, N. K. (2012) Activity-Based Protein Profiling of the Escherichia coli GlpG Rhomboid Protein Delineates the Catalytic Core, *Biochemistry 51*, 7794-7803.

111. Lazareno-Saez, C., Arutyunova, E., Coquelle, N., and Lemieux, M. J. (2013) Domain swapping in the cytoplasmic domain of the Escherichia coli rhomboid protease, *J Mol Biol 425*, 1127-1142.

112. Sampathkumar, P., Mak, M. W., Fischer-Witholt, S. J., Guigard, E., Kay, C. M., and Lemieux, M. J. (2012) Oligomeric state study of prokaryotic rhomboid proteases, *Biochimica et biophysica acta 1818*, 3090-3097.

113. Meissner, C., Lorenz, H., Weihofen, A., Selkoe, D. J., and Lemberg, M. K. (2011) The mitochondrial intramembrane protease PARL cleaves human Pink1 to regulate Pink1 trafficking, *Journal of Neurochemistry 117*, 856-867.

114. Lemberg, M. K. (2011) Intramembrane proteolysis in regulated protein trafficking, *Traffic (Copenhagen, Denmark) 12*, 1109-1118.

115. Knopf, R. R., Feder, A., Mayer, K., Lin, A., Rozenberg, M., Schaller, A., and Adam, Z. (2012) Rhomboid proteins in the chloroplast envelope affect the level of allene oxide synthase in Arabidopsis thaliana, *The Plant journal : for cell and molecular biology 72*, 559-571.

116. Wolf, E. V., Zeißler, A., Vosyka, O., Zeiler, E., Sieber, S., and Verhelst, S. H. L. (2013) A New Class of Rhomboid Protease Inhibitors Discovered by Activity-Based Fluorescence Polarization, *PLoS ONE 8*, e72307.

117. Adrain, C., Strisovsky, K., Zettl, M., Hu, L., Lemberg, M. K., and Freeman, M. (2011) *Mammalian EGF receptor activation by the rhomboid protease RHBDL2*, Vol. 12.

118. Maegawa, S., Koide, K., Ito, K., and Akiyama, Y. (2007) The intramembrane active site of GlpG, an E. coli rhomboid protease, is accessible to water and hydrolyses an extramembrane peptide bond of substrates, *Molecular microbiology 64*, 435-447.

119. Paetzel, M., Dalbey, R. E., and Strynadka, N. C. (1998) Crystal structure of a bacterial signal peptidase in complex with a beta-lactam inhibitor, *Nature 396*, 186-190.

120. Cox, J., and Mann, M. (2011) Quantitative, high-resolution proteomics for data-driven systems biology, *Annual review of biochemistry 80*, 273-299.

121. Bogyo, M., Verhelst, S., Bellingard-Dubouchaud, V., Toba, S., and Greenbaum, D. (2000) Selective targeting of lysosomal cysteine proteases with radiolabeled electrophilic substrate analogs, *Chemistry & biology 7*, 27-38.

122. Sadaghiani, A. M., Verhelst, S. H., and Bogyo, M. (2007) Tagging and detection strategies for activity-based proteomics, *Current opinion in chemical biology 11*, 20-28.

123. Gillet, L. C., Namoto, K., Ruchti, A., Hoving, S., Boesch, D., Inverardi, B., Mueller, D., Coulot, M., Schindler, P., Schweigler, P., Bernardi, A., and Gil-Parrado, S. (2008) In-cell selectivity profiling of serine protease inhibitors by activity-based proteomics, *Molecular & cellular proteomics : MCP 7*, 1241-1253.

124. Evans, M. J., Saghatelian, A., Sorensen, E. J., and Cravatt, B. F. (2005) Target discovery in small-molecule cell-based screens by in situ proteome reactivity profiling, *Nature biotechnology 23*, 1303-1307.

125. Yang, Y., Hahne, H., Kuster, B., and Verhelst, S. H. (2013) A simple and effective cleavable linker for chemical proteomics applications, *Molecular & cellular proteomics : MCP 12*, 237-244.

126. Yang, Y., and Verhelst, S. H. (2013) Cleavable trifunctional biotin reagents for protein labelling, capture and release, *Chemical communications (Cambridge, England) 49*, 5366-5368.

127. Böttcher, T., and Sieber, S. A. (2008) β-Lactones as Privileged Structures for the Active-Site Labeling of Versatile Bacterial Enzyme Classes, *Angewandte Chemie International Edition 47*, 4600-4603.

128. Staub, I., and Sieber, S. A. (2008) Beta-lactams as selective chemical probes for the in vivo labeling of bacterial enzymes involved in cell wall biosynthesis, antibiotic resistance, and virulence, *J Am Chem Soc 130*, 13400-13409.

129. Sieber, S. A., Niessen, S., Hoover, H. S., and Cravatt, B. F. (2006) Proteomic profiling of metalloprotease activities with cocktails of active-site probes, *Nat Chem Biol 2*, 274-281.

130. Krysiak, J. M., Kreuzer, J., Macheroux, P., Hermetter, A., Sieber, S. A., and Breinbauer, R. (2012) Activity-based probes for studying the activity of flavin-dependent oxidases and for the protein target profiling of monoamine oxidase inhibitors, *Angewandte Chemie (International ed. in English) 51*, 7035-7040.

131. Weerapana, E., Simon, G. M., and Cravatt, B. F. (2008) Disparate proteome reactivity profiles of carbon electrophiles, *Nat Chem Biol 4*, 405-407.

132. Haedke, U., Kuttler, E. V., Vosyka, O., Yang, Y., and Verhelst, S. H. (2013) Tuning probe selectivity for chemical proteomics applications, *Current opinion in chemical biology 17*, 102-109.

133. Haedke, U. R., Frommel, S. C., Hansen, F., Hahne, H., Kuster, B., Bogyo, M., and Verhelst, S. H. (2014) Phosphoramidates as novel activity-based probes for serine proteases, *Chembiochem 15*, 1106-1110.

134. Speers, A. E., and Cravatt, B. F. (2004) Profiling enzyme activities in vivo using click chemistry methods, *Chemistry & biology 11*, 535-546.

135. Willems, L. I., Li, N., Florea, B. I., Ruben, M., van der Marel, G. A., and Overkleeft, H. S. (2012) Triple bioorthogonal ligation strategy for simultaneous labeling of multiple enzymatic activities, *Angewandte Chemie (International ed. in English) 51*, 4431-4434.

136. Willems, L. I., Verdoes, M., Florea, B. I., van der Marel, G. A., and Overkleeft, H. S. (2010) Two-step labeling of endogenous enzymatic activities by Diels-Alder ligation, *Chembiochem 11*, 1769-1781.

137. Saxon, E., and Bertozzi, C. R. (2000) Cell surface engineering by a modified Staudinger reaction, *Science (New York, N.Y.) 287*, 2007-2010.

138. Verdoes, M., Florea, B. I., Hillaert, U., Willems, L. I., van der Linden, W. A., Sae-Heng, M., Filippov, D. V., Kisselev, A. F., van der Marel, G. A., and Overkleeft, H. S. (2008) Azido-BODIPY acid reveals quantitative Staudinger-Bertozzi ligation in two-step activity-based proteasome profiling, *Chembiochem 9*, 1735-1738.

139. Hang, H. C., Loureiro, J., Spooner, E., van der Velden, A. W., Kim, Y. M., Pollington, A. M., Maehr, R., Starnbach, M. N., and Ploegh, H. L. (2006) Mechanism-based probe for the analysis of cathepsin cysteine proteases in living cells, *ACS Chem Biol 1*, 713-723.

140. Speers, A. E., Adam, G. C., and Cravatt, B. F. (2003) Activity-based protein profiling in vivo using a copper(i)-catalyzed azide-alkyne [3 + 2] cycloaddition, *J Am Chem Soc 125*, 4686-4687.

141. Debets, M. F., van Berkel, S. S., Dommerholt, J., Dirks, A. T., Rutjes, F. P., and van Delft, F. L. (2011) Bioconjugation with strained alkenes and alkynes, *Accounts of chemical research 44*, 805-815.

142. van der Linden, W. A., Li, N., Hoogendoorn, S., Ruben, M., Verdoes, M., Guo, J., Boons, G. J., van der Marel, G. A., Florea, B. I., and Overkleeft, H. S. (2012) Two-step bioorthogonal activity-based proteasome profiling using copper-free click reagents: a comparative study, *Bioorg Med Chem 20*, 662-666.

143. Bachovchin, D. A., Brown, S. J., Rosen, H., and Cravatt, B. F. (2009) Identification of selective inhibitors of uncharacterized enzymes by high-throughput screening with fluorescent activity-based probes, *Nat Biotech 27*, 387-394.

144. Adibekian, A., Martin, B. R., Chang, J. W., Hsu, K.-L., Tsuboi, K., Bachovchin, D. A., Speers, A. E., Brown, S. J., Spicer, T., Fernandez-Vega, V., Ferguson, J., Hodder, P. S., Rosen, H., and Cravatt, B. F. (2012) Confirming Target Engagement for Reversible Inhibitors in Vivo by Kinetically Tuned Activity-Based Probes, *Journal of the American Chemical Society 134*, 10345-10348.

145. Bachovchin, D. A., Wolfe, M. R., Masuda, K., Brown, S. J., Spicer, T. P., Fernandez-Vega, V., Chase, P., Hodder, P. S., Rosen, H., and Cravatt, B. F. (2010) Oxime esters as selective, covalent inhibitors of the serine hydrolase retinoblastoma-binding protein 9 (RBBP9), *Bioorganic & Medicinal Chemistry Letters 20*, 2254-2258.

146. Dillon, M. B. C., Bachovchin, D. A., Brown, S. J., Finn, M. G., Rosen, H., Cravatt, B. F., and Mowen, K. A. (2012) Novel Inhibitors for PRMT1 Discovered by High-Throughput Screening Using Activity-Based Fluorescence Polarization, *ACS Chemical Biology 7*, 1198-1204.

147. Knuckley, B., Jones, J. E., Bachovchin, D. A., Slack, J., Causey, C. P., Brown, S. J., Rosen, H., Cravatt, B. F., and Thompson, P. R. (2010) A fluopol-ABPP HTS assay to identify PAD inhibitors, *Chemical Communications 46*, 7175-7177.

148. Lone, A. M., Bachovchin, D. A., Westwood, D. B., Speers, A. E., Spicer, T. P., Fernandez-Vega, V., Chase, P., Hodder, P. S., Rosen, H., Cravatt, B. F., and Saghatelian, A. (2011) A Substrate-Free Activity-Based Protein Profiling Screen for the Discovery of Selective PREPL Inhibitors, *Journal of the American Chemical Society 133*, 11665-11674.

149. Tsuboi, K., Bachovchin, D. A., Speers, A. E., Spicer, T. P., Fernandez-Vega, V., Hodder, P., Rosen, H., and Cravatt, B. F. (2011) Potent and Selective Inhibitors of Glutathione S-Transferase Omega 1 That Impair Cancer Drug Resistance, *Journal of the American Chemical Society 133*, 16605-16616.

150. Chung, C. T., Niemela, S. L., and Miller, R. H. (1989) One-step preparation of competent Escherichia coli: transformation and storage of bacterial cells in the same solution, *Proceedings of the National Academy of Sciences 86*, 2172-2175.

151. Käll, L., Krogh, A., and Sonnhammer, E. L. L. (2007) Advantages of combined transmembrane topology and signal peptide prediction—the Phobius web server, *Nucleic Acids Research 35*, W429-W432.

152. Oakley, B. R., Kirsch, D. R., and Morris, N. R. (1980) A simplified ultrasensitive silver stain for detecting proteins in polyacrylamide gels, *Analytical biochemistry 105*, 361-363.

153. Zhang, J.-H., Chung, T. D. Y., and Oldenburg, K. R. (1999) A Simple Statistical Parameter for Use in Evaluation and Validation of High Throughput Screening Assays, *Journal of Biomolecular Screening 4*, 67-73.

154. Antos, J. M., Chew, G.-L., Guimaraes, C. P., Yoder, N. C., Grotenbreg, G. M., Popp, M. W.-L., and Ploegh, H. L. (2009) Site-Specific N- and C-Terminal Labeling of a Single Polypeptide Using Sortases of Different Specificity, *Journal of the American Chemical Society 131*, 10800-10801.

155. Hope, M. J., Bally, M. B., Mayer, L. D., Janoff, A. S., and Cullis, P. R. (1986) Generation of multilamellar and unilamellar phospholipid vesicles, *Chemistry and physics of lipids 40*, 89-107.

156. Reeves, J. P., and Dowben, R. M. (1969) Formation and properties of thin-walled phospholipid vesicles, *Journal of Cellular Physiology 73*, 49-60.

157. Walde, P., Cosentino, K., Engel, H., and Stano, P. (2010) Giant vesicles: preparations and applications, *Chembiochem 11*, 848-865.

158. Hishida, M., Seto, H., Yamada, N. L., and Yoshikawa, K. (2008) Hydration process of multi-stacked phospholipid bilayers to form giant vesicles, *Chemical Physics Letters 455*, 297-302.

159. Halgren, T. A. (1996) Merck molecular force field. I. Basis, form, scope, parameterization, and performance of MMFF94, *Journal of Computational Chemistry 17*, 490-519.

160. Trott, O., and Olson, A. J. (2010) AutoDock Vina: Improving the speed and accuracy of docking with a new scoring function, efficient optimization, and multithreading, *Journal of Computational Chemistry 31*, 455-461.

161. Humphrey, W., Dalke, A., and Schulten, K. (1996) VMD: Visual molecular dynamics, *Journal of Molecular Graphics 14*, 33-38.

162. de Hoon, M. J. L., Imoto, S., Nolan, J., and Miyano, S. (2004) Open source clustering software, *Bioinformatics 20*, 1453-1454.

163. McWilliam, H., Li, W., Uludag, M., Squizzato, S., Park, Y. M., Buso, N., Cowley, A. P., and Lopez, R. (2013) Analysis Tool Web Services from the EMBL-EBI, *Nucleic Acids Research 41*, W597-W600.

164. Tamura, K., Stecher, G., Peterson, D., Filipski, A., and Kumar, S. (2013) MEGA6: Molecular Evolutionary Genetics Analysis version 6.0, *Mol Biol Evol 30*, 2725-2729.

165. Rzhetsky, A., and Nei, M. (1992) A Simple Method for Estimating and Testing Minimum-Evolution Trees, *Molecular Biology and Evolution 9*, 945.

166. Felsenstein, J. (1985) Confidence Limits on Phylogenies: An Approach Using the Bootstrap, *Evolution 39*, 783-791.

167. Jones, D. T., Taylor, W. R., and Thornton, J. M. (1992) The rapid generation of mutation data matrices from protein sequences, *Computer applications in the biosciences : CABIOS 8*, 275-282.

168. Nei, M., and Kumar, S. (2000) *Molecular evolution and phylogenetics*, Oxford University Press, Oxford ; New York.

169. Saitou, N., and Nei, M. (1987) The neighbor-joining method: a new method for reconstructing phylogenetic trees, *Mol Biol Evol 4*, 406-425.

170. Bachovchin, D. A., Mohr, J. T., Speers, A. E., Wang, C., Berlin, J. M., Spicer, T. P., Fernandez-Vega, V., Chase, P., Hodder, P. S., Schürer, S. C., Nomura, D. K., Rosen, H., Fu, G. C., and Cravatt, B. F. (2011) Academic cross-fertilization by public screening yields a remarkable class of protein phosphatase methylesterase-1 inhibitors, *Proceedings of the National Academy of Sciences 108*, 6811-6816.

171. Kidd, D., Liu, Y., and Cravatt, B. F. (2001) Profiling Serine Hydrolase Activities in Complex Proteomes†, *Biochemistry 40*, 4005-4015.

172. Haedke, U., Götz, M., Baer, P., and Verhelst, S. H. L. (2012) Alkyne derivatives of isocoumarins as clickable activity-based probes for serine proteases, *Bioorganic & Medicinal Chemistry 20*, 633-640.

173. Zeiler, E., Braun, N., Böttcher, T., Kastenmüller, A., Weinkauf, S., and Sieber, S. A. (2011) Vibralactone as a Tool to Study the Activity and Structure of the ClpP1P2 Complex from Listeria monocytogenes, *Angewandte Chemie International Edition 50*, 11001-11004.

174. Pitscheider, M., Mausbacher, N., and Sieber, S. A. (2012) Antibiotic activity and target discovery of three-membered natural product-derived heterocycles in pathogenic bacteria, *Chemical Science 3*, 2035-2041.

175. Morein, S., Andersson, A.-S., Rilfors, L., and Lindblom, G. (1996) Wild-type Escherichia coli Cells Regulate the Membrane Lipid Composition in a Window between Gel and Non-lamellar Structures, *Journal of Biological Chemistry 271*, 6801-6809.

176. Oursel, D., Loutelier-Bourhis, C., Orange, N., Chevalier, S., Norris, V., and Lange, C. M. (2007) Lipid composition of membranes of Escherichia coli by liquid chromatography/tandem mass spectrometry using negative electrospray ionization, *Rapid Communications in Mass Spectrometry 21*, 1721-1728.

177. Rigaud, J.-L., and Lévy, D. (2003) Reconstitution of Membrane Proteins into Liposomes, In *Methods in Enzymology* (Nejat, D., Ed.), pp 65-86, Academic Press.

178. Schubert, R. (2003) Liposome Preparation by Detergent Removal, In *Methods in Enzymology* (Nejat, D., Ed.), pp 46-70, Academic Press.

179. Ruozi, B., Belletti, D., Tombesi, A., Tosi, G., Bondioli, L., Forni, F., and Vandelli, M. A. (2011) AFM, ESEM, TEM, and CLSM in liposomal characterization: a comparative study, *International Journal of Nanomedicine 6*, 557-563.

180. Käll, L., Krogh, A., and Sonnhammer, E. L. L. (2004) A Combined Transmembrane Topology and Signal Peptide Prediction Method, *Journal of Molecular Biology 338*, 1027-1036.

181. Serim, S. (2014) The development of activity-based probes for serine proteases, In *Fakultät Wissenschaftszentrum Weihenstephan*, p 154, Technische Universität München.

182. Jackson, D. S., Fraser, S. A., Ni, L. M., Kam, C. M., Winkler, U., Johnson, D. A., Froelich, C. J., Hudig, D., and Powers, J. C. (1998) Synthesis and evaluation of diphenyl phosphonate esters as inhibitors of the trypsin-like granzymes A and K and mast cell tryptase, *J Med Chem 41*, 2289-2301.

183. Smith, H. J., and Simons, C. (2002) *Proteinase and peptidase inhibition : recent potential targets for drug development*, Taylor & Francis, London ; New York.

184. Holmes, O., Paturi, S., Ye, W., Wolfe, M. S., and Selkoe, D. J. (2012) Effects of membrane lipids on the activity and processivity of purified gamma-secretase, *Biochemistry 51*, 3565-3575.

185. Winkler, E., Kamp, F., Scheuring, J., Ebke, A., Fukumori, A., and Steiner, H. (2012) Generation of Alzheimer disease-associated amyloid beta42/43 peptide by gamma-secretase can be inhibited directly by modulation of membrane thickness, *The Journal of biological chemistry 287*, 21326-21334.

186. Lei, X., and Li, Y.-M. (2009) The Processing of Human Rhomboid Intramembrane Serine Protease RHBDL2 Is Required for Its Proteolytic Activity, *Journal of Molecular Biology 394*, 815-825.

187. Wolfe, M. S., and Selkoe, D. J. (2014) gamma-Secretase: a horseshoe structure brings good luck, *Cell 158*, 247-249.

188. Cheng, T. L., Wu, Y. T., Lin, H. Y., Hsu, F. C., Liu, S. K., Chang, B. I., Chen, W. S., Lai, C. H., Shi, G. Y., and Wu, H. L. (2011) Functions of rhomboid family protease RHBDL2 and thrombomodulin in wound healing, *The Journal of investigative dermatology 131*, 2486-2494.

189. Pascall, J. C., and Brown, K. D. (2004) Intramembrane cleavage of ephrinB3 by the human rhomboid family protease, RHBDL2, *Biochemical and biophysical research communications 317*, 244-252.

190. Liao, H. J., and Carpenter, G. (2012) Regulated intramembrane cleavage of the EGF receptor, *Traffic (Copenhagen, Denmark) 13*, 1106-1112.

# Publications

Parts of this thesis have been or will be published in international, peer-reviewed journals.

### *Research Papers*

"A new class of rhomboid protease inhibitors discovered by activity-based fluorescence polarization." PLoS One. 2013 Aug 22;8(8):e72307. doi: 10.1371/journal.pone.0072307
**Wolf EV**, Zeißler A, Vosyka O, Zeiler E, Sieber S, Verhelst SH.

"Activity-based probes for rhomboid proteases discovered in a mass spectrometry-based assay." Proc Natl Acad Sci USA. 2013 Feb 12;110(7):2472-7. doi: 10.1073/pnas.1215076110.
Vosyka O, Vinothkumar KR, **Wolf EV**, Brouwer AJ, Liskamp RM, Verhelst SH.

"Inhibitor fingerprinting of rhomboid proteases reveals inhibitor selectivity and rhomboid auto-processing**.**" (*Manuscript in preparation*)
**Wolf EV**, Zeißler A, […], Verhelst SH.

"Activity-based protein profiling of rhomboids in liposome environments."
(*Manuscript in preparation*)
**Wolf EV**, Seybold M, Langosch D, Verhelst SH.

### *Review / Book chapter*

"Tuning probe selectivity for chemical proteomics applications." Curr Opin Chem Biol. 2012 Dec 27. pii: S1367-5931(12)00159-7. doi: 10.1016/j.cbpa.2012.11.024.
Haedke U, **Küttler EV**, Vosyka O, Yang Y, Verhelst SH.

"16. Activity-based protein profiling" book chapter in the book „*Chemoselective and Bioorthogonal Ligation Chemistries: Concepts and Applications*" to be published 2015 by Wiley-VCH; chapter submitted 2013, accepted 02/2014
**Wolf EV**, Verhelst SH.

## Acknowledgements

First of all, I would like to express the deepest appreciation and special thanks to my PhD supervisor **Prof. Dr. Steven Verhelst**. You have been an incredible mentor to me, encouraging me to always aim as high as possible and to never give up. Not only have you helped me grow as a researcher and a person, but you have also taught me to laugh in the face of difficulty. I feel privileged to have done my PhD under your supervision.

Furthermore, I am also deeply grateful to **Prof. Dr. Dieter Langosch**, head of the biopolymer chemistry group and my committee chair, for supporting my research through very helpful comments, ideas, and a wonderful POLARstar plate reader. I have enjoyed working at your chair tremendously, and I will miss our philosophical talks during lunches and excursions.

I would like to thank my committee members, **Prof. Dr. Stefan Lichtenthaler** and **Prof. Dr. Iris Antes**, for talking the time and acting as examiners.

I am very grateful to the **Elite Network of Bavaria** for funding my PhD thesis through a scholarship. Without this stipend I wouldn't have been able to work on this exciting project.

**Prof. Dr. Matthew Freeman**, **Prof. Dr. Sinisa Urban**, **Prof. Dr. Joanne Lemieux**, and **Dr. Marius Lemberg** I would like to thank for providing me with many rhomboid plasmids, as well as lots of advice and positive feedback at various conferences.

Special thanks I want to bestow upon **Dr. Kvido Strisovsky**. I had the pleasure of visiting your lab in Prague twice. Thank you and everyone in your group and department for performing the TEM and EDMAN experiments.

For trying to produce a crystal structure from EcGlpG with a β-lactone I want to thank **Dr. Kutti Vinothkumar** .

I would like to thank **Prof. Dr. Stephan Sieber** and his whole group for providing our lab with a lot of compounds, especially **Dr. Evelyn Zeiler** for my favorite β-lactones.

Thank you **Prof. Dr. Renier van Der Hoorn** for your letter of support enabling me to attend the Lindau Nobel Laureate Meeting, and also for many inspiring conversations!

My "Doktor-Opa", **Prof Dr. Hermen Overkleeft**, I would like to acknowledge for an outstanding lecture on the design of ABPs for especially difficult proteases.